# A study of novel filiform corrosion phenomena on hot dip organically coated Zn-Al-Mg steel.

**Eaves, David Richard**

# A study of novel filiform corrosion phenomena on hot dip organically coated Zn-Al-Mg steel

David Richard Eaves

Submitted to the University of Wales in fulfilment of the requirements for the Degree of Doctor of Engineering

2013

# Summary

Hot dip coated steel is a high volume engineering material with a range of applications from automotive to white goods and construction. In recent years there has been a drive to increase the corrosion resistance of hot dip coated steels, and reduce the dependence upon carcinogenic and toxic corrosion inhibitors such as hexavalent chromium VI. In order to meet these targets steel companies globally are developing a new generation of galvanised steel coatings with novel zinc based alloys, with increasing additions of aluminium and magnesium. However although the corrosion resistance of these materials has been shown to increase in salt spray tests, these new alloys have also been proven to be susceptible to other types of corrosionThis thesis studies filiform corrosion on hot dip galvanised steel, with a hot dip coating composed mainly of zinc, but with additions of aluminium and magnesium. It is found that acetic acid can reproducibly initiate filiform corrosion on these Zn-Al-Mg hot dip steel coatings. The composition of the hot dip coating is also studied, and this is found to be critical to the corrosion resistance of the coating. Zinc-Magnesium coatings are found to be susceptible to filiform corrosion. However the addition of aluminium increases the filiform corrosion resistant of these coatings and above a critical point of approximately 3wt% aluminium, the sample is resistance to filiform attack. This is due to the increased amount of aluminium promoting the formation of a passive aluminium oxide surface layer on the sample.

A second method of inhibiting filiform corrosion is also tested where hydrotalcite, an anion exchange clay, which is incorporated into a model polyvinylbutyral organic coating system. Hydrotalcite scavenges aggressive anions from the coating / metal interface and in this case removes acetate via an anion exchange reaction. The use of hydrotalcite is found to inhibit filiform corrosion, and reduce the rate of filament propagation over time. However hydrotalcite cannot stop initiation of filiform corrosion as the concentration of acetic acid during initiation exceeds the finite capacity of the hydrotalcite exchange reaction.

A third method for the inhibition of filiform corrosion was tested where phenylphosphonic acid (PPA) is incorporated into the model polyvinylbutyral organic coating system. The addition of PPA reduces the pH at the coating / hot dip coating interface when the coating is applied. PPA will dissociate to give the PP2- di-negative anion which forms an insoluble salt with the $Zn^{2+}$ cation and so leads to the precipitation of a solid layer of ZnPP. This insoluble layer acts as a barrier to electron transfer, reducing the rate of the cathodic reaction, and therefore reducing the rate of corrosion. After 5 weeks the total amount of surface corrosion on samples containing 10wt% PPA were found to be over 80% less than on uninhibited samples.

# Declarations and Statements

DECLARATION

This work has not previously been accepted in substance for any degree and is not being concurrently submitted in candidature for any degree.

Signed ..... (candidate)

Date 28.07.14

STATEMENT 1

This thesis is the result of my own investigations, except where otherwise stated. Where correction services have been used, the extent and nature of the correction is clearly marked in a footnote(s).

Other sources are acknowledged by footnotes giving explicit references. A bibliography is appended.

Signed ..... (candidate)

Date 28.07.14

STATEMENT 2

I hereby give consent for my thesis, if accepted, to be available for photocopying and for inter-library loan, and for the title and summary to be made available to outside organisations.

Signed ..... (candidate)

Date 28.07.14

**NB:** *Candidates on whose behalf a bar on access has been approved by the University (see Note 7), should use the following version of Statement 2:*

I hereby give consent for my thesis, if accepted, to be available for photocopying and for inter-library loans **after expiry of a bar on access approved by the Swansea University.**

Signed .. ..... (candidate)

Date 28.07.14

# Contents

# Acknowledgements

First and foremost I would like to thank Professor Neil McMurray and Dr Geraint Williams, without whom this project would not have been possible. Their continued support and ideas, along with their open door policy on their offices has been a great help over the years. They have also proved to be a wealth of information, not just about corrosion but also good holiday (conference) destinations, investments including visits to the Australian royal mint to buy gold certificates, and prolonged conversations about the economic issues in the UK. In addition I would like to extend special thanks to Dr Jon Elvins, my industrial supervisor for offering support, access to equipment and people and for his technical expertise. He has also been a good friend on many of our business trips away, and always offered good advice.

There are many other people and organisations to thank; obviously Tata steel and EPSRC for funding. Professor David Worsley for what seems like an infinite amount of effort to organise SPECIFIC which has given us a much better environment to carry out our work. Other people to thank are Dr David Penney, Dr Jim Sullivan, Dr Mabbs, and so many more, who without them the previous four years would of been significantly harder and a lot less enjoyable.

My friends outside of university have also contributed to success in my EngD. A big inspiration has been Adrian who was a bit of a "model PhD student" and showed me the ropes! I would also like to thank Dyfrig and Julie who have literally put up with me talking about corrosion for hours over the past year without too much complaining. There are also many more people so thank you, you know who you are.

I have thoroughly enjoyed my 4 years on the EngD at Swansea University. There have been so many good times, and trips. It has also been a great opportunity to gain an insight in to how a multination engineering company works, both good and bad, and I think this will be an invaluable eye opener for the future.

# List of Abbreviations

| | | |
|---|---|---|
| AFM | : | Atomic Force Microscope |
| EDS | : | See EDX |
| EDX | : | Energy Dispersive X-ray |
| FFC | : | Filiform corrosion |
| GDP | : | Gross Domestic Product |
| HDG | : | Hot dip Galvanized |
| HT | : | Hydrotalcite |
| LDH | : | Layered Double Hydroxides |
| REDOX | : | Reduction and Oxidation |
| RH | : | Relative Humidity |
| PPA | : | Phenyl phosphoric acid |
| PTFE | : | Polytetrafluoroethylene |
| PVB | : | Polyvinylbutyral |
| PVD | : | Physical Vapour Deposition |
| SEM | : | Scanning Electron Microscope |
| SKP-FM | : | Scanning Kelvin Probe Force Microscopy |
| XRD | : | X-Ray Diffraction |

# Chapter 1: Introduction and Literature Review

## 1.1 General introduction

In 2011 over 1.52 mega tonnes of steel was produced (1), a large proportion of which was used in corrosive environments. Steel is a widely used construction and engineering material due to its mechanical properties; manufacturing properties such as formability and weld ability, and economic reasons such as cost. Many different grades of steel are manufactured, with a wide range of mechanical properties, resulting in the use of steel in a varied range of applications, from architectural, to automotive, to specialist applications such as transistors. However one significant drawback of steel is its low level of corrosion resistance in its unprotected form, when compared to other materials such as aluminium alloys and polymers. In the context of this thesis corrosion is defined as the detrimental deterioration of a material by an electro-chemical interaction with its environment. The term corrosion is sometimes also applied to the degradation of plastics, concrete and wood, but in this thesis it will be used solely to describe electrochemical corrosion on metals.

The main detrimental physical consequence of corrosion is metal loss. The reduction in metal thickness due to metal loss, will result in changes in the mechanical properties of components, such as reduced strength, or increased strain, which may result in structural failures. When metal loss occurs in localized regions it can form a crack like structure, which can result in considerable weakening of the component, as these defects can act as stress raisers. The corrosion of components can also have an associated human risk arising from structural failures (e.g. bridges, cars, and aircraft). Corrosion can lead to the reduction in the value of an asset, either by reduced physical performance or future working life time, or simply due to reduced aesthetic appearance. When corrosion occurs in an aqueous environment, there will also be some contamination of fluids due to the leaching out of metal anions from the corroding metal. This issue can be highly relevant for some applications such as the corrosion of pipe lines in a process where the product is a fluid (e.g. the manufacture

of petrochemicals, or shampoo). A human hazard can be caused in the case of corrosion of drinking water pipelines. When heavy metals such as nickel corrode, this leaching of anions into the water system may also cause environmental issues (2).

The costs of corrosion can be broken down in to direct and indirect costs. Direct costs are costs that can be directly attributed to corrosion, or corrosion prevention. Some examples of direct costs are:

- Capital costs - the cost of replacing corroded components
- Control costs : the cost associated with maintaining, repairing, repainting components due to corrosion
- Design costs – extra cost of using corrosion resistant alloys, protective coatings and corrosion inhibitors

Indirect costs are costs that can be associated with the effect of corrosion. Some examples of indirect costs are:

- Loss of earnings due to shutting down a factory or power station for issues due to corrosion of assets.
- Loss of product due to leakage
- Contamination of a product and subsequent loss of earnings

Several studies have been undertaken to estimate the annual cost of corrosion in industrialized economies. The first comprehensive landmark study was carried out in America in 1978. This study found that in 1975 the total estimated cost of metallic corrosion was $70 billion for the US economy, which was approximately 5% of national gross domestic product (GDP) at the time (3). A more recent study carried out again in America, found the cost of corrosion between 1999 and 2001 to average approximately $276 billion in the US, which is ~3% of US national GDP (4). Numerous other studies have been carried out, and the economic cost of corrosion is consistently calculated to be between 3-5% of an industrialized nations GDP. Assuming the conservative figure of 3% of global GDP, this extrapolates to a global annual cost of corrosion over £1.4 trillion per year in 2011.

## 1.2 Introduction to Corrosion

Most engineering metals naturally occur in the form of an ore, which is most commonly an oxidised form of the metal, however ores can also be a metal sulphides or silicates. The production of a pure metal requires processes that expend large amounts of energy, in order to reduce and separate the metal from its ore. In their metallic form, most engineering metals can therefore be regarded as being in a metastable state, as there is an electrochemical driving force for the metal to revert back to its oxide form. Corrosion is the electrochemical process in which this occurs. Corrosion does not usually occur by a direct chemical reaction of a metal with its environment, rather through the operation of coupled electrochemical half-cell reactions, in the form of an electrochemical corrosion cell. This electrochemical corrosion cell can be separated into anodic and cathodic reactions, which are also commonly described as reduction and oxidation reactions or REDOX reactions. An electrochemical reaction is defined as a chemical reaction involving the transfer of electrons between a solid and liquid species. (5)

### 1.2.1 Anodic corrosion reaction

During the anodic half-cell reaction in an electrochemical corrosion cell, the metallic element will lose electrons from its outer sub shell and become a positively charged ion. The charge of this ion will correspond to the number of electrons lost, for example when one electron is removed, the ion will have a charge of +1. The process of stripping electrons from an atom is known as oxidation. In corrosion terminology, an oxidation reaction is also called an anodic reaction (3).

The location where the anodic reaction takes place is often considered to be the site of physical corrosion, as this is where metal loss occurs. At the anodic reaction site, positively charged ions leave the metals surface. The corresponding negatively charged electrons leave the anodic reaction site and flow via the metal or an external

conductor. The simplest form of an anodic corrosion reaction is shown in equation 1.1.

$$M \rightarrow M^{+} + e^{-} \tag{1.1}$$

An anodic reaction that can be observed during the corrosion of iron to form iron oxide *(rust)* is shown in equation 1.2.

$$Fe(s) \rightarrow Fe^{2+}(aq) + 2e^{-} \tag{1.2}$$

In the case of iron, solid metallic iron is oxidised to form $Fe^{2+}$ ions, which are soluble within aqueous electrolytes. The two electrons are transported away from the anodic site via conduction through the metallic iron. This is shown in the schematic diagram figure 1-1.

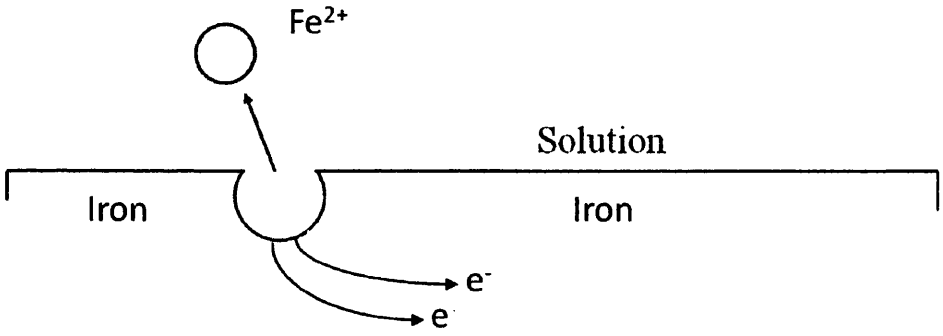


**Figure 1-1** : Schematic diagram of an anodic half cell reaction on an iron substrate in immersion conditions. Solid metallic iron is oxidised to form $Fe^{2+}$ ions which are soluble within most aqueous electrolytes, and two electrons are conducted away from the anodic site through the metallic iron

During an anodic half-cell reaction, the metal will always undergo an oxidation reaction and therefore its oxidation number will increase, as there is a loss of electrons at the anodic site. Therefore corrosion can be described electrochemically as the simultaneous transformation of mass and charge across a metal / solution interface (5)

### 1.2.2 Cathodic corrosion reaction

A corrosion cell consists of oxidation and reduction reactions happening simultaneously at equivalent rates. As the anodic oxidation reaction takes place, the corresponding cathodic reduction reaction must simultaneously occur. The electrons generated at the anode are conducted through the metal to the cathodic reaction sites. At the cathodic reaction site electro neutrality is conserved by reducing hydrogen ions to hydrogen gas, or by the reduction of oxygen and water to hydroxyl ions (5)

During the cathodic reaction a given species always undergoes reduction, and therefore the oxidation number of that species will reduce, as electrons are consumed by the reduction reaction. There is no metal loss at the cathodic reaction site, and the reaction happens on the metallic surface.

There are various specific cathodic reactions that can take place in a corrosion cell. The type of cathodic reaction is governed, largely by the pH of the electrolyte, and by the oxidation reduction potential of the metal. The two most common cathodic reactions are the formation of hydrogen gas from two $H^+$ ions and two electrons or the reduction of oxygen and water to form hydroxyl ions. In an acidic electrolyte there is an excess of $H^+$ ions. As a result of this the most common cathodic reaction in acidic electrolytes is the reduction of $H^+$ to form hydrogen gas as shown in equation 1.3. This is also shown in figure 1-2 (6)

$$2H^+(aq) + 2e^- \rightarrow 2H_2(g) \qquad (1.3)$$

This hydrogen reduction cathodic reaction can also occur in neutral solutions, as there will be some disassociation of water to produce equal quantities of $H^+$ and $OH^-$ ions.

$$H_2O \leftrightarrow H^+ + OH^- \qquad (1.4)$$

However in neutral and alkali conditions, the predominant driving force for the cathodic reaction is excess of dissolved oxygen. Aqueous solutions contain dissolved

oxygen from the air. When this dissolved oxygen and water are present, they can be reduced at the cathodic site to form hydroxyl ions. This is the predominant cathodic reaction in neutral or basic solutions and is shown in equation 1.5 and figure 1-3 (6).

$$O^2(g) + 2H_2O + 4e^- \rightarrow 4OH^-(aq) \qquad (1.5)$$

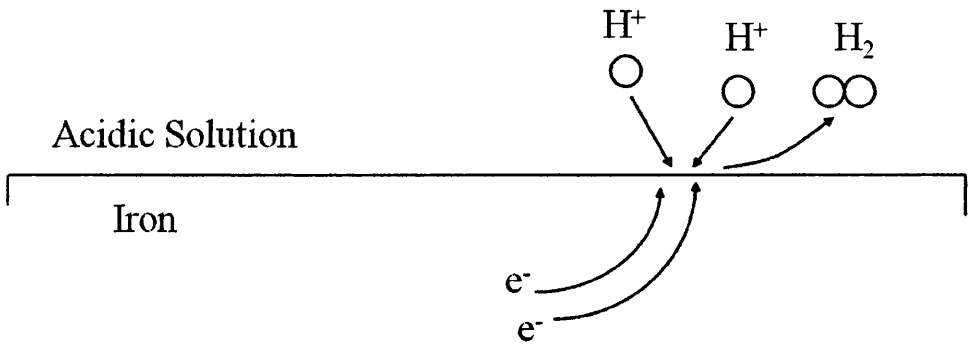


**Figure 1-2 :** Schematic diagram of the cathodic reduction reaction on iron in an acidic environment where an excess of H+ ions are present. $H^+$ is reduced on the metallic surface to form hydrogen gas.

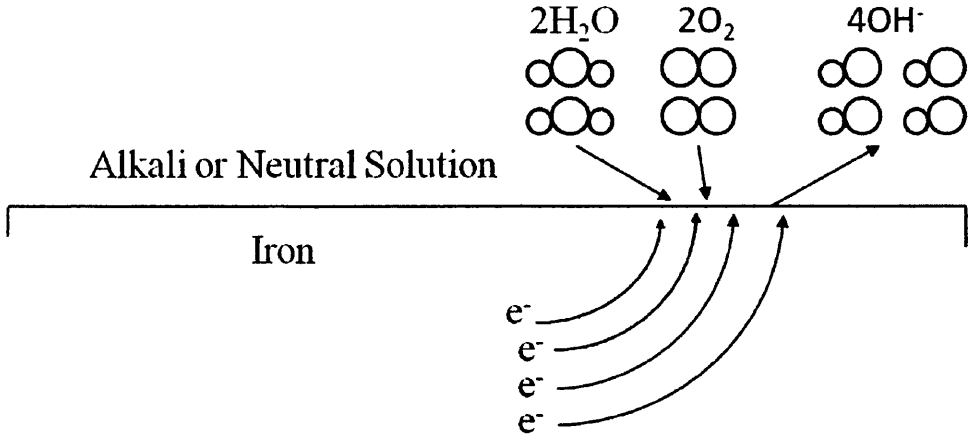


**Figure 1-3 :** Schematic diagram of the cathodic half cell reaction on iron in an oxygenated neutral and alkali environment. When dissolved oxygen and water are present, they can be reduced at the cathodic site to form hydroxyl ions.

### 1.2.3 Electrochemical Corrosion cell

There are four essential ingredients to an electrochemical corrosion cell, **(i)** the anode; **(ii)** the cathode; **(iii)** an electrolyte and **(iv)** a conductive circuit. An electrolyte is a solution capable of conducting a charge ionically. Water can be considered as an electrolyte due to the disassociation of $H^+$ and $OH^-$ shown in equation 1.4; however the ionic conductivity of pure water is very low. Many chemical compounds are made up of two or more ions of opposite charge. When these compounds are dissolved in water, they can spontaneously disassociate into two or more separate ions, which have opposite charges. This process is called ionization, and ionization significantly increases the ionic conductivity of aqueous solutions. Electrolytes also have an associated pH, which has an effect on the corrosion mechanism (7). The level of acidity or alkalinity is due to the excess of $H^+$ (hydrogen ions) or $OH^-$ (hydroxyl) ions present. An excess of $H^+$ ions is found in an acid, and an excess of $OH^-$ ions is found in an alkali. In a neutral solution, pH7, the amount of $H^+$ and $OH^-$ ions are equal. pH is the negative logarithm of the hydrogen ion concentration (7).

During corrosion in immersion conditions, the electrolyte is considered to be an aqueous solution in which the metal is immersed. In atmospheric conditions, the electrolyte can be perceived to be a thin film of aqueous solution on the surface of the metal. The conductive circuit required can simply be the metal its self. Electrons pass through this circuit from the anodic to the cathodic half-cell reaction sites, therefore coupling the two reactions. Electrons can also be conducted via an external circuit. As a result of this coupling, the physical location of the anodic and cathodic reaction sites can be separated on the surface of the metal by a significant distance. Electron coupling is shown in the schematic diagram in figure 1-4; which illustrates a typical scenario for the corrosion of iron in an acidic electrolyte. (8)

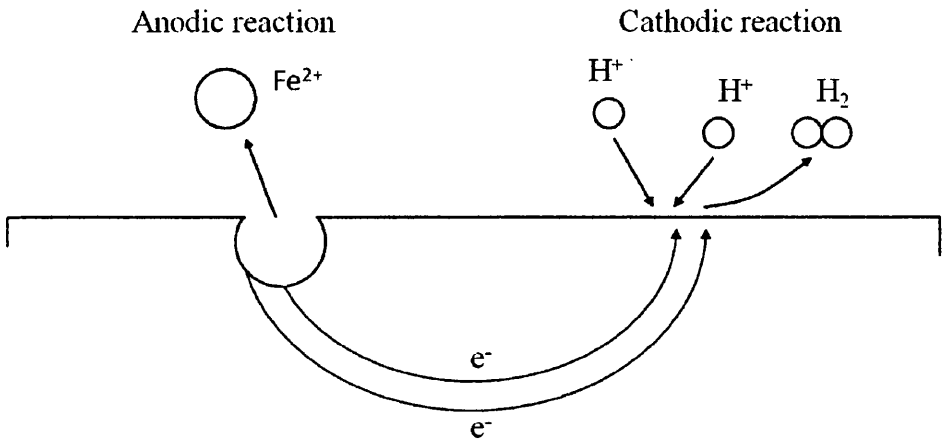


**Figure 1-4 :** Schematic diagram showing the coupled electrochemical anodic and cathodic half-cell reactions, on iron in an acidic electrolyte

### 1.2.4 Differential Aeration

The presence of oxygen can not only support the cathodic reduction half-cell reaction, it can actually promote one. Local concentrations of dissolved oxygen at the electrolyte / metal interface will vary depending on factors such as, temperature, the thickness or depth of electrolyte films or droplets, and the topography of the metallic surface. As the REDOX corrosion reaction is an equilibrium reaction, local excesses of dissolved oxygen concentration can promote the formation of local cathodes, therefore increasing the number of reaction sites and subsequently the rate of the cathodic half-cell reaction. When there is a variance in the concentration of dissolved oxygen at the metallic surface, the region of the surface where the higher concentration of dissolved oxygen is will become cathodic. As a result of this, the area of the metallic surface where the oxygen concentration is lowest will become anodic, and undergo localised corrosion. This phenomena is known as differential aeration (8).

## 1.3 Galvanic Corrosion

Most alloys or structures are composed of a range of more than one metal. Within an individual metal there are different phases. Dissimilar metals have different electrode potentials, and when there is a conductive path between dissimilar metals immersed

in an electrolyte, one metal will preferentially act as anode, and the other metal will act as cathode. The potential difference between the dissimilar metals is the driving force for the accelerated material removal rate of the more anodic metal in the galvanic couple. As the anodic reaction preferentially occurs on the anodic metal, this is the site of metal loss. As metallic ions can migrate from the anode to the cathode through the electrolyte, the anodic metal will corrode more quickly than it otherwise would, whilst the corrosion of the cathodic metal is retarded. This reaction is sometimes intentionally induced, such as in the case of batteries (8).

### 1.3.1 Electro galvanic series

Corrosion potentials of metals in solution can be measured in a relative sense by comparing one metal to another in the same solution. When two metals with different surface potentials are present in an electrolyte, a current will flow around an external circuit from the metal with the more negative surface potential, to the more positive metal. Therefore by measuring the direction of this current it is possible to deduce which metal will undergo anodic attack due to an anodic oxidation reaction, and which will act as the cathodic site and therefore support cathodic reduction reaction.

There is no absolute value of electrode potential for an individual metal, as the surface electrode potential will depend on factors such as the chemistry of the electrolyte, aeration and temperature. However the relative tendencies of metals to corrode in relation to each other can generally be considered to remain constant in most environments in which they are likely to be used. The order of metals potentials in relation to each other is shown in the galvanic series. The metallic elements most likely to support anodic oxidation reactions are shown as more negative metals in the series, and the elements most likely to support a cathodic reduction reaction at the more positive metals. When two different metals are electronically connected, which is known as galvanic coupling, the more negative metal will act as the anode, and will undergo metal loss at an accelerated rate due to the more positive metal acting as a cathode. The intensity of the galvanic effect can be measured by measuring the current flowing between the anodic and cathodic metal. The galvanic series for various commercial metals in 0.1 Molar NaCl is shown in table 1-1 (9).

| | |
|---|---|
| Cathodic (+) | Platinum |
| | Gold |
| | Graphite |
| | Silver |
| | Titanium |
| | Brasses / Bronzes |
| | Tin |
| | Stainless Steels |
| | Steels |
| | Aluminium Alloys |
| | Galvanised Steels |
| | Zinc |
| | Magnesium Alloys |
| Anodic (-) | Magnesium |

**Table 1-1** : Galvanic series for a range of commonly used commercial metals in a 0.1 mol/dm$^3$ NaCl environment (9)

### 1.3.2 Oxidation reduction potentials

All metals have a unique oxidation reduction potential. The oxidation reduction potential can be defined as the relative potential of an electrochemical reaction under equilibrium conditions or non-reacting (zero current flow) conditions. Oxidation-reduction potentials can be used to predict whether a metal will corrode in a given environment. The reason for this is that in an electrochemical REDOX reaction, the most negative half-cell will be oxidised, and therefore become the anode, and the most positive half-cell will be reduced and therefore become the cathode. When a metal is corroding in acidic conditions, the predominant cathodic reaction is the formation of hydrogen gas. This reaction shown in equation 1.5 is the same reaction that is used as a reference for oxidation reduction potentials. As a result of this any element with a negative oxidation reduction potential will undergo corrosion in an acidic environment, as it will have an electrochemical driving force for the hydrogen evolution cathodic reaction to occur. In basic or alkali environments the main cathodic reaction is oxygen reduction. The standard oxidation reduction potential for the reduction of oxygen is 1.23V, and therefore any element with an oxygen reduction potential below 1.23V will be susceptible to corrosion in the oxygenated environments. Elements such as platinum and gold, with oxidation reduction

potentials above 1.23V can be considered to be corrosion resistant, or passivated in both acids, and oxygenated environments. The oxidation reduction potentials for some commonly used elements are listed in table 1-2.

| REDOX reaction | Oxygen reduction potential |
|---|---|
| $Au \leftrightarrow Au^{3+}+3e^-$ | 1.42 |
| $Pt \leftrightarrow Pt^{2+}+2e^-$ | 1.2 |
| **$O_2+4H^+ \leftrightarrow 2H_2O$** | **1.23** |
| $Ag \leftrightarrow Ag^+ + e^-$ | 0.799 |
| $Fe^{3+}+e^- \leftrightarrow Fe^{2+}$ | 0.771 |
| **$2H^+ + 2e^- \leftrightarrow H_2$** | **0.00** |
| $Fe \leftrightarrow Fe^{2+}+2e^-$ | -0.44 |
| $Zn \leftrightarrow Zn^{2+}+2e^-$ | -0.763 |
| $Al \leftrightarrow Al^{3+}+3e^-$ | -1.66 |
| $Mg \leftrightarrow Mg^{2+}+2e^-$ | -2.38 |
| $K \leftrightarrow K^+ + e^-$ | -2.92 |

**Table 1-2 :** Oxygen reduction potentials with reference to a standard hydrogen electrode for various relevant elements. The oxidation reduction potentials shown in table 2 are for standard conditions and therefore must be corrected for (temp, concentration etc)

## 1.4 Corrosion Kinetics

Various factors dictate the rate of a corrosion reaction. As the REDOX reactions are in equilibrium, anything that limits the rate of either the anodic or cathodic reactions, will have a limiting effect on the overall rate of corrosion. Both the anodic and cathodic reactions produce reaction products. At the anodic reaction positively charged metal ions are produced. These positively charged ions can react with negatively charged ions which occur in the electrolyte, and form compounds such as oxides, chlorides or nitrides. These products can precipitate out of the electrolyte on to the metallic surface. This in turn can cover a reaction site reducing its efficiency. This mechanism can also be used to enhance the corrosion resistance of a metal, as these precipitates act as a mass transport barrier for other species, and can reduce the overall rate of corrosion. (9)

The reaction products from the cathodic reaction are either hydrogen gas or $OH^-$ ions. These can slow down the rate of the cathodic reaction by cathodic

polarization. There are two main forms of cathodic polarization, which are activation polarization and concentration polarization (9).

### 1.4.1 Activation polarization

During the cathodic reaction in an acidic electrolyte, there will be a limit to the rate hydrogen ions can be reduced, to form hydrogen gas. This limit will be a function of a variety of factors such as hydrogen ion concentration within the electrolyte, the speed of electron transfer to the hydrogen ion at the metal surface, and the temperature of the system. The speed of electron transfer to the hydrogen ion at the metal surface is highly metal dependant. Each metal has specific properties such as the band gap which will have an effect on the efficiency of this electron transfer. This efficiency will in turn lead to a fixed kinetic limit for a cathodic reaction on a single metal type. As a result of this, the rate of hydrogen evolution has been observed to be highly dependent on the type of metal which is supporting the cathodic reaction (9) (10)

### 1.4.2 Concentration Polarization

When a cathodic reaction is proceeding at a high rate, there is a constant movement of species to and from the cathode. This movement of species is known as mass transport. Cathodic reactions consume $H^+$ ions or $O_2$ gas at the cathodic reaction site, and therefore the local concentration of these ions or species around the cathodic reaction site will be depleted in the electrolyte. Using the example of $H^+$ ions in an acidic electrolyte, in order to replenish the local concentration of $H^+$ around the local reaction site, more $H^+$ ions have to diffuse through the electrolyte from the surrounding area. The diffusion of ions through an electrolyte is time dependant, and therefore the diffusion rate or mass transport rate of species, can be the limiting factor on the reaction kinetics of the cathodic reaction. Furthermore the lower the total concentration of $H^+$ in the electrolyte, the greater the distance $H^+$ ions will have to diffuse from. As a result of this concentration polarization is a large factor for both electrolytes with low overall concentrations of required species, and for reactions with a very high rates of kinetics. Unlike *activation polarization*, it is possible to increase

the rate of reaction if the reaction rate is limited by a mass transport issue (11). Inducing movement and mixing in the electrolyte by either stirring or ultrasound will increase the amount of required species at the cathodic reaction site, and therefore increase the rate of the reaction (9)

### 1.4.3 Area Effects

Another important factor influencing the rate of corrosion is known as the area effect. This is the relative ratio of the area of the anodic and cathodic reaction sites. As the overall rates of reaction are equal at the anodic and cathodic reaction sites, the magnitude of current per unit area at each reaction site, will correlate to the total area of the reaction site. This is known as the current density. If the reaction area of a half cell electrode reaction is smaller at one electrode than the other, the current density at the smaller electrode will be higher, as the same amount of current must pass through a smaller area. If the area of the cathode is small this may lead to activation polarization limiting the rate or corrosion. This is because the overall current is limited by the size and efficiency of the cathodic reaction. For anodic reactions low current densities are favourable, as the local rate of metal dissolution is low. In scenarios where the current density of anodic reactions is high, this can lead to very aggressive and localised dissolution of metal ions at the anode, and therefore aggressive localised corrosion (9,12)

## 1.5 Corrosion Products

The term corrosion product refers to the substances that are produced during a corrosion reaction. When metal ions are formed at the anodic reaction, these ions go on to migrate through the electrolyte, and may enter in to further reactions with other ionic species in the electrolyte. The result of these reactions can be the formation of insoluble corrosion products such as oxides, chlorides, nitrates or sulphates. These insoluble chemical compounds may precipitate out of the electrolyte on to the metal surface to form layers of corrosion product. Corrosion products and other surface

films can have a profound effect on the corrosion behaviour of the metal as they act as a barrier to mass transport (13).

Oxide films occur naturally on virtually all metals when they are exposed to the air, and can provide substantial protection for the underlying metal against further corrosive attack. If it were not for these oxide films, many of the common engineering metals such as aluminium and magnesium, which are near the top of the electromotive series, would corrode rapidly when exposed to air and water.

The effect of oxygen and other oxidizing agents with regards to corrosion mechanisms is variable and complex. Oxygen can accelerate corrosion by promoting oxygen reduction cathodic reactions. However oxygen and other oxidizing agents can also reduce the rate of corrosion of the underlying metal by the formation of protective films on the metal surface. Metals, such as aluminium, form continuous thin protective oxide films on their surfaces. These films act as a barrier to mass transport of species to and from anodic and cathodic corrosion sites, to the point that the metal is deemed to be passive. Passivity is when the measured potential of a metal in electrolyte resembles that of a noble metal *(eg platinum or gold)* rather that the potential of the unfilmed metal. It can also be defined as the loss of chemical activity (9). In the case of aluminium this leads to levels of corrosion resistance which are in orders of magnitude greater than the unfilmed of non-passivated "active metal". Other examples of metals that become passive in certain environments due to the formation of oxide films are, chromium, nickel, titanium and alloys containing these elements (9).

## 1.6 Corrosion mechanisms

### 1.6.1 Cathodic Disbondment

In many practical applications the corrosion resistance of metals is increased by coating the metal with an organic coating. When used in this way inert organic coatings inhibit corrosion by acting as a barrier coating. Organic coatings can be damaged, or contain defects or holidays which leave the underlying steel exposed to

potential corrosive attach. For this reason an additional method of protecting steel is cathodic protection. Cathodic protection is often used in-situ with organic coatings. The principle of cathodic protection is to polarise the steel surface to a sufficiently negative potential, so that all oxygen present at the steel surface is reduced, and no anodic attack will occur on the steel (14) (15)

Cathodic disbondment is an organic coating delamination mechanism which is driven by cathodic surface activity on the underlying metal. Due to the negative polarisation of the underlying metal, a loss of coating adhesion can occur, starting from the edge of the coated defect. Coating adhesion loss as a result of cathodic protection is a distinguishable phenomenon compared to other methods of coating disbondment such as water absorption. During the initial stages of cathodic disbondment, water creeps along the interface between the organic coating and the steel. Water ingress starts at a defects, or coating holidays and can be drawn up the interface due to osmosis. Within this moisture layer a corrosion cell will form, where the area near the hydrated metal, organic coating interface becomes cathodic, and the exposed metal surface away from the defect will become an active anode. The corrosion cell is distributed in this way due to differential aeration; oxygen concentrations are lower at the metal, coating interface than they are on the exposed metal surface. The cathodic reaction near the interface will release hydroxyl ions increasing the local pH of the hydrated interface layer. Along the metal / organic coating interface local pH's as high as 13 have been measured (14-17). Excess hydroxyl ions from the cathodic interface region may chemically bond with other ions in the electrolyte such as Na to form compounds such as NaOH. Organic coating delamination is due to the presence of strong alkali such as NaOH. The exact mechanism of coating delamination is still debated; however the surface tension of water will be reduced by the alkalinity (5), increasing the amount of water ingress along the metal / coating interface. Furthermore high concentrations of compounds such as NaOH will have the effect of alkali cleaning the metal (18).

### 1.6.2 Anodic Disbondment

When moisture and oxygen are present at the coating metal interface, anodic attack can also occur on the metal surface causing the organic coating to delaminate. This most commonly happens in acidic environments, and on materials such as aluminium and magnesium alloys. One of the consequences of the anodic reaction of a material is metal loss, and as a result of this, the metal at the metal / coating interface may be dissolved, and therefore the coating will become delaminated as the metal surface it was adhering to has been removed. Anodic disbondment is highly pH dependant. In some cases low levels of oxygen are required to ensure the pH is low. The two main forms of anodic disbondment are filiform corrosion and pitting corrosion (19).

## 1.7 Filiform corrosion

Filiform corrosion is the main form of corrosive attack studied in this thesis. Filiform corrosion was first formally described in 1944 by Sharman, as a form of atmospheric corrosion phenomenon found on steel lacquered tobacco cans (20). Sharmann found that in atmospheres containing acetic acid and water vapour, "hair like areas of corrosion grew", which could have a length of several hundred times their own width. Filiform corrosion is generally considered to be an aesthetic issue. However in some cases, damage to surface layers can be a precursor to secondary corrosion which can lead to structural issues. This could be the case on thin section materials, or coated materials (21).

Filiform corrosion will only occur in specific conditions. In order for filiform corrosion to initiate, and propagate, oxygen, aggressive anions, and a high relative humidity's must all be present. The initiation sites are usually defects, where the organic coating / metallic interface is exposed, in the presence of a soluble ionic species (21). The appearance of filiform filaments can be varied, for a range of reasons such as metallic composition and properties, propagation conditions and surface morphology. The familiar appearance of filiform corrosion on an organically coated steel ruler is shown in figure 1-5.

**Figure 1-5 :** Typical visual appearance of filiform corrosion filaments on an organically coated steel ruler

Filiform corrosion is of particular concern to industries and material applications where aesthetic appearance is of high importance, such as the automotive industry, and on products where thin metallic coatings provide corrosion protection, as the filament corrosion depth may be sufficient to expose the underlying substrate, and leave it susceptible to further corrosion. Filiform corrosion has been reported on a range of substrates such as Iron and Steel (22), Aluminium (23), Magnesium (24). As previously mentioned filiform corrosion will only initiate and propagate under certain conditions. Therefore it is necessary for a combination of several factors to exist simultaneously for filiform corrosion to occur. There are explained in more detail below.

### 1.7.1 Relative Humidity

Water is required for filiform corrosion to initiate, and propagate, as this water hydrates the salts in the filament head (25). Typical relative humidity's for filiform corrosion are in the range of 60%-95%. However the specific minimum humidity will depend on the composition of the salt in the filament head. If the humidity it to high,

filiform corrosion mechanism can be less favourable than blistering of the coating (21).

### 1.7.2 Coating Defect

Salts must be present on the surface of the metal for filiform corrosion to initiate and propagate. As the metal must be organically coated, the initial presence of salts on the metallic surface is most commonly due to a mechanical defect in the organic coating, such as a scratch, a coating holiday or a cut edge.

### 1.7.3. Oxygen

The corrosion processes required for filiform corrosion are redox reactions, and therefore oxygen is required. However the pH of the filament head will also depend on the amount of oxygen present. As oxygen can increase the pH of the filament head by reacting with $H^+$ ions, there are instances where filiform corrosion will only occur in a low oxygen environment. (26)

### 1.7.4 Corrosive Anions

Filiform corrosion is an anodic form of corrosive attack, and therefore aggressive anions such as chloride and acetate are required to make corrosive salts, which will from the electrolyte in the filament head. The filiform corrosion properties of a metal will be specific to an individual anion (20).

### 1.7.5 Nature of the Substrate

Some metallic substrates are significantly more prone to filiform corrosion than others. Filiform corrosion is known to occur on a range of substrates, as has been previously mentioned. However, even seemingly similar substrates by elemental composition may have dramatically different susceptibilities to filiform corrosion. A Afseth *et al* (27) did a study on aluminium alloys, where alloys of the same composition of aluminium alloys were tested for their filiform resistance before and after annealing. He found that some alloys which did not show filiform corrosion before annealing, were highly prone to filiform attack after the annealing process. The reason for this is

still open to debate, but it has been theorised that there is a large difference (>200mV) in the phase potentials of different microstructural phases present, and this potential difference may be sufficient to support micro-galvanic corrosion on aluminium-copper alloys.

### 1.7.6 Morphology of a filiform corrosion filament

A filiform corrosion filament is composed of two areas. The front of the filament is known as the head, and then linking this head to the initiation site is the tail. The tail is composed of dry porous corrosion product, and acts as a diffusion pathway for oxygen to get to the active cathode which is located to the rear of the filament head. Filament heads are filled with electrolyte, containing metal cations and aggressive anions such as $[Cl^-]$ and acetates $[CH_3COO]^-$. Filament advance is driven by differential aeration rising from oxygen freely diffusing through the porous filament tail to the trailing edge of the head. As a result of this the primary site for cathodic oxygen reduction lies towards the trailing edge of the filiform head, as this is the area with the highest oxygen concentration (28) (29). A schematic diagram of a model filiform corrosion filament on organically coated aluminium is shown in figure 1-6.

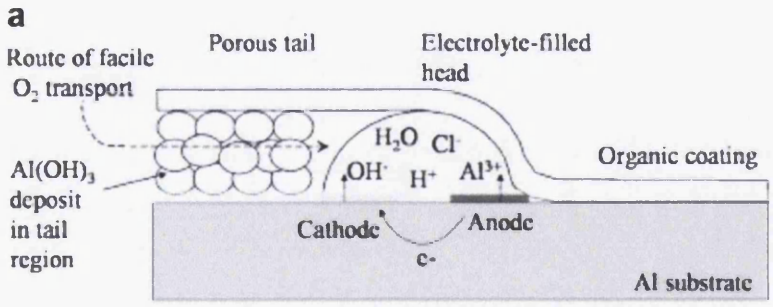


**Figure 1-6:** :Schematic diagram of a filiform corrosion filament on an organically coated aluminium substrate (30).

### 1.7.7 Filiform initiation

The exact mechanism for filiform initiation is still remains unclear. Mechanical prising by osmotic forces, anodic undercutting and cathodic delamination have all been suggested as principal causes (31).

### 1.7.8 Filament propagation

The widely supported mechanism for filament propagation suggests an anodic mechanism for organic coating delamination (32). Following initiation the filiform filament is composed of two discreet parts; a head which acts as an active corrosion cell, and travels over the surface of the metal substrate, and a tail which is the path of inert corrosion product left behind from the head (33).

The filament head is composed of a drop of electrolyte, which contains aggressive salts. The leading and trailing edges of the head are by nature asymmetric due to differential aeration. Oxygen is supplied to the head, via passing through the porous corrosion product in the tail. For this reason, the trailing edge of the head, where it has an interface with the tail has a higher oxygen concentration, and will become strongly cathodic. The leading edge of the filament head is highly anodic, with a typical pH of between 1-4 (34). The underlying metallic substrate is anodically attacked at the leading edge of the head leading to localised anodic coating disbondment or undercutting. During propagation the electrolyte in the head is effectively sealed, and filiform filament can only propagate if the humidity is high enough to effectively "wet" the hygroscopic salts present in the head (26).

## 1.8 Corrosion Inhibition techniques

As has previously been shown, the rate of corrosion, and also the subsequent amount of metal loss relies upon a range of complex processes. Various alterations can be engineered into the metal or alloy to offer significant improvements in corrosion resistance. The composition of the alloy can be varied, or additional alloying elements

can be added to promote the formation of passive surface oxides. This is the reason for chromium additions to iron to make stainless steel. Cathodic protection is also commonly used to inhibit corrosion, by electronically connecting, or by coating the underlying base metal with a more anodic sacrificial metal. In this case the underlying metal will preferentially become the site for the cathodic reduction reaction, and not undergo any metal loss. However the rate of metal loss at the anodic reaction will be increased, unless the anodic metal is also protected by either an oxide film, or an organic coating or both.

### 1.8.1 Pourbaix diagrams

Pourbaix diagrams are a plot of oxidation reduction potentials as a function of solution pH (5). Oxidizing conditions are portrayed by the upper section of the diagram where there are high positive electrode potentials. Reducing conditions are portrayed by the lower section of the diagram where the low negative potentials are shown. Electrode potentials are quantified on the Y axis, pH is displayed by the x axis. Acidic solutions are shown to the left hand side of the diagram, and alkaline solutions are displayed to the right. The diagram shows what corrosion products will be formed under a certain electrode potential at a certain pH. For example on iron, potentials more positive than -0.6, and pH values above 9, ferrous iron is the formed reaction product. At potentials of less than -0.6V iron will be passive. At high potentials iron will form $Fe^{3+}$ which forms a continuous corrosion product, which will act as a physical barrier for species in the electrolyte to interact with the iron surface, therefore reducing corrosion rates (35). The objective of anodic or cathodic corrosion protection techniques, applied either through an impressed current, or impressing a current due to galvanic potentials, is to change the electrode potential of the iron. Cathodic corrosion protection techniques reduce the electrode potential of the iron to below the -0.6 V level, so that even exposed iron will not corrode. Anodic corrosion protection techniques will increase the potential of the iron to above 0.8, so that a protective continuous surface oxide forms on any exposed iron surface, inhibiting corrosion (5). An example of a pourbaix diagram for iron is shown in figure 1.7.

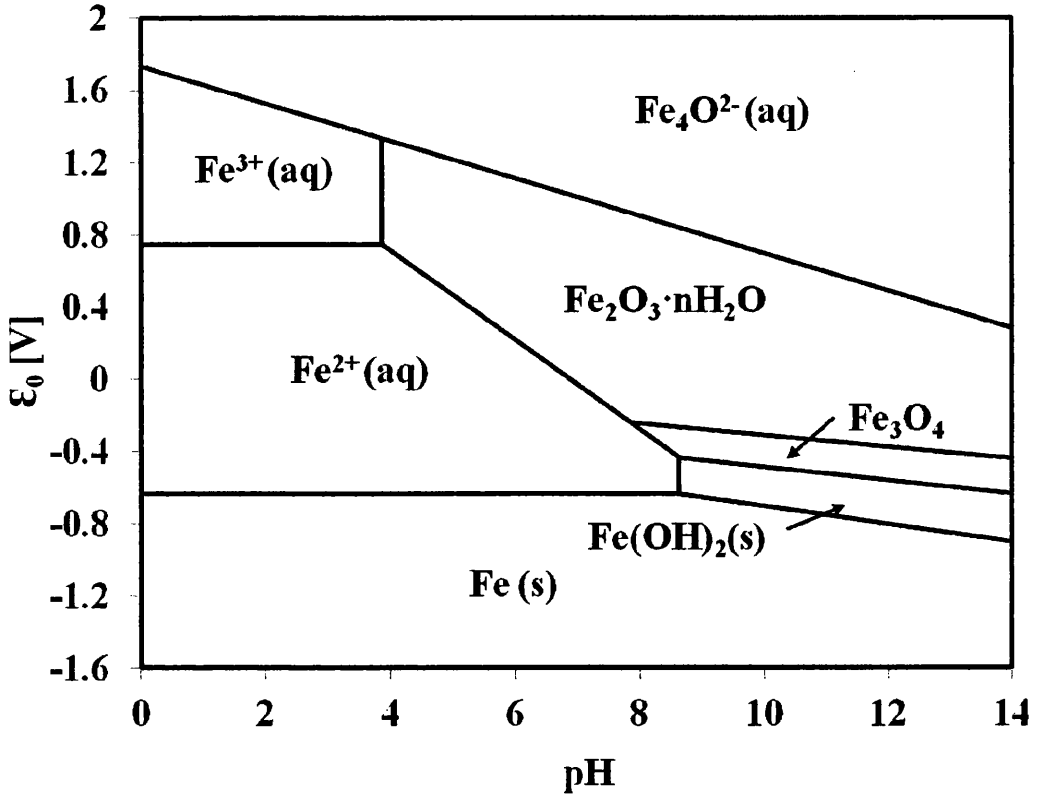


**Figure 1-7 :** Simplified potential vs pH (pourbaix) diagram for iron in an aqueous environment. This diagram can be used to predict the form of oxide that will form on iron at a given pH value

### 1.8.2 Cathodic Protection

In a similar manner to protecting a steel ship with anodic blocks, steel can be protected from corrosion by being coated with a layer of a more anodic metal. The main metals which have been used for the protection of sheet steel in this way are zinc, aluminium, manganese and cadmium. As well as offering galvanic protection, these metallic coatings will also act as a physical barrier to inhibit the corrosion of the underlying steel. In order to reduce the rate of anodic dissolution of the anodic coating as much as possible, coating alloys will often be formulated so that they form stable continuous oxides, which will therefore protect the coating. Therefore the three main ways in which these coatings offer protection to the steel are:

- By acting as a barrier coating
- Secondary barrier action by the formation of a corrosion product layer (stable oxide)
- Galvanic protection with the coating acting as a sacrificial anode.

Sacrificial metal coatings are characterized by their galvanic action. When the underlying metal is exposed to the atmosphere at a cut edge, the underlying metal will become polarized cathodically in relation to the anodic coating metal. As a result of this the underlying metal may be passive. Furthermore the surrounding anodic coating will corrode around exposed areas of the underlying steel substrate, potentially coating the substrate with corrosion product from the anodic coating. This corrosion product will act as a physical barrier and inhibit future corrosion, effectively plugging the defect (36).

Sacrificial metal coatings protect the underlying metal against corrosion via two mechanisms. Firstly the sacrificial coating acts as a barrier coating, and secondly via galvanic protection. The sacrificial coating is self-protected from rapid corrosion by the formation of a surface oxide layer. The main form of long term protection for the whole coating system is this stable oxide layer, as without it, the sacrificial coating would undergo rapid anodic dissolution, leaving the underlying metal exposed. As a result of this the metals and alloys that are often chosen to be used as sacrificial coatings are chosen, not just because of their galvanic properties, but also because they form a stable protective oxide layer.

Aluminium is commonly used as a coating system as it is highly anodic, and as has been discussed previously. Aluminium also instantaneously forms a stable, continuous protective oxide, which renders the underlying aluminium coating passive. An advantage of protection by an oxide films is that if this film gets damaged, a new film will form, effectively "healing" the oxide barrier coating. Zinc is the most commonly used coating material to protect steel. The reasons for this are that it is highly anodic in the galvanic series in relation to iron, so offers high levels of galvanic protection, it has a relatively low melting temperature (*420°c compared to 660°c for aluminium*) so processing costs for hot dip lines are competitive, and it is priced well in comparison to other possible elements. Zinc coated steel products are also highly

workable and weld-able for potential future processes. Zinc oxide is not as insoluble, or passive as aluminium oxide, and therefore it is considered to offer a lower level of corrosion resistance. For this reason higher performance cathodic protection systems are based on zinc aluminium alloys, as these incorporate some of the economic advantages of zinc, with the stability of an aluminium oxide protective film (37) (38).

Zinc also offers high levels of corrosion resistance due to having a large cathodic over potential(5) The cathodic over potential is the potential difference between the cathodes thermodynamically determined reduction potential, and the potential at which a REDOX reaction is experimentally observed. The reason this over potential occurs is due to inefficiencies in electron transfer at the cathodic site. At the cathodic site, an electron has to transfer from the solid metal, to a compound or ion in solution. For this to occur, a driving force is required, and the magnitude of this driving force that is required is quantified as the cathodic over potential. Zinc having a large cathodic over potential, means that a large voltage is required for the electron transfer reaction to take place, and the result of this is that zinc is inefficient at supporting a cathodic reaction. The result of this is that the overall corrosion rate of pure zinc is low, as the cathodic reaction is highly inefficient. Some elements have very low cathodic over potentials such as iron, copper and carbon, and these elements are therefore highly efficient at supporting a cathodic reaction (39)

## 1.9 Galvanized Steel

Protecting steel with zinc and zinc alloy coatings is commercially one of the most important and wide spread techniques used to protect steel against corrosion. Zinc coatings protect the steel from corrosion by two main methods, firstly acting as a barrier coating, and secondly by galvanic protection. In barrier protection, the zinc coating simply acts as a physical barrier between corrosive species in the environment and the underlying steel substrate. During galvanic protection, the zinc is less noble than the iron, and will therefore sacrificially corrode to protect the steel substrate. Galvanic protection is effective in areas where the underlying steel is exposed, such

as cut edges and defects (40). Zinc and zinc alloy coatings are most commonly applied to steel either through hot dip coating, or electro deposition. The scope of this thesis will be limited to hot dip coated steel.

### 1.9.1 Introduction to Hot Dip galvanizing

Hot dip galvanizing, the immersion of a steel substrate in a molten bath of zinc or zinc alloy, can be a batch or continuous process. Zinc is commonly used because it offers a high level of sacrificial protection to the steel, along with a relatively low melting point. Batch processing is most commonly used for components, whilst a continuous process is used for sheet steel (41). Hot dip coatings are composed of two main regions, the main bulk of the coating known as the overlay, and the intermetallic layer at the zinc / steel interface. Both of these regions are affected by coating composition, bath time, bath temperature, cooling rates and substrate composition (40).

### 1.9.2 Hot dip galvanizing process

The most commonly used commercial method for hot dip galvanizing, is the Sendzimir hot line process, although the Cook-Norteman cold line process is also used for batch hot dipping, and some continuous processes. During both processes continuous cold rolled welded steel sheets can be coated at a rate of up to 200m/min. The first stage is an alkali cleaning stage, followed by an electrolytic cleaning stage. The steel then passes through a drying furnace. Oxides are removed by reduction, either in a reduction furnace followed by a gas cooling stage as in the Sendzimir process, or by chemical fluxing in the Cook-Norteman process. After oxide removal the sample is hot dipped. After hot dipping, the coating weight, and cooling rates of the coating are controlled by air knives, and finally the coating is cooled, sometimes via a heat treatment (42).

#### 1.9.2.1 Alkali Cleaning

Initially the cold rolled sheet steel strip goes through an alkali cleaning process in which rolling oils, surface contaminants, surface carbon and iron fines are removed from the steel surface. This is done by immersing, or spraying the strip with a 1.5 – 2.5% sodium hydroxide solution, and followed by a rinsing stage (40).

#### 1.9.2.2 Electrolytic cleaning

In the electrolytic cleaning stage contaminants which are tightly adhered to the strip are removed. This is done by passing a current through the strip whilst it is immersed in water. This hydrolizes the water, to form hydrogen and oxygen bubbles on the surface. This bubbling action of the surface of the strip removes contaminants from the surface. Some hot dip processes rely entirely on alkali cleaning, and do not use electrolytic cleaning.

#### 1.9.2.3 Drying

The clean strip is dried using a high volume, low pressure air blower. This is used as it removes moisture, yet prevents oxidation.

#### 1.9.2.4 Oxide removal

Oxide removal is carried out in a reducing furnace during the Sendzimir process,
During the cold rolling process, the surface of the sheet steel is spontaneously oxidized to form a layer of iron oxide, and iron hydroxide. This layer must be removed, to ensure good adhesion between the hot dip coating, and the surface of the steel. In order to do this, the surface oxide is reduced by heating the steel in a $N_2/H_2$ atmosphere to a temperature of 500-760°c (40). Surface oxides are reduced using the processes shown in equations 1.6 and 1.7. This process will also reduce any residual organic surface contaminants.

$$Fe_3O_4 + 4H_2 \rightarrow ZnCl_2 + ZnO \quad (1.6)$$

$$FeO + H_2 \rightarrow Fe + H_2O \quad (1.7)$$

Chemical fluxing is used to remove this oxide layer in the Cook-Norteman cold line process. Chemical fluxing is an important stage for adhesion properties of the hot dip coating, as it removes surface oxides, so that the coating can adhere to the metal substrate, and not the substrates oxide layer. On a steel substrate the most common chemical flux is hydrochloric acid. This removes the oxide layer by the process shown in equation 1.8.

$$FeO + 2HCl \rightarrow Fe + H_2O + 2Cl \quad (1.8)$$

As a general rule a chemical flux bath is most commonly used in batch processes, as components can be submersed in HCl, and then submersed in a hot dip melt bath. However it is still used commercially for some continuous sheet steel processes as well. (43)

#### 1.9.2.5 Cooling and hot dipping

After passing through the reducing furnace, the steel sheet is cooled to the approximate temperature of the hot dip bath. A small amount of under cooling can be induced on the strip to increase nucleation rates. Typical bath temperatures for a conventional zinc hot dip coating (Zn +Al (0.1wt%) are in the region of 450-490°c (44). During the hot dip process, as soon as the steel substrate is immersed in the melt bath, a chemical reaction will occur at the interface between the melt bath, and the steel surface metal. This reaction will largely depend on the chemistry of the melt bath and substrate, the amount of time the substrate is in the melt bath, and the difference in temperature between the substrate and melt bath. Diffusion, and chemical interactions between the sheet steel substrate and melt alloy in the hot dip bath, cause the formation of intermetallic phases on the surface of the substrate (45). The least desirable intermetallic phases are Zn-Fe intermetallic which may form at the steel, coating interface. The addition of aluminium to the hot dip coating alloy will repress the formation on Zn-Fe intermetallic, preferentially promoting the formation of $Fe_2(Al,Zn)_5$. This will result in a more formable metal coating interface. For this reason practically all zinc coatings contain at least low level additions (<0.15wt%) of

aluminium. This is discussed in greater detail by Marder (40). When the steel substrate leaves the hot dip bath, it will pass through a pair of air knives. These are two air jets that cool the hot dip coating causing it to solidify. They also remove any excess coating ensuring a consistent and controlled coating thickness[9].

### 1.9.3 Hot dip galvanized coating compositions

Commercially the addition of aluminium to the zinc bath results in three main types of coating, Galvatite (0.15wt% Al), Galfan (5wt% Al) and Galvalume(55wt% Al). A 4$^{th}$ type of coating will be studied in this thesis which contains an alloy of zinc, aluminium and magnesium. Galvalume is typically used for high temperature applications, such as car exhausts, but due to it having a significantly higher aluminium content than other coatings, it will not be further discussed in this thesis.

#### 1.9.3.1 Galvatite

Galvatite coatings, also referred to as conventional hot dip coatings, and HDG are composed of zinc and low level additions of aluminium (<0.15wt%). Galvatite coatings are often used as the bench mark coating, which other coatings are compared to (40).

#### 1.9.3.2 Galfan

Galfan is a hot dip coating composed of a zinc alloy, with a composition of Zn + Al(4.5wt%). This is the composition of the eutectic point on the Zn-Al binary phase diagram. Due to the high cooling rates found on hot dip coating lines, non-equilibrium phases form and therefore Galfan does not have an entirely eutectic structure. Galfan has a two part microstructure, composing of a primary zinc dendritic phase, and a Zn-Al lamella eutectic phase. The coarseness, and resultant lamella spacing of this eutectic is dependant upon the cooling rates during solidification (46).

Galfan has increased formability over Galvatite, which is ascribed to the increased ductility found in the eutectic structure. Galfan also has increased corrosion resistance, and cut edge protection when compared to Galvatite. This is due to the formation of an adherent aluminium oxide surface layer.

## 1.10 Zn-Al-Mg hot dip galvanized coatings

### 1.10.1 Evolution of Zinc based hot dip coatings

As previously mentioned hot dip galvanized coatings have traditionally consisted primarily of zinc, with small additions of aluminium and in some cases silicon. In the last two decades there have been environmental and economic pressures requiring a new generation of hot dip coatings, which will not rely on chromium containing pre-treatments to inhibit cathodic disbondment. As a result of this over the past 35 years a significant body of research has been carried out improving the corrosion resistance of hot dip coated steel by increasing the alloying additions of aluminium and magnesium.

The corrosion resistance of hot dip coatings can be improved by increasing the alloying addition levels of aluminium. Good examples of these coatings are Galfan Zn+Al(5wt%) and Galvalume Al(55wt%)+Zn(43.5wt%)+Si(1.5wt%). These coatings offer increased levels of corrosion resistance in relation pure zinc, because they combine the sacrificial protection of zinc, and a long lasting physical barrier of aluminium oxide.

Ternary coatings containing zinc, aluminium and magnesium (Zn-Al-Mg coatings) have also been developed. The commercial compositions for these hot dip coatings are in the range of 1-11wt% aluminium and 1-6wt% Magnesium and the remaining part of the coating been zinc (47, 48).

| Manufacturer | Product Name | Coating composition |
|---|---|---|
| Tata | Magizinc | Zn + Al*(1.5wt%)* + Mg*(1.5wt%)* |
| Arcelormittal | Magnelis | Zn + Al*(3.5wt%)* + Mg*(3wt%)* |
| Nippon Steel | Super Dyma | Zn + Al*(11wt%)* + Mg*(3wt%)* + Si*(0.2wt%)* |
| Nippon Steel | Super Zinc | Zn + Al*(4.5wt%)* + Mg*(0.1wt%)* |
| Nippon Steel | Dyma Zinc | Zn + Al*(0.2wt%)* + Mg*(0.5wt%)* |
| Nisshin Steel | ZAM | Zn + Al *(6wt%)* + Mg *(3wt%)* |
| Thyssenkrupp | Zn-ecoprotect | Zn + Al *(1wt%)* + Mg *(1wt%)* |

**Table 1-3** : Table of commercially produced Zn-Al-Mg hot dip galvanised steel coatings

The earliest commercial ternary Zn-Al-Mg coatings were developed by Nippon steel in 1984, and known as Super Zinc. Super Zinc (Zn + 4.5wt% Al + 0.1wt%Mg) has a composition that is similar to that of Galfan, with a small magnesium addition at 0.1wt% (49). ZAM (Zn+Al*(6wt%)*+Mg*(3wt%)*) and Super Dyma (Zn+Al*(11wt%)*+Mg*(3wt%)*+Si*(0.2wt%)*) can be considered one of the first true ternary systems. These alloys were commercialized in the late 1990's by Nishin steel for highly corrosive architectural environments (50).

At the same time European steel makers were developing lower alloyed Zn–Al–Mg hot-dip-coated steel products, typically in the Al*(1-3wt%)* and Mg*(1-3wt%)* range (51) (52). Zn-Mg coatings are also been developed using physical vapour deposition (PVD), with the aim of increasing ductility for the automotive sector over Zn+Al+Mg hot dip coatings (53). PVD coatings are produced by sputtering a thin layer of magnesium on to a hot dip zinc, or electroplated zinc coating, and then heat treating the resultant coating to diffuse the magnesium and zinc and improve adhesion (50). Some Zn-Mg hot dip coatings have also been produced, however due to magnesium's high affinity for oxygen, there are issues with large amounts of dross formations in the hot dip melt bath. One of the reasons for the addition of aluminium is that is reduces this dross formation, and therefore creates a much more stable melt bath (54). As a result of this most commercial hot dip Zn+Al+Mg hot dip coatings contain at least equal amounts of aluminium and magnesium, and usually an excess of aluminium.

### 1.10.2 Zinc Magnesium PVD coatings

The addition of magnesium to sacrificial zinc coatings on a steel substrate has been shown to significantly increase corrosion resistance. In the literature most zinc-magnesium alloy coatings are made by depositing a thin layer of magnesium using physical vapour deposition (PVD) onto a hot dip zinc or electroplated zinc substrate. The zinc-magnesium coating is then formed through diffusion by heating the sample to a temperature of 250°c for a period of time. This allows the magnesium to diffuse in to the zinc (55). The reason zinc-magnesium coatings are not usually made using a hot dip process is because the magnesium in the hot dip bath will rapidly oxidise. M.Duttsa *et al* (54) did make Zn-Mg hot dip coatings Zn+Mg(2.5wt%), however there were significant issues with the large amount of dross formation on the surface of the hot dip bath, due to the magnesium oxidising. Production of Zn+Mg coatings by hot dipping can be achieved via the addition of aluminium to the molten metal pot to avoid dross formation, and therefore improve the quality of the coating (47). Without the addition of higher levels of aluminium significant amounts of Zn-Fe intermetallics will form at the steel-coating interface, these are detrimental for the adhesion of the coating. The addition of an excess of aluminium reduces the level of the Zn-Fe intermetallic (47).

#### 1.10.2.1 Morphology of PVD Zn-Mg coatings

PVD coatings are composed of a layer of magnesium which has been deposited on a layer of zinc. The coating is then heat treated at >250°c for a period of time to allow diffusion of the magnesium and zinc. The magnesium and zinc will also chemically bond to form intermetallic phases. The main intermetallic phases that are formed after heat treatment are $MgZn_2$ and $Mg_2Zn_{11}$ (22). The equilibrium phase diagram for zinc and magnesium is shown in figure 1-8. However it must be noted that the phases present on hot dip coatings may not correlate to this diagram as a result of high cooling rates meaning non equilibrium phase's form.

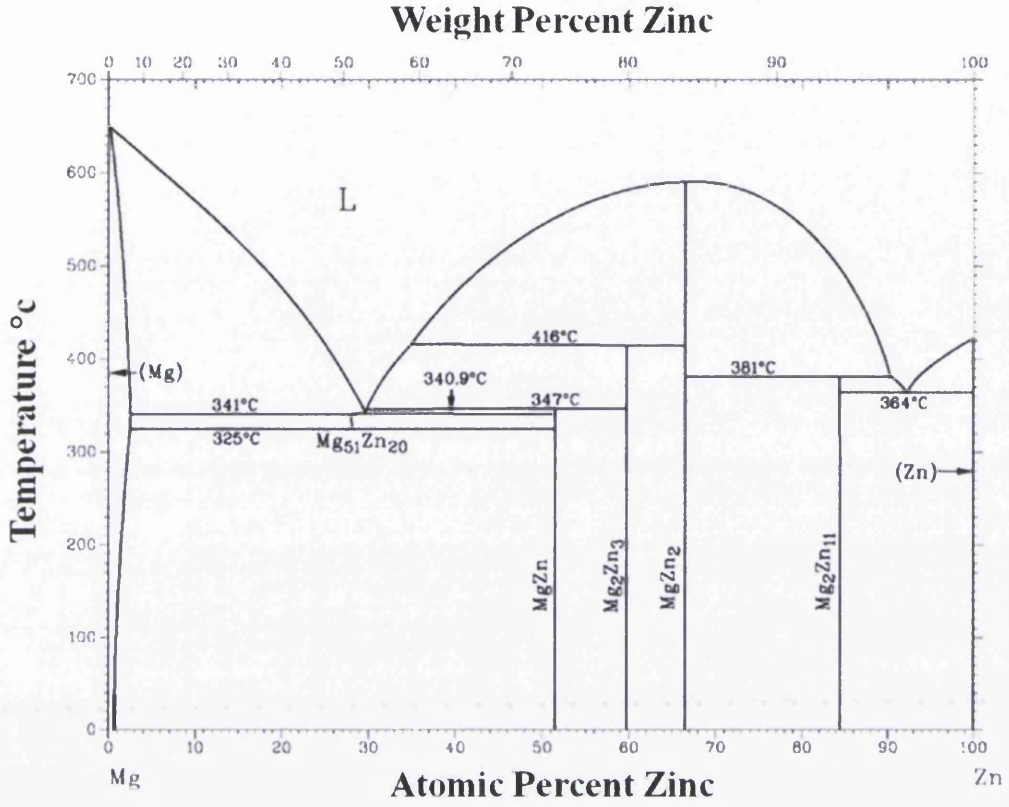


**Figure 1-8** : Binary phase diagram for zinc and magnesium showing the equilibrium phases that will be preferentially formed at a range of compositions (23)

XRD analysis carried out by Kawafuku *et al* (56) and Morishita *et al* (57) has shown these PVD Zn-Mg coatings to be composed of two layers. The upper surface layer is composed of $MgZn_2$. This is shown in the schematic diagram in figure 1-9. This is the equilibrium phase when 8-16wt% magnesium is present. The surface will be enriched in magnesium as this is where the magnesium is deposited during the PVD process. The remainder of the underlying coating has a lower concentration of magnesium and is composed of $Mg_2Zn_{11}$ intermetallic. The thickness of each layer will depend on the levels of diffusion that have occurred, and therefore the heat treatment process, along with the amount of magnesium deposited on to the surface. Variables such as temperature, and annealing time will have an effect on the diffusion of magnesium in the coating (58)

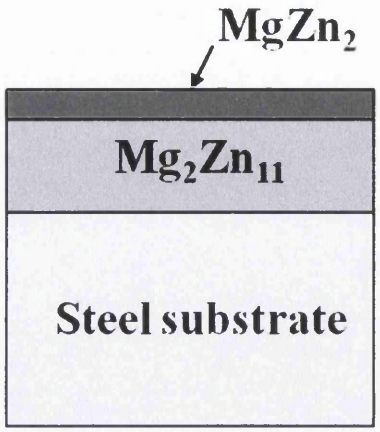


**Figure 1-9 :** Cross sectional schematic illustration showing the structure of a PVD Zn-Mg steel coating. PVD is deposited on top of a zinc layer on hot dip coated steel and then thermally diffused to form a thick layer of $Mg_2Zn_{11}$ and a thin surface layer of $MgZn_2$.

### 1.10.2.2 Morphology of hot dip Zn-Mg-Al coatings

Various studies have characterized the composition and phases found in Zn-Al-Mg hot dip coatings. Dutta *et al* (47) studied a range of Zn-Al-Mg hot dip compositions using EDX and XPS. At a composition of Mg 2.5wt% and Al 0.01wt% the only intermetallic phase present was $MgZn_2$. Schuerz *et al* (48) studied coatings with a composition of Mg 2wt% and Al 2wt% and found that microstructure consisted of a primary zinc phase, containing very little magnesium or aluminium, a binary eutectic composed of zinc and non-equilibrium $MgZn_2$ intermetallic, and a ternary eutectic phase composed of zinc, aluminium and $MgZn_2$. They also reported some equilibrium $Mg_2Zn_{11}$. Prosek *et al* (50) studied hot dip Zn-Al-Mg coatings with a composition range of Mg 1-2wt% and Al 1-2wt% and found the only intermetallic phase present to be $MgZn_2$. An SEM micrograph showing the visual appearance of a cross section of ZnMg(1.5wt%)Al(1.5wt%) hot dip coating is shown in figure 1-10.

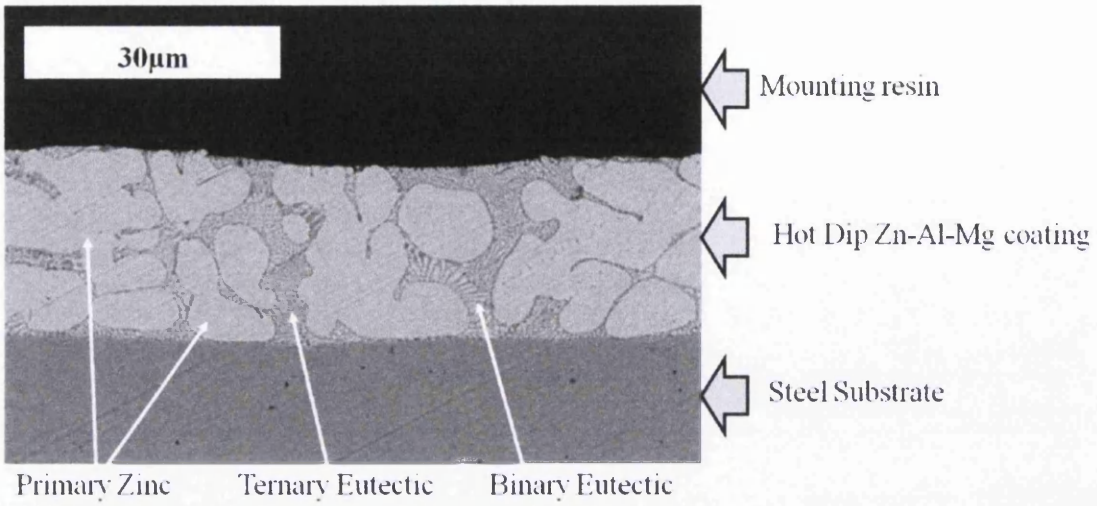


**Figure 1-10** : SEM Micrograph of a resin mounted Zn-Al(1.5wt%)-Mg(1.5wt%) hot dip coating on a steel substrate. The steel substrate is shown towards the bottom of the image and the black region at the top is the mounting resin. Microstructural phases of primary zinc, binary and ternary eutectic are visible and labelled.

### 1.10.3 Corrosion resistance of Zn-Mg and Zn-Al-Mg coatings

There are many examples in the literature of Zn-Mg and Zn-Mg-Al coatings showing an increase in corrosion resistance in chloride salt spray tests when compared to conventional hot dup zinc coatings. Vlot *et al* (58) studied Zn-Al-Mg hot dip coatings with a composition of Zn+Al*(1.5-2wt%)*+Mg*(1.5-2wt%)*. The time to red rust in salt spray tests was increased by 20 times when compared to conventional hot dip zinc coatings, Zn+Al*(0.2wt%)* of a similar coating thickness. Similar results have been shown on Zn-Mg coatings. Koll *et al* (59) tested hot dip zinc coatings with a layer of magnesium deposited on to the surface by PVD. After thermal diffusion these coatings were shown to contain mostly $MgZn_2$ intermetallic along with some $Mg_2Zn_{11}$. The time red rust was tested in a humidity-salt spray cyclic corrosion test. Compared to a similar thickness conventional hot dip zinc coating the time to red rust was delayed by a factor of 8-13 times (59). In a similar study Similar to Koll, Schwerdt *et al* (60) produced PVD coatings, but, this time on electroplated zinc rather that hot dip galvanised zinc coatings. When characterized the total coating thickness was 7.5µm, with $MgZn_2$ making up a surface layer approximately 0.8-1.6 µm thick. During salt spray tests the corrosion resistance of the coating containing magnesium, showed an

improvement in time to red rust by a factor of 10 compared to the electroplated steel without the magnesium layer (60).

Furthermore hausbrand *et al* (61) have demonstrated that the corrosion resistance of zinc can be enhanced by adding magnesium to the electrolyte. Magnesium chloride was added to a salt solution in the proportion 0.1mol/L $MgCl_2$ in 0.5mol/L NaCl. Galvanized sheet steel was immersed in the magnesium containing salt solution at 40°c. After a period of 4 days there was almost no corrosion on the material surface. Immersion of galvanised sheet steel in 0.5mol/l NaCl solution without magnesium under the same conditions would result in "severe" corrosive attack (59).

The exact mechanism in which magnesium improves the corrosion resistance of sacrificial zinc coatings is still open to some debate in the literature. Kawafuku et al (56) propose that the superior corrosion resistance of zinc-magnesium coatings is due to the formation of a dense adherent layer of an insoluble compound known as simonkolleite ($Zn_5(OH)_8Cl_2.H2O$. Simonkolleite acts as a barrier coating to inhibit further corrosion. Using XRD simonkolleite was detected on the surface along with zinc oxide (ZnO). It is suggested that the improvement in corrosion resistance is due to the formation of simonkolleite alone, and irrespective of zinc oxide (ZnO). Other studies back up this proposal. Tsujimura *et al* (62) also used XRD to study corrosion products on Zn-Al-Mg hot dip coatings. This time on a hot dip coating with a composition of Zn+Al*(6wt%)*+Mg*(3wt%)*, the only corrosion product found was simonkolleite after immersion testing in 5%NaCl. On samples with the composition Zn+Al*(4.5wt%)*+Mg*(0.1wt%)* tested in the same conditions the main corrosion product again was simonkolleite. However zinc oxide and zinc hydroxide carbonate were also found. The authors proposed magnesium enhanced corrosion resistance of hot dip zinc coated steel due to the formation of simonkolleite.

Prosek *et al* (50) did a systematic study of zinc-magnesium alloys to try and gain an understanding of the corrosion products and oxide layers that form. On un-corroded zinc the surface was shown to be coated in a thin layer of zinc oxide. However on alloys containing as little as Mg*(2wt%)* this layer was almost completely substituted with a layer of magnesium oxide. Due to magnesium's high affinity with oxygen, this oxide film forms rapidly, and is much thicker than the zinc oxide film

found on pure zinc. For example a zinc oxide film is typically 3nm thick, whilst magnesium oxide films on a Zn-Mg(8wt%) alloy were found to be 25nm thick.

The corrosion products that are formed on the surface of zinc magnesium alloys containing primary zinc, $Mg_2Zn_{11}$ and $MgZn_2$ intermetallic have been studied in the literature using Fourier transform infrared spectroscopy (FTIR). The samples were corroded in an aqueous sodium chloride (NaCl) environment. The dominant corrosion products were found to be hydrozincite ($Zn_5(OH)_6(CO_3)_2$ and simonkolleite ($Zn_5(OH)_8Cl_2 \cdot H_2O$). A range of coating compositions were tested from Zn(99wt%) + Mg(1wt%) to Zn(92wt%) + Mg(8wt%) with very little difference in the composition of corrosion product observed. It is proposed by the authors that magnesium ions in magnesium oxide can rapidly react with hydroxide ions at the cathode, effectively neutralising them. This then will allow insoluble simonkolleite to form over the entire corroding surface. Simonkolleite is highly insoluble, and therefore acts as a barrier for further corrosion to occur (63).

The corrosion process found on Zn-Al-Mg hot dip coatings and Zn-Mg PVD coatings differ significantly. On Zn-Mg PVD coatings the surface is uniform $MgZn_2$, and most studies report that the only surface layer that is found is simonkolleite. As a result of this the corrosion inhibition mechanism seems to be that the magnesium oxide liberates magnesium cations which contribute to the formation of homogenous simonkolleite by neutralising hydroxyl ions. Significant amounts of $Na^+$ is also absorbed in the oxide layer, which may increase the concentration of $Cl^-$ in hydrated films on the surface, again improving conditions for simonkolleite formation.

As previously discussed the microstructure of Zn-Al-Mg hot dipped steel is composed of various different phases. S.Schuerz *et al* (48) have shown that anodic dissolution initiates in the $MgZn_2$ phase. $MgZn_2$ that is present at the surface of the Zn-Al-Mg coating is initially rapidly removed, potentially exposing the underlying steel substrate. During this phase of corrosion the zinc dendrites remain intact. The reason for this preferential attack is most likely due to $MgZn_2$ been less noble in comparison to zinc, and it is therefore corroded preferentially.

Initially when Zn-Al-Mg coatings are exposed to NaCl a layer approximately 1μm thick containing zinc, oxygen and remarkable amounts of aluminium and magnesium forms on the surface. After further corrosion dark regions start to appear

on the surface. At these regions the former Zn-Al-Mg coating has totally transformed to form a dark grey oxide layer. No red rust is seen in these areas, and only low levels of white rust are observed. The thickness of this oxide layer corresponds to the original thickness of the Zn-Al-Mg coating. After time the entire coating will become much darker, due to the entire coating transforming to this oxide layer. Using EDX this dark oxide layer has been shown to be depleted in zinc, and to have a higher aluminium content than the underlying alloy. There is also a second surface corrosion layer which has been shown to contain small amounts of chlorine. This indicates the presence of simonkolleite on the surface of the aluminium rich oxide layer. Over time this simonkolleite layer increased in thickness. After formation the aluminium rich oxide layer appears to shown no change over time meaning that it is very stable against corrosive media. The main form of protection for the underlying steel substrate is therefore aluminium rich oxide layer. However this oxide layer is also protected by a thin layer of simonkolleite. It's hypothesised that this synergistic effect of aluminium and magnesium promoting the formation of an insoluble simonkolleite over a passive aluminium oxide layer that allows Zn-Al-Mg coatings to offer such improvements in corrosion resistance.

### 1.10.4 Corrosion of painted Zn-Al-Mg coatings

The majority of hot dip coatings are organically coated in their final application. The knowledge in the open literature with regards to corrosion mechanisms specific to painted zinc-magnesium coated steel is minimal. Hausbrand and Stratman *et al* [35] reported that the corrosion resistance of organically coated $MgZn_2$, one of the main intermetallics found in Zn-Mg and Zn-Al-Mg coatings is very high when compared to zinc. The improvement in corrosion resistance can be attributed to the complete inhibition of cathodic delamination. Hausbrand and Stratman (61) actually predict that the potential between a defect and the intact metal oxide / polymer interface will be such that the galvanic coupling needed for cathodic delamination will not be possible (61). The potentials at locations on the coating are ascribed to the oxygen reduction properties of the passive oxides. A defect on Zn-Al-Mg hot dip coated steel will contain mostly zinc oxide, as this will sacrificially corrode and is the main element in the hot dip coating. However the metal oxide / polymer interface on $MgZn_2$ has

been shown to be composed of magnesium hydroxide, which has a potential significantly more negative than the zinc oxide found in the defect. The result of this is that the defect will become cathodic, and the intact coating will be anodic. In this situation cathodic disbondment will not occur, and the expected form of corrosive attack will be of an anodic nature.

Stratmann *et al* (61) also state the nature of the oxides is of high importance. Many metal oxides act as a semiconductor, and therefore the rate of electron transfer will depend on the electron concentration at the surface. The band gap of a compound has a significant role to play in electron transfer efficiency. The band gap is equivalent to the amount of energy required to free an outer shell electron from its orbit about the nucleus to become a mobile charge carrier, Simply put semiconductors with a wide band gap have very poor electron transfer efficiencies, and therefore oxygen reduction rates are expected to be low as they are poor at supporting a cathodic reaction. For this reason these semiconductors are preferable as passive oxides. For example, iron oxide has a band gap of ~2eV, zinc oxide ~3.3eV and magnesium oxide ~7.8eV. Due to magnesium been highly electronegative, and the high band gap of magnesium oxide, the most probably form of disbondment between a coating and a substrate will be anodic.

## 1.11 Corrosion inhibition on organically coated steels

### 1.11.1 Organically coated steels

#### 1.11.1.1 Introduction to organic coated steels

As has been previously mentioned hot dip steels are often coated with an organic coating to improve their corrosion resistance. This coating system usually consists of a pre-treatment, which will contain active corrosion inhibitors, and this pre-treatment directly coats the hot dip coating. This pre-treatment layer is then covered with a topping coat, which acts as a physical barrier for species, includes pigments for cosmetic appearances, and may also contain UV protection (64).

### 1.11.1.2 Production of organic coated steels

Organic coatings can be applied either by spraying, or by dipping the steel in a coating bath. For components with complex geometry electrostatic spraying is commonly used. However for hot dip coated sheet steel the most common method of applying an organic coating is to pass the strip through a coating bath, and then cure the coating in a drying oven. Traditionally the most common corrosion inhibitor that is incorporated into the pre-treatment layer is hexavalent chromium VI. There is legislation been introduced to stop the use of chromium VI in the automotive industry by 2018 in Europe, due to its toxicity, and its carcinogenic effects. This thesis focuses on two potential alternatives for hexavalent chromium, one is an anion exchange clay, and one is a variation of phosphate coatings.

### 1.11.4 Hydrotalcite

Hydrotalcite (HT) is a commercially available white anionic clay. HT is a viable chromium free alternative and is classed as an ion-exchange mineral or so-called "smart-release" pigment, which can be incorporated within an organic polymer binder. It has been known for some time that hydrotalcite ($Mg_6Al_2(OH)_{16}(CO_3 + 4H_20)$ and hydrotalcite like compounds act as effective halogen scavengers in polymer systems, and a halide getters in aqueous solutions (65). Hydrotalcites and calcined hydrotalcites are also known to neutralize aqueous acids (30). The appeal of such systems lies in the ability to release inhibitor species and sequester aggressive ions such as chloride or $H^+$ only when a corrosive aqueous environment is encountered (30). Intelligent release of stored corrosion inhibitor species can be triggered by the presence of aggressive ions, which initiates a subsequent ion-exchange process, or by changes in local pH and/or metal substrate potential. (66) Hydrotalcite has been shown to inhibit filiform corrosion on aluminium alloys (67)

Crystalline hydrotalcite (HT) clays are layered materials, which can either be natural or synthetic, consisting of a lamella of positively charged layers, separated by negatively charged anions (68). A wide range of HT clays exist, with different chemical compositions, or crystallographic properties. However all these types of

clays fall under the title of hydrotalcites or layered double hydroxides (LDH) (69). In this work, the term Hydrotalcite is used to refer to a specific Mg/Al hydroxycarbonate which is known for its ease, and low cost of synthesis. The general formula of this anionic clay is shown in equation 1.9:

$$[M^{2+}_{1-x}M^{3+}_{x}(OH)_2]^{x+}[A^{n-}_{x/n}\cdot yH_20] \quad (1.9)$$

$M^{2+}$ and $M^{3+}$ are divalent and trivalent metal ions respectively. $A^{n-}$ is the interlayer exchangeable anion and x has valance in the range of ca0.25-0.33 (65)

The structure of Hydrotalcite is a layered type lattice structure, consisting of a positively charged brucite cation layer, and a negatively charged exchangeable anion layer. The brucite cation layer is composed of an isomorphous substitution of metal atoms such as $Al^{3+}$ and $Mg^{2+}$ in octahedral positions, which results in these brucite layers becoming positively charged. It is possible to incorporate other cations, provided that they have a higher charge than $Al^{3+}$ and a similar atomic radius (70) Electro neutrality of the HT structure is maintained by the anion layer between these positively charged layers. A large variety of anions can be incorporated in to this interlayer space, although hydrated carbonate is the most common anion ($CO_3^{2-}\cdot 4H_2O$), and the only anion which is used in this thesis. In naturally occurring Hydrotalcite clays carbonate is the preferred anion, with only very few other variations. However synthetic hydrotalcite clays have been made with a wide range of anions, allowing the creation of tailor made exchange clays for a specific reaction (71). Due to the large variety of potential exchange reactions Hydrotalcite clays have found a varied range of industrial applications from medication to increasing the corrosion resistance of metals. (72)

The anions present in the interlayer regions can be easily exchanged, with an anion from an external media, and it is this anion exchange mechanism than enables hydrotalcite reduce the rate of corrosion. The effectiveness in which HT can exchange its anions with an external media depends on the nature of the intercalated and external anion exchange equilibrium. This essentially means the ease in which external anions can fit in to the vacant spaces created form the removal of the original anions present in the HT. Therefore certain anions will exchange with a much higher efficiency than others. Essentially the more similar the anions being exchanged are in size and charge, the easier and more efficient the exchange process will be (73).

These anions can then be exchanged with aggressive anions found within corrosive electrolytes, or to neutralize aqueous acids. Anion exchange is an equilibrium process. However the process can become one way due to the exchanged anions inducing a crystal change in the Hydrotalcite, reducing anionic mobility, or by released anions undergoing further chemical reactions in solution to form gaseous substances which may be released. A schematic diagram showing the structure of a hydrotalcite clay is shown in figure 1-11.

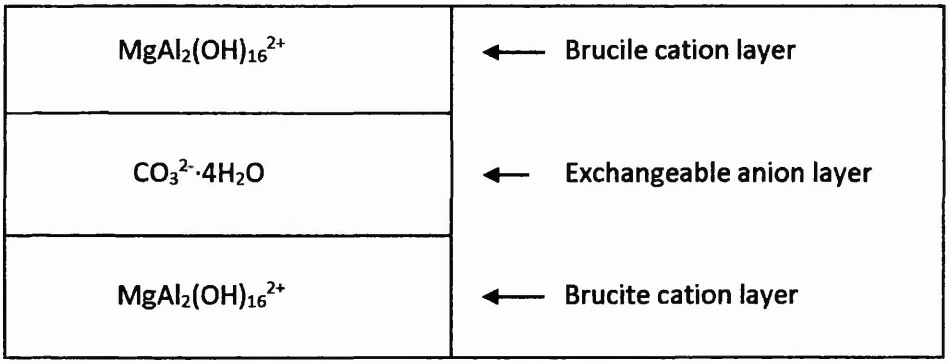


**Figure 1-11** : The layered structure of a hydrotalcite clay, with brucite cation layers sandwiching an exchangeable anion layer in-between.

Hydrotalcite pigments can work as a corrosion inhibitor by rapidly exchanging aggressive anions out of aqueous solution, and substituting these anions for non-aggressive anions.

### 1.11.5 Phosphate

Phosphate has been used to protect metallic surfaces for over 60 years. Phosphate treatments have been used to protect mainly steel and zinc coated steel products, however there are also examples of phosphate treatments on aluminium, magnesium, cadmium and various other metals. The main method of applying phosphate is immersion. During application by immersion, the metal product will firstly be cleaned by immersed in a degreasing bath, typically composed of concentrated acids such as hydrogen chloride and sulphuric acid, or concentrated alkalis such as sodium

hydroxide and potassium hydroxide. Secondly the metal will be immersed in a tank containing a phosphating solution. The amount of time the metal spends in the phosphating tank will have an effect on the thickness of the phosphate later. Phosphating tanks usually contain a variant of phosphoric acid. When a metal is immersed in dilute phosphoric acid, the phosphoric acid will react with the surface of the metal. The reaction between iron and phosphoric acid is shown in equation 1.10.

$$Fe + 2H_3PO_4 \rightarrow Fe(H_2PO_4)_2 + H_2 \quad (1.10)$$

As can be seen in equation 1.10, iron and phosphoric acid react to form iron (III) phosphate and hydrogen gas. The reaction with zinc is shown in equation 1.11, however in this case zinc phosphate and hydrogen gas are formed.

$$3Zn + 2H_3PO_4 \rightarrow Zn_3(PO_4)_2 + 3H_2 \quad (1.11)$$

These phosphates are known as primary phosphates. When primary phosphates are formed phosphoric acid is broken down in to neutral metal phosphates and hydrogen gas (5). The result of this is that there is a reduction in local phosphoric acid concentrations, and therefore an increase in local pH. In a solution, a certain percentage will be unreacted phosphoric acid, and the remainder will be metal phosphate reaction products. The unreacted phosphoric acid is known as free phosphoric acid, and the relationship between the amount of free phosphoric acid and metal phosphate reaction products is known as the acid ratio. Primary phosphates will disassociate readily under neutral and weakly acidic conditions by the equations 1.12, 1.13 and 1.14. M represents a metal.

$$M(H_2PO_4) \leftrightarrow MHPO_4 + H_3PO_4 \quad (1.12)$$

$$3MHPO_4 \leftrightarrow M_3(PO_4)_2 + H_3PO_4 \quad (1.13)$$

$$M_3(PO_4)_2 \leftrightarrow M_3(PO_4)_2 + 4H_3PO_4 \quad (1.14)$$

The reason for this disassociation is that primary metal phosphates which are formed in equations 1.10 and 1.11 are soluble in neutral conditions. Neutral conditions are likely to prevail due to free phosphoric acid consumed by the formation of primary metal phosphates. When this happens the equilibrium changes and metal phosphates can disassociated as is shown in equation 1.12 and 1.13 forming secondary phosphates. These are again soluble in neutral conditions and will go on to form a

ternary free phosphate as shown in equation 1.14. This ternary phosphate is insoluble and will precipitate out on to the metal surface. As a result of this, the acid ratio must be controlled during the formation of phosphate layers, because if the pH is to low primary and secondary phosphates will not be soluble, and the insoluble ternary phosphate will not form. The kinetics of this reaction will also depend on the metallic species that is present. As a general rule zinc phosphate will form more rapidly that iron phosphate.

Another factor in the initiation of the phosphate coating reaction is the presence of suitable sites for the reaction to occur. Colloidal suspensions of fine particles can be added to the phosphating solution. These fine particles act as seed crystals and increase the rate of ternary phosphate formation. These fine particles also increase the number of phosphate crystals, and therefore a coating can be made up of more fine phosphate crystals, which will form a more continuous surface layer. These coatings are smoother, and offer higher levels of corrosion resistance than a coating made of fewer larger particles (74).

#### 1.11.5.1 Accelerators

Most immersion phosphate processes today are "accelerated" so that shorter treatment times, and lower temperatures can be obtained. The most common mode of acceleration is the addition of oxidising agents such as nitrates and hydrogen peroxide. The resultant coatings are smoother and thinner which leads to better aesthetic appearances when they have been painted. Heavy phosphate coatings do not necessarily have increased corrosion resistance than lighter coatings. Finally phosphate coatings must be sealed with an organic coating film, or a layer of oil or grease to offer high levels of corrosion resistance improvements. Porosity of the sealing medium must be kept to a minimum (74)

### 1.11.5.2 In situ phosphating

Phosphating is one of the most widely used pre-treatment process for the surface finishing of metals in order to increase their corrosion resistance. The corrosion protection performance of such finished metals is determined mainly by the quality of the phosphating coating (75). Normally, the metal surface is degreased, rinsed, phosphated, sealed, dried, and finally painted (76) However, multi-stage commercial phosphating processes are error-prone, costly and produce waste products including organic solvents and heavy metals.

Commercial phosphate coatings have a typical porosity of between 0.5%-1.5% of the total substrate surface area (77). As a result of this a subsequent rinsing and sealing procedure, which traditionally utilizes highly toxic hexavalent chromate ($Cr^{6+}$) compounds is critical to the corrosion protective performance of the pre-treated surface (77). If these pores are not quickly sealed, they begin to deteriorate rapidly after the phosphating coatings application. Future legislation is generating a large driving force to reduce waste, and end the use of hexavalent chromate by 2018. For these targets to be met, there will need to be radical changes to current phosphating processes.

### 1.11.5.3 Etch Primers

One potential solution it to use phosphate containing etch primers. Etch primers are primer organic coatings, which contain an acid or alkali, and will chemically react with the surface of the metal. Phenylphosphonic acid is a phosphate containing acid ($H_2PP$), which can be readily dissolved in ethanolic polymers such as Poly Vinyl Butyral (78). When a phenylphosphonic acid containing organic coating is applied to a metal surface, a phosphating process takes place via a reaction with the metal surface. Phenylphosphonic acid will react will react with metals such as magnesium, aluminium and zinc to form insoluble metal phosphonates, which will act as a protective barrier. Furthermore phenylphosphonic acid will also react with the polymer, forming strong covalent bonds of (phosphorous-oxygen-carbon), linking the metal phosphate film and the polymer resin matrix (79). These "simultaneous" reactions provide metal substrates with a corrosion protective barrier without the need

for a chromate or primer finishing step. It might also be possible to eventually eliminate the pre-treatment and/or post-treatment steps and to obtain a coating providing a better adhesion and corrosion inhibition to the substrate (77) (79). This increase in corrosion resistance has been demonstrated by various groups. Specifically is has been observed that the doping of polyaniline coatings, and organoalkoxysilane sol-gel coatings (80) with phenylphosphonic acid significantly reduces the rate of filiform corrosion, and pitting corrosion, on aluminium alloy substrates. Furthermore Coleman *et al* have demonstrated that doping PVB ethanolic primers with phenylphosphonic acid produced up to a 95% reduction in filiform corrosion on aluminium alloys (78) (79).

## 1.12 Conclusion and project aims

Globally many steel companies are developing organically coated Zn-Al-Mg hot dip coatings, due to their improved resistance to cathodic disbondment, and therefore potentially offering a chromium free coating system. The aim of this project is to investigate the anodic corrosion performance of these coatings. A Bennet has previously shown that these coatings are susceptible to filiform corrosion, so this project plans to expand on this and identify which electrolytes can initiate filiform corrosion on organically coated Zn-Al-Mg hot dip coatings, and what the effect of coating composition and thickness is on the corrosion resistance.

Finally corrosion inhibition will be investigated using novel methods such as hydrotalcite and etch primers (phenylphosphonic acid), which will be incorporated with model organic coatings systems. Systematic studies of these inhibitors on Zn-Al-Mg substrates are discussed in this thesis.

# Chapter 2: Experimental Techniques

## 2.1 Filiform corrosion testing

A significant proportion of work carried out during this thesis involves testing filiform corrosion resistance of hot dip Zn+Al+Mg coated steel. All filiform corrosion tests are carried out using the following methodology:

### 2.1.1 Sample preparation

Surface properties, specifically morphology, topography and any surface contamination can have a considerable effect on the filiform corrosion properties of the substrate. Conventional surface preparation techniques, such as sanding and polishing were kept to a minimum for hot dip coated samples, as they would cause a significant reduction in coating thickness and could potentially expose the underlying steel substrate if not carefully controlled or have an effect on the corrosion performance of the material. For all filiform corrosion tests, hot dip coated steel samples are cut in to 5cm square coupons with a guillotine. The surface on which the corrosion test takes place is then abrasively cleaned using an aqueous slurry of 5μm polishing alumina powder and deionised water. The sample is hand polished with this slurry, and a paper towel in a circular motion for approximately two minutes. After polishing the sample is rinsed with deionised water. Following rinsing with deionised water, samples are immersed in hexane, in a beaker placed in an ultrasound tank, to remove any residual organic contamination from the surface. The beaker is placed in an ultrasound bath at a temperature of 20°c for 10 minutes. The sample is then removed from the beaker using Teflon (PTFE) tweezers to avoid contamination of the sample surface. The sample is rinsed with ethanol and allowed to air dry.

### 2.1.2 Organic coating production

Filiform corrosion occurs at the organic coating / metallic interface and therefore requires the sample to be coated with an organic coating. A model clear polyvinylbutyral (PVB) coating is used as a control coating. A model organic coating was used, instead of a commercially available organic coating because the model coating does not contain stabilizers, pigments or other additives which could act as uncontrolled variables, inducing an effect on the corrosion performance of the substrate. Dry PVB is mixed with 15.5% w/w ethanol. Initially the solution is stirred using a glass rod, to promote initial mixing. As the viscosity becomes more homogeneous the PVB ethanolic solution is further stirred with a magnetic stirrer bar, in a sealed glass container to avoid the ethanol from evaporating, for 12 hours, or until it has a completely homogeneous appearance and viscosity. This PVB 15.5 w/w ethanolic solution is then stored for 24 hours before use, to ensure that air bubbles are not trapped in the solution. If the solution is not left to stand these air bubbles may cause defects in the final dry film coating, which can behave as coating holidays. PVB ethanolic solutions must be stored in a sealed container to avoid the ethanol evaporating from the coating, and the viscosity increasing.

### 2.1.3 Coating application

Samples prepared as described in section 2.1.1 have a 5mm wide strip of 50μm thick vinyl tape placed down two parallel sides of the sample. PVB 15.5% w/w ethanolic solution is then rod cast with a glass bar down the sample and allowed to air dry. The dry film thickness for all PVB coatings tested in this thesis is ~30μm, as measured with a micrometer screw gauge. All coatings are allowed to air dry for 24 hours to ensure that the coating has completely cured before any corrosion tests begin.

### 2.1.4 Corrosion initiation and propagation

Filiform corrosion must be initiated along an area where the coating / metal interface is exposed such as a surface defect, cut edge, or coating holiday. For this reason a 10mm long penetrative defect is scribed in to the sample with a scalpel. This defect must penetrate through the organic coating, and hot dip coating to expose the steel substrate. Two defects are scribed on each sample. Corrosion is initiated by injecting

2µl of electrolyte in to each penetrative defect. After initiation the samples are placed in a sealed dessicator, with a relative humidity of 86% and a temperature of 25°c. Relative humidity is controlled with a desiccant (sodium sulphate decahydrate, as a saturated salt solution at the bottom of the dedicator). Temperature is controlled by placing the dedicator in an oven at 22°C measured using a digital thermometer. This temperature was chosen because it is slightly warmer than room temperature, so we could ensure that temperature is controlled, but as low as possible because of the volatility of some initiants. The duration of the filiform experiment is stated in the relevant results sections. The appearance of a coupon and a schematic of a filiform corrosion test coupon are shown in figure 2-1.

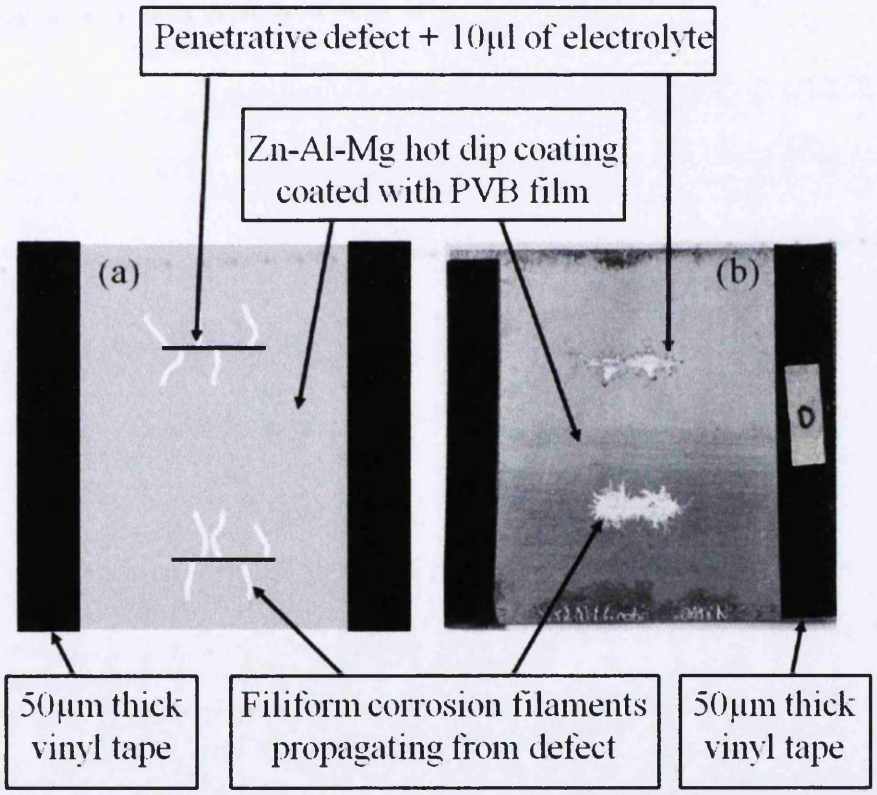


**Figure 2-1** : A schematic diagram of Zn-Al-Mg hot dip coated filiform corrosion test sample **(a)** schematic diagram of a standard test sample **(b)** optical image of a laboratory sample

## 2.2 Microscopy and optical imaging

Samples are imaged using Meiji Techno EMZ-8TRD low magnification optical stereo microscope and an Infinity 1 microscope digital camera.

### 2.2.1 Illumination

Metallic samples are reflective by their nature. Due to this characteristic, having controlled lighting conditions is essential in order to obtain detailed macro images of fine features, such as filiform corrosion filaments. Firstly background light must be minimised, as this will create uncontrolled reflections, so all images are taken in a dark room. The light source for all images is an 11W fluorescent bulb, illuminating a matt black light tube, 30cm long, and 5cm in diameter. This light tube ensures that only a 5cm diameter beam of light is present increasing the signal to noise ratio of the image.

The angle light hits the sample at is known as the angle of incidence. As the sample is reflective, a significant proportion of this light will be reflected off the sample. The angle of incidence is always equal the angle of reflectance on a flat sample, as shown in figure 2-2.

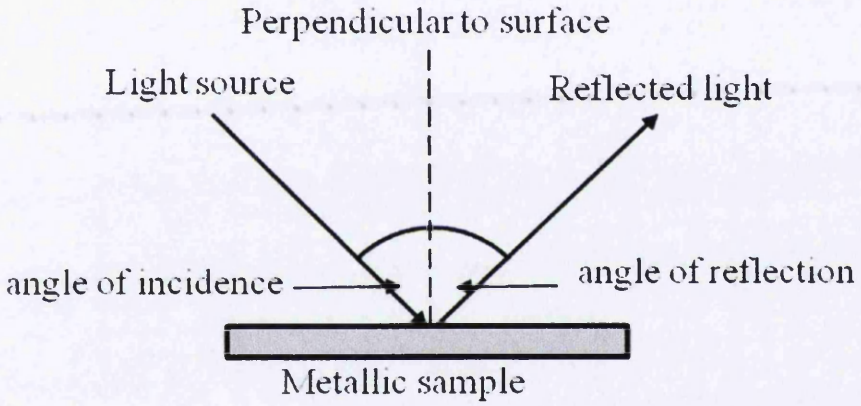


**Figure 2-2 :** Illustration to show the angle of incidence and reflectance on a reflective sample. Imaging should be perpendicular to the surface if it is been used for digital image analysis to remove the effect of distortion. Imaging must also be taken away from the angle of reflectance to minimise glare.

As a result of this, the camera or detector cannot be in the area where reflected light will be projected. The reason for this is that the image will have a lot of light reflected from the sample, saturating the image and reducing optical definition of fine surface features. Therefore the camera / detector is placed perpendicular to the surface of the sample. This is desirable for several reasons. Firstly it minimises glare, secondly features can be directly measured from an image, as there are no perspective issues due to the image been taken at an angle, and thirdly the entire surface of the flat sample is in focus.

The appearance of the reflective surface to the camera / detector will be a reflection of what surrounds the sample. As the main corrosion product (zinc oxide) on zinc based coatings is white, it is desirable to make the reflective surface a darker colour. This is done by placing the photographic set up (*sample, light source, and camera / detector)* in to a black box. When black is reflected of the reflective metal surface in to the detector, this gives the surface a darker appearance, improving the contrast between the reflective surface and the white corrosion product. For digital image analysis maximum contrast is essential to generate accurate measurements and clearly define corrosion features.

### 2.2.2 Camera and lighting setup

As images are to be used for digital image analysis, all images are taken under control conditions to ensure consistency and reproducibility when quantified. Images are taken on a Miji Techno EMZ-8TRD stereo microscope with an infinity 1 digital camera add on. The pixel image size is 2048 x 1536 pixels. The physical camera settings are, working distance 10.5cm, magnification 0.7 (minimum magnification) and the angle of incidence of light is 60 degrees. All images are taken with a dark background to ensure maximum contrast between the reflective intact metal surface, and white corrosion product.

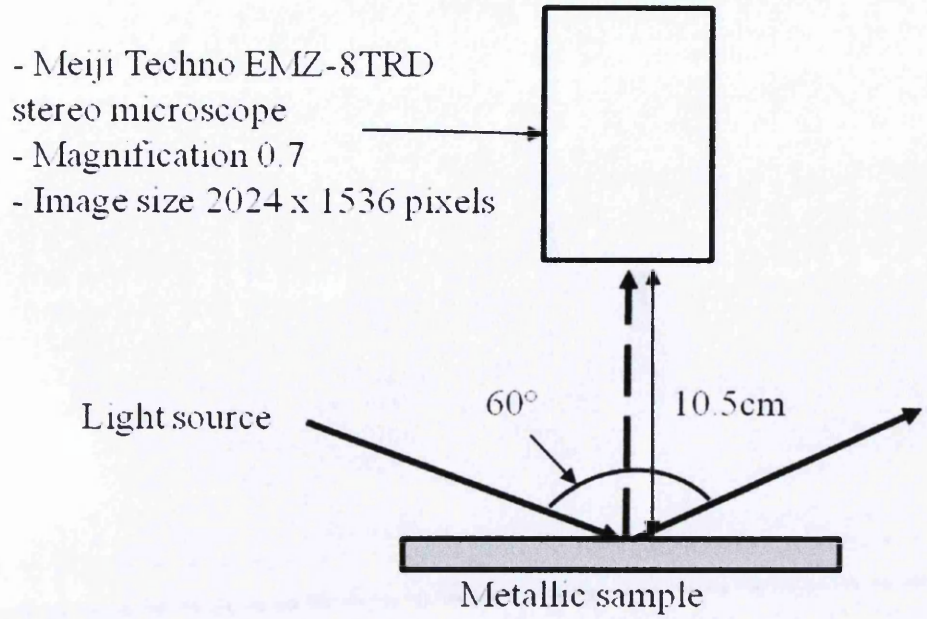


**Figure 2.-3** Schematic diagram showing the optical digital camera set up used for digital image analysis

## 2.3 Sigma Scan Pro, digital image analysis

The fractional area of the sample that is corroded is measured using digital image analysis software. Sigma scan pro 5 is an automated image analysis program that enables data on images such as surface area, or the number of features to be quantified.

### 2.3.1 Surface area measurement

In order to measure the percentage of the surface which has been subjected to corrosion there must be a contrast between the corrosion product and back ground metal. Images are then converted to a grey scale and areas lighter than input x are measured. The area to be analysed must then be selected around the image. In order to make direct comparisons between images it is imperative that the digital image was taken under control conditions as explained in section 2.2. When the image is opened the first stage is to select the area to be analysed. The area of the screen to be measured is measured using, X and Y coordinates with the unit been the number of pixels. All

images used for filiform corrosion analysis were cropped to an area of 700 x 400 pixels around each penetrative defect. The size of this cropped area in relation to the defect is shown in figure 2-4.

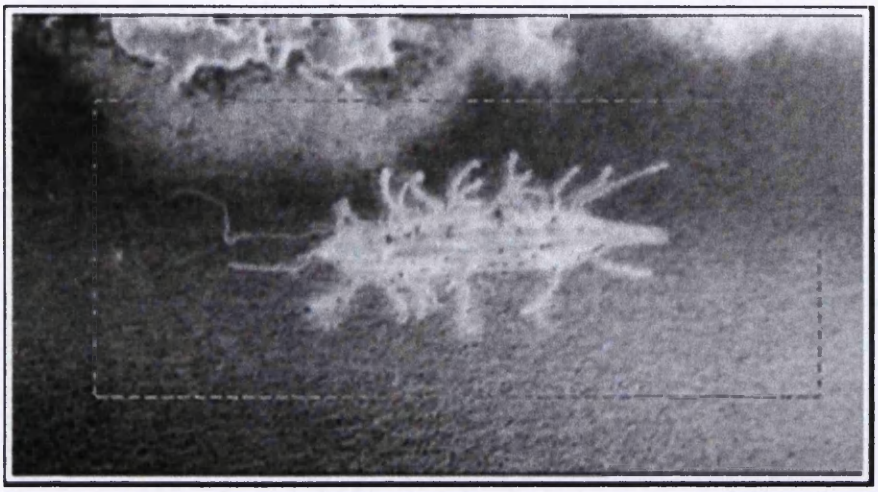

**Figure 2-4** : Cropped area of image used for digital image analysis. The area is constant across all images by taking the image under control conditions, and cropping to a size of 700 x 400 pixels

When measuring the total corroded area, the area to be measured becomes red when selected as is shown in figure 2-5. It is important to visually inspect this process to ensure the red area closely correlates to the corroded area before quantifying the total corroded area. The contrast threshold can be adjusted until a good correlation is obtained. This area of set up is subjective, so a potential cause for error.

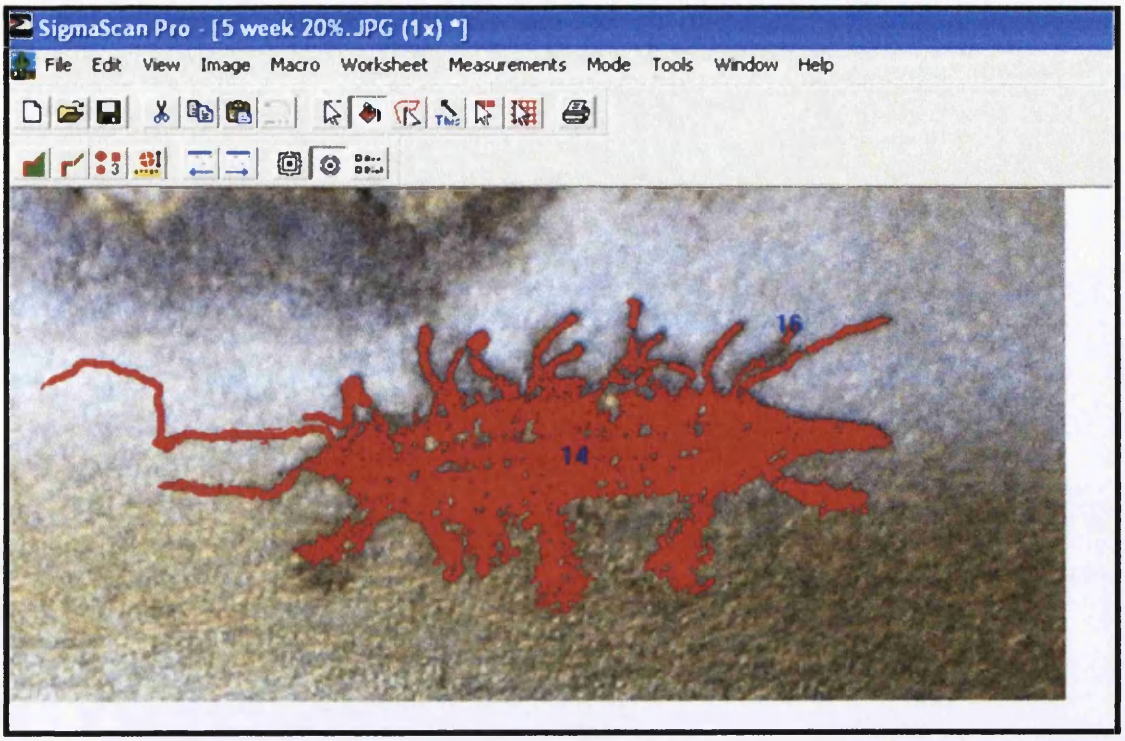


**Figure 2-5 :** Area to be measured is highlighted in red by digital image analysis software. This is done by contrasting the corrosion colour with the background metal.

### 2.3.2 Sigma Scan Data analysis

Data output for sigma scan threshold area is given in the number if pixels that are shaded in red, during the threshold area measurement. The fractional area of the sample that is corroded, is the number of pixels measured during the threshold area measurement divided by the total area. Multiplying the fractional area of the sample that is corroded, by 100 gives the percentage of the image surface area which has been corroded.

## 2.4 Measuring Filament Length

Filament lengths are measured by placing circles with a 70 pixel diameter on the digital image of the filament. Using control camera settings, a 70 pixel circle, is the equivalent of a 0.25 mm on the sample. The next circle is placed adjacent to the first circle, and the total number of circles that can be placed on a filament are counted. From this the overall length of the filament can be calculated. The reason this method is chosen is due to the filaments not travelling in straight lines, and therefore this is a

consistent way of measuring a curved filament. An illustration of this method is shown in figure 2.6.

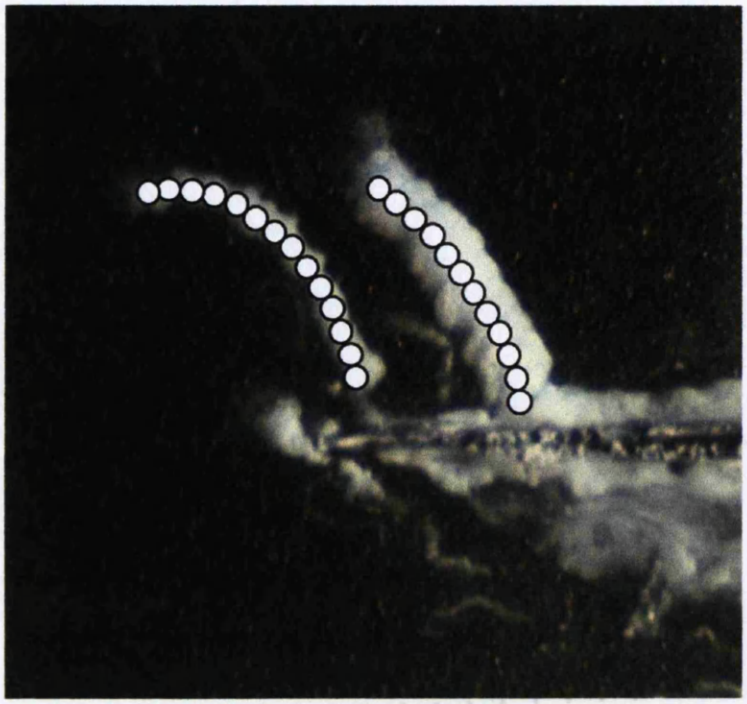

**Figure 2-6 :** Filament length is measured by placing 70 pixel (0.25mm) circles along the filament length, and then counting the total number of circles. This method can be used to measure the irregular curves found on filiform filaments

For example the 2 filaments shown in figure have a length of 14 and 12 circles respectively, giving them a physical length on the sample of 4 and 4.5mm. On wider filament dots are drawn as close to the centre of the filament as possible.

## 2.5 SEM imaging and EDX

### 2.5.1 Scanning Electron Microscope Imaging

A Hitachi TM3000 desktop scanning electron microscope (SEM) is used to image samples at a magnification of between 100 and 3000 times. All samples are prepared by cleaning with a 5μm alumina slurry, rinsing with deionised water then degreasing by immersion in hexane for 5 minutes, to remove any organic residue, unless stated otherwise. Finally samples are rinsed with deionised water and allowed to air dry.

Backscatter detection is used so that contrast between the different microstructural phases is observed. All samples are imaged with an accelerating voltage of 15keV.

### 2.5.2 EDX analysis

EDX stands for Energy Dispersive X-ray analysis. It is also sometimes referred to as EDS or EDAX analysis. EDX is a semi-quantitive technique, used for characterizing the elemental composition of a specimen, or an area of interest within a specimen. It is an integrated feature of a scanning electron microscope (SEM), and cannot operate without the latter.

During EDX analysis, the specimen in bombarded with electrons via an electron beam. The electrons in the electron beam will interact with the outer electron subshells of the atoms that make up the specimen. Every atom is made up of a positively charged nucleus, containing protons and neutrons, and orbiting this nucleus are negatively charged electrons. These electrons are arranged in electron sub shells, as shown in table 2-1.

| Subshell | Maximum number of electrons |
|---|---|
| K | 2 |
| L | 8 |
| M | 18 |
| N | 32 |

**Table 2-1** : Electron subshell name and number of electrons contained within each subshell

When incoming electrons in the incident electron beam interact with the electrons in the subshells of the sample atoms, they can displace an electron from an inner subshell. When a position vacated by an ejected inner sub shell electron it will be re-occupied by a higher-energy electron from an outer shell. In order for this to occur the transferring outer electron must release some energy, and this is done by emitting an X-ray. The magnitude of the drop in energy is a fixed, defined amount for individual elements and there resultant subshell reduction. The energy of the x-ray which is emitted directly correlates to the energy difference between the sub shells.

EDX identifies the elements are present in the sample by measuring the energy of the x-ray radiation been emitted from a sample that is been bombarded with electrons.

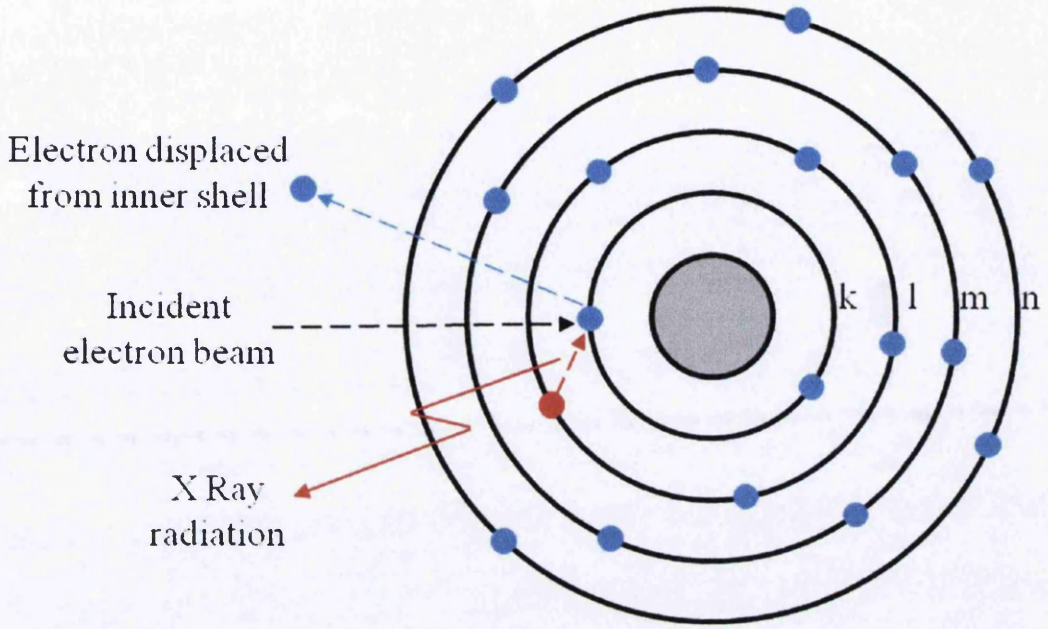


**Figure 2-7** : During EXD analysis electrons from atomic subshells in the sample are displaced by incoming electron beams from the electron gun. When an inner subshell electron is displaced, outer subshell electrons will drop in to the inner sub shell. When this happens energy is released in the form of an X-ray. EDX characterizes the sample by measuring the energy of these radiated Xrays.

The EDX detector measures the energy of each x-ray emitted from the sub shell as shown in figure 2-7, and counts the number of x-rays been detected of each specific energy. Each specific energy level of an xray will be plotted to form a graph as shown in figure 2-8. The element is identified by the energy of the x-ray, and the approximate abundance of that element can be predicted by the number of counts per second or the height of the peak of the x-rays for a given energy (81,82)

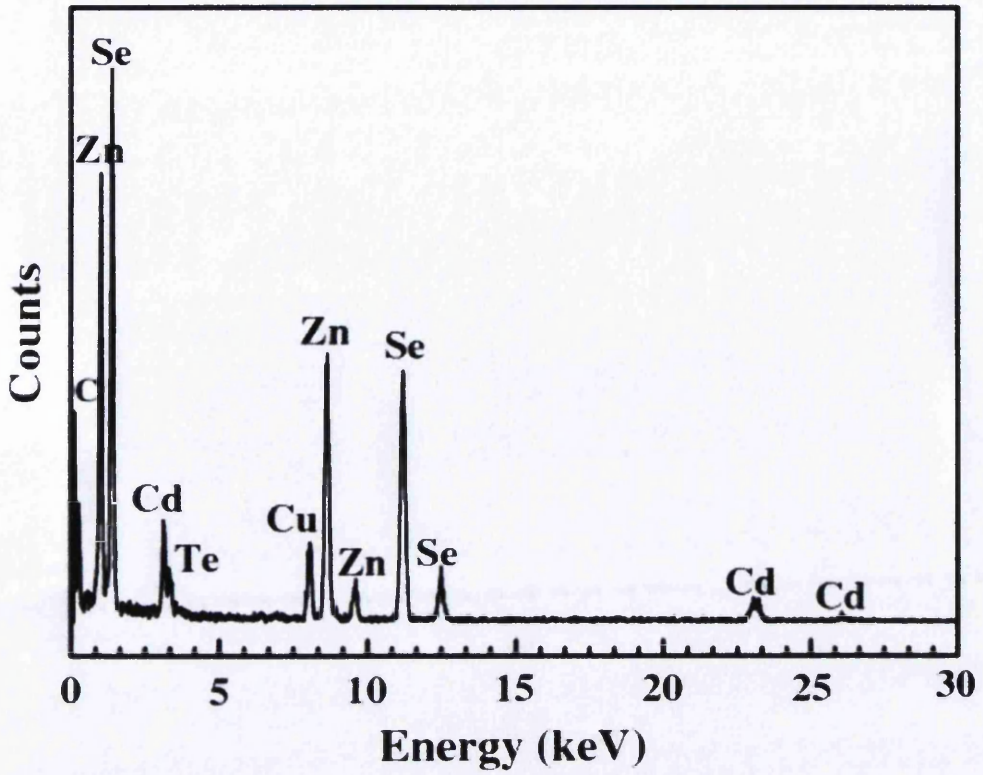


**Figure 2-8 :** Typical EDX plot showing the energy of x-rays detected, and the abundance of energy peaks in counts per second. The element is characterized by the energy of the x-ray, and the relative abundance is calculated from the count per second of x-rays at a given energy.

### 2.5.3 EDX Interaction volume

When the incident electron beam interacts with a sample, electrons will have an associated penetration depth with that specific sample. The depth the electrons penetrate in to the sample depends on the accelerating voltage of the incident electron beam, and the composition and density of the sample. An approximate calculation for electron penetration depth is given in equation 2.1 (81)

$$X(\mu m)= \frac{0.1{E_0}^{1.5}}{\rho} \qquad (2.1)$$

X = Penetration depth in μm

E0 = Accelerating voltage keV

P = Sample density ($g/cm^3$)

For all EDX analysis discussed in this thesis the Hitachi TM3000 SEM used was operated with an accelerating voltage of 10keV. At 10keV the electron penetration depths for relevant metals is shown in table 2-1.

| Element | Density ($g/cm^3$) | Electron penetration depth ($\mu m$) |
|---|---|---|
| Zinc | 7.14 | 0.44 |
| Magnesium | 1.74 | 1.82 |
| Aluminium | 2.70 | 1.71 |
| Iron | 7.87 | 0.40 |

**Table 2-1 :** Penetration depth of electrons on various metallic samples during EDX analysis with an accelerating voltage of 10keV

### 2.5.4 Sample Preparation for EDX

#### 2.5.4.1 Organically coated samples

All samples used in an SEM must be conducting, or they will charge up when bombarded with electrons. For this reason insulating organic coatings must be removed. PVB based coatings are removed by immersing the sample in acetone, in an ultrasound bath for 10 minutes at 20°c. The coating is then removed by abrading it with a lint free cloth.

#### 2.5.4.2 Non organically coated samples

Uncoated samples must be washed and degreased to remove any electrolytes, salt solution / salt crystals, or organic contaminants off the surface. Firstly the sample is rinsed with deionised water, and then immersed in hexane for 5 minutes. When the sample is removed from immersion it is rinsed with deionised water, and ethanol and air dried.

## 2.6 Time dependant EDX etching

In order to investigate the corrosion mechanism of samples in selected environments, samples are immersed in an electrolyte, and then removed at systematic time periods and studied using EDX. The same area of the sample is repeatedly studied at different time periods under a Scanning Electron Microscope, and using EDX analysis, in order to investigate the effect of immersion in a corrosive medium, over the time period, on the sample. The sample is then further immersed, and this process continues until the desired level of corrosion has been achieved.

### 2.6.1 Sample preparation

Samples are firstly chopped in to 25mm x 25mm coupons using a guillotine. A right angle is then scribed on to the surface of a sample using a scalpel, as shown in figure 2-9. The reason for this scribe, is the two lines can be used as reference marks when locating the sample for imaging, and this ensures that the same area of the surface is imaged reproducibly. For imaging the sample surface is abrasively cleaned using an aqueous slurry of 5μm polishing alumina powder and deionised water. Any organic components on the surface are then removed by immersing the sample in hexane for 5 minutes.

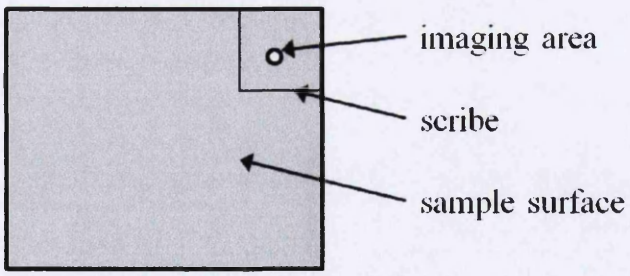


**Figure 2-9** : Schematic diagram showing the layout of a sample for kinetic EDX studies. The scribed marks are reference marks used for image location. Imaging is done a significant distance away from these scribes, as the scribes can have an effect of corrosion phenomena

### 2.6.2 Kinetic EDX Imaging

SEM imaging is carried out in a Hitachi TM3000 SEM. The first stage of imaging is to find the reference lines at a low magnification. Reference lines are then lined up so that they line up with the X and Y edges of the image at a magnification of x 100, and a working distance of 10mm as shown in figure 2-10.

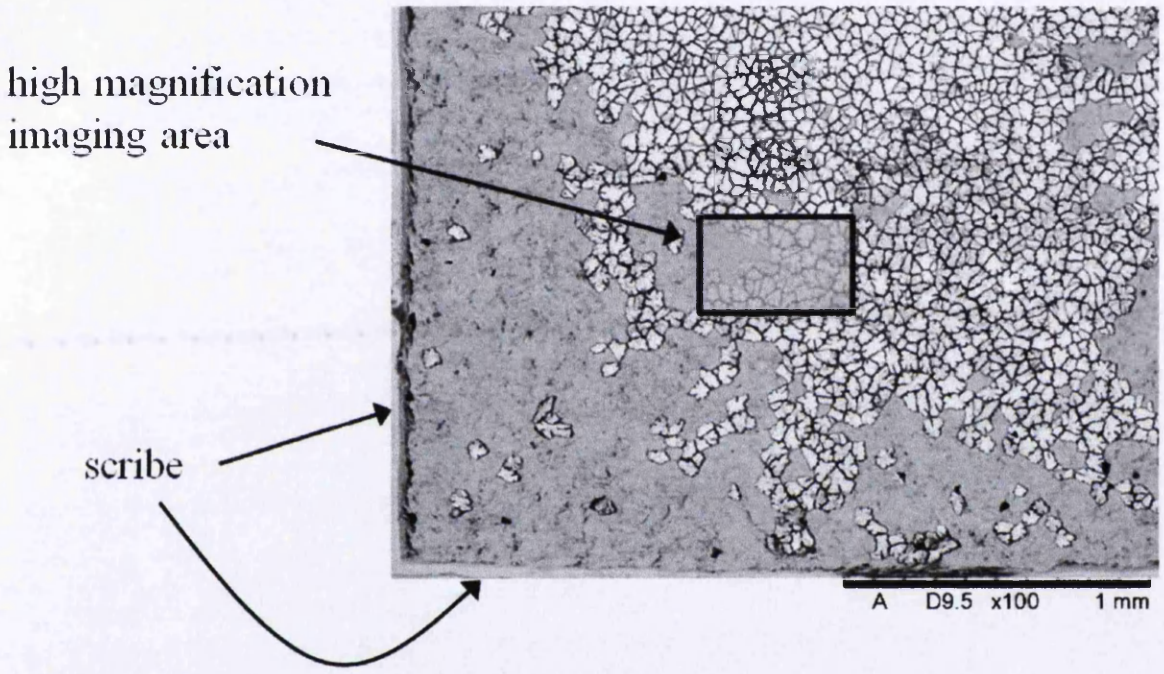


**Figure 2-10** : Reference lines on image location of a sample for SEM EDX time dependant analysis. The effect of steel exposure form the reference lines can be observed. Exposing the cathodic steel increases the rate of corrosion on the anodic Zn-Al-Mg coating.

When the image position has been calibrated the magnification is increased systematically in order to alter the position of the image and finally locate the sample so the same sample area is analysed. All kinetic EDX analysis discussed in this thesis is carried out at a magnification of x3000. EDX elemental maps showing the distribution of iron are made using Quantax 70 EDX. Finally the surface composition for each area is measured also using EDX.

### 2.6.3 Immersion Etching

Cleaned and polished hot dip coated steel samples are immersed in the specified electrolyte (specified in relevant results chapter) in a petri dish placed in a fume cupboard. Immersion times between imaging will be noted in the relevant results. When the sample is removed from the electrolyte, it is rinsed with deionised water, and then immersed in hexane for 5 minutes in an ultrasound bath to remove corrosion product. Corrosion product is removed so that the underlying coating surface can be observed. The sample is now dried and placed in an SEM for EDX analysis.

## 2.7 AFM and SKP-FM

### 2.7.1 Introduction to AFM

Atomic force microscopes (AFM's) provide a 3D profile map of the surface of a sample at a nm – μm scale. This is done by measuring forces between a sharp probe *(typical probe radius <10nm)* and its interaction with the sample surface charge layer *(probe–surface distance is typically 0.2 – 10nm)*. The probe is supported at the end of a flexible cantilever, which acts like a spring. The surface of the sample is mapped by following the movement of the cantilever with a laser. The movement of the cantilever with regards to the surface will depend upon the spring constant *(stiffness of the cantilever)* and the distance between the probe and the sample surface. The force upon the cantilever can be described using Hooke's law, $F = -k\text{-}x$ where F = force, k = spring constant and x = cantilever deflection. The motion of the probe is detected by reflecting a semiconductor diode laser off the back of the cantilever, on to a position sensitive photodiode detector. This position is then relayed in to a feedback loop, and piezoelectric scanners control the cantilever. The photodiode detector is also used to detect the position of the cantilever; this data of cantilever deflection is used to generate a map of the samples surface topography (83,84).

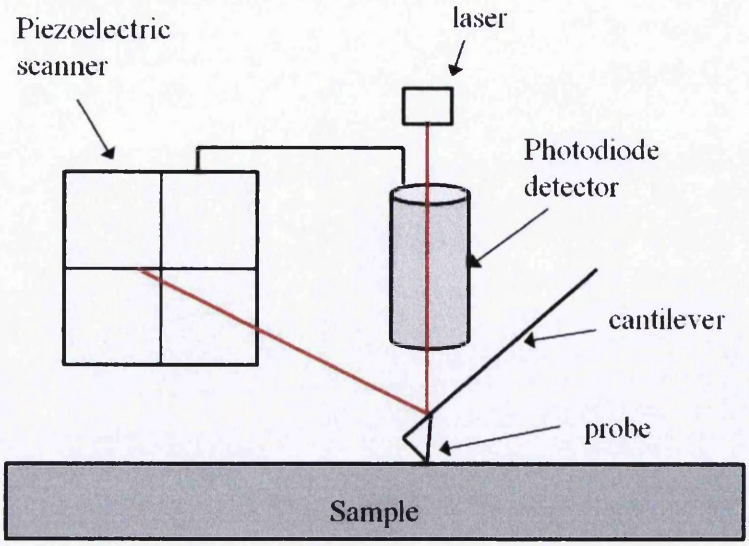


**Figure 2-11 :** A schematic diagram of an atomic force microscope. The cantilever interacts with the surface charge layer of the sample. A laser tracks this movement, and amplifies it on to a detector. AFMs are used to measure the surface topography of a sample

### 2.7.2 Introduction to SKPFM

Kelvin probe microscopy is an additional working mode supported by some commercial atomic force microscopes (AFM's). All work carried out in this thesis is carried out using a JPK nanowizard 3 AFM, with JPK SKPFM. Scanning Kelvin probe force microscopy (SKPFM) allows the measurement of surface potentials over a nm to μm scale. This is favourable over standard Kelvin probe in some situations, as standard Kelvin probes do not allow for a high enough resolution to resolve the surface potentials of sub- μm microstructural phases.

The potential surface contrast between the phases present in a metallic microstructure will have a large effect on the corrosion mechanism of the material, therefore SKPFM can provide significant amounts of information on the potential mechanisms for delamination and corrosion on a metallic coating. As with other scanning Kelvin probe (SKP) techniques, the resolution for SKPFM is highly dependent on the distance between the tip and the surface (85).

The reference electrode used for potential measurements are pseudo-references since volta potentials may vary from tip to tip, due to slight differences in the oxide covering the tip, contaminants on the tip, or variation in tip composition.

The scanning procedure for an SKPFM scan is to do alternating line scans, the first been a topographical scan measuring the height of the sample surface, and then a second lift scan which traces the topographical scan, but with the probe lifted a set distance above the surface. Typical probe measurement heights are in the region of 20 – 100nm (86).

During SKPFM measurements a constant bias, and a superimposed alternating bias are applied between the tip and the sample. The alternating bias induces an alternating charge between the AFM tip and the sample surface, which then induces an alternating modulation of the force on the tip. The force being induced upon the tip at frequency $\omega$ which is the resonant frequency of the cantilever, is used to determine the surface potential as shown in equation 2.2

$$F\omega = \upsilon_{dc}\upsilon_{ac} d\,C/d\,z = 0 \text{ at } \upsilon_{dc} = \Delta\Psi - \upsilon_{dc,\,applied} = 0 \qquad (2.2)$$

$F\omega$ = tip force

$\upsilon_{dc}$ = dc voltage tip / sample

$\upsilon_{ac}$ = ac bias tip / sample

C = capacitance

z = distance tip / sample

$\upsilon_{dc\ applied}$ = applied control bias tip / sample

$\Delta\Psi$ = volta potential difference

The interaction of the tip and the sample when this potential is induced will depend on the surface potential of the sample. The output of this interaction will be a variation in tip movement which will be detected by the AFM. This can then be used to calculate the surface potential of the sample (83).

### 2.7.3 AFM and SKPFM methodology

#### 2.7.3.4 AFM sample preparation

Polished samples should show no significant topography. However when a sample has undergone corrosion, the rate of corrosion will not be equal of all micro structural phases. As a result of increased anodic dissolution in some phases, corrosion will induce a topography upon the surface. During AFM topographical measurements, this topography is measured. The removed phases can then be correlated to the micrographs and the phase most susceptible to anodic dissolution can be defined. Sample preparation is kept to a minimum as it may have an effect on results. However corrosion products must be removed. This is done by immersing the sample in hexane, in an ultrasound bath for 10 minutes. Samples are then scanned using tapping mode in there as seen state.

#### 2.7.3.4 SKPFM Sample preparation

In order to obtain a good SKPFM map samples must be as flat as possible, as this will reduce the error signal by enabling the AFM to maintain the distance between the sample and the tip as constantly as possible. In order to produce a flat sample, samples are firstly cleaned with an aqueous slurry of 5μm polishing alumina powder and deionised water. Any residual slurry is then rinsed using deionised water. Organic contaminants are removed by immersing the sample in hexane, and subjecting it to ultrasound for 5 minutes. Finally samples are rinsed with more deionised water (86).

To ensure the sample is flat the surface is lightly polished. This is done using 1μm diamond polishing paste and paraffin. Water is not used, as it will etch the sample slightly creating topography, and removing some of the anodic phases which we wish to see the potential of on the SKPFM. After a light polish *(coating thickness is 10μm, and the coating must not be removed)* the sample is degreased by immersing in hexane and placing in an ultrasound bath for 10 minutes. The sample is finally rinsed with ethanol and allowed to air dry.

### 2.7.3.5 Sample set up AFM / SKPFM

All work in this thesis is carried out using Nano World FM-50 doped silicon SPM cantilever, with dimensions of thickness 3μm, length 225μm, width 28μm, force Constant 2.8N/m, and resonance Frequency ~75kHz. Sample set up is identical for form AFM and SKPFM measurements, apart from for SKPFM the reference contact lead must be attached to the sample. This is done by clipping it to the sample with the crocodile clip on the end, ensuring that it does not touch the metallic base. Metallic samples must be securely mounted on a glass slide, to ensure that they do not move. This is done using double sided adhesive tape, and then the slide is clipped in to the AFM base.

### 2.7.3.6 Scanning

Firstly the AFM is setup and calibrated as according to the user handbook. All topographical scans are carried out in tapping mode. For SKPFM measurements it is important to ensure that the sample is flat (+/- 200nm). For this reason a topographical scan is always carried out first. All scanning is carried out as per the handbook.

# Chapter 3 Filiform corrosion of Zn+Al+Mg hot dip coated steel in atmospheric conditions

## 3.1 Introduction

A commercial widely used technique for protecting steel against corrosion in atmospheric environments is galvanic protection via metallic hot dip coatings. These metallic coatings often undergo further coating with an organic polymer film or lacquer. These organic films and lacquers act as a barrier for corrosion species such as oxygen and electrolytes (87). This further increases the corrosion resistance of the underlying steel. Hot dip galvanized coatings have traditionally consisted primarily of zinc, with small additions of aluminium and silicon to improve adhesion and ductility (88). In the last two decades there have been environmental and economic pressures requiring a new generation of chromium free hot dip coating systems, with increased levels of corrosion resistance, in relation to conventional hot dip zinc coatings. As a result of this pressure, new alloy compositions for hot dip coatings containing increased additions of aluminium, and magnesium have been developed. Current commercially available variants of Zinc+Aluminium+Magnesium (Zn-Al-Mg) coatings have compositions in the range of 1-11wt% aluminium and 1-6wt% Magnesium, with the remaining part of the coating consisting of zinc (58).

The aim of this chapter is to investigate the primary corrosion mechanisms found to occur on Zn-Al-Mg hot dip coated steels. It has been suggested by Stratman *et al* that alloying highly anodic elements such as magnesium with zinc based coatings, could make Zn-Al-Mg hot dip coatings susceptible to anodic forms of attack (61).

## 3.2 Materials

All experimental work in this chapter is carried out on commercially produced hot dip galvanised steel samples, with a mild steel substrate gauge of 0.7mm. The substrate is symmetrically hot dip coated on both sides with a Zn-Al-Mg coating, with

a bath composition of Zn+Al*(1.5wt%)*+Mg*(1.5wt%)* and a coating thickness of 10 μm, which has a corresponding coating weight of 140g/m$^2$. All other chemicals and materials used are supplied by the Aldrich chemical company in analytical grade purity. All samples are coated with an un-pigmented PVB model lacquer as described in section 2.1

## 3.3 Methodology

Corrosion experiments are carried out using the standard filiform corrosion / anodic disbondment test methodology described in section 2.1. The range of electrolytes used to initiate corrosion are shown in table 3-1: in all scenarios 2μl of electrolyte is used to initate corrosion per defect.

| Electrolyte | Electrolyte concentration (mol/dm$^3$) |
|---|---|
| HCl | 1, 2, 3, 4 |
| NaCl | 1, 2, 3, 4 |
| $FeCl_2$ | 0.5, 1, 1.5, 2 |
| $Cl_3COOH$ | 0.5, 1, 1.5, 2 |

**Table 3-1:** Compositions and concentrations of electrolyte matrix used to initiate anodic corrosion experiments. In all scenarios 2μl of electrolyte is used for corrosion initiation per defect.

## 3.4 Sample characterization

Due to the high cooling rates found on commercial hot dip galvanizing lines, the microstrucutral phases present in hot dip coatings are often non equilibrium phases, and therefore the hot dip coating alloy cannot be accurately characterized using an equilibrium ternary phase diagram (89). Studies of similar coating compositions described in chapter 1 predict that the phases present in Zn+Al(*1.5wt%*)+Mg(*1.5wt%)* hot dip coatings are likely to be an equaixed or dendritic primary zinc phase, a course binary eutectic composed of $MgZn_2$ and Zinc, and a finer ternary eutectic composed of $MgZn_2$, Zinc and aluminium (90).

Samples are characterised using energy dispersive X-ray spectroscopy (EDX) in a Hitachi TM3000 scanning electron microscope as described in section 2.3. Elemental maps are composed to show the presence and distribution of element densities. These maps are correlated to scanning electron microscope back scatter images to show the element densities with respect to phase location. Due to the interaction volume of electrons discussed in section 2.3, EDX can only be used as a semi quantitive technique. However the physical location of elements in relation to microstructural phases is observed, and this information is correlated with the literature to give a predicted characterization.

## 3.6 Characterization Results

An SEM backscatter image of a typical area of Zn-Al(*1.5wt%*)-Mg(*1.5wt%)* hot dip coating is shown in figure 3-1. The main phases present in the coating are a homogeneous primary dendritic phase, and two eutectic phases. After EDX analysis, it is proposed that a dendritic primary zinc phase is present, which is composed almost entirely of zinc, with small amounts of aluminium (<0.25wt%) and magnesium (<0.1wt%) also present. Elemental analysis map for Zinc, Magnesium and Aluminium are shown in figure 3-2. The primary zinc phase covers approximately 30% of the overall hot dip coating surface area. A course binary eutectic phase is also present, with an average lamella spacing of approximately 1μm. The binary eutectic is composed of lamella of zinc, and $MgZn_2$, and virtually no aluminium is observed in this phase. A finer ternary eutectic phase is also observed, and this phase shows high levels of zinc, aluminium and magnesium. The ternary eutectic phase has a lamella spacing of approximately 400nm. The average EDX compositions of each phase is calculated from the k shell counts per second reading.

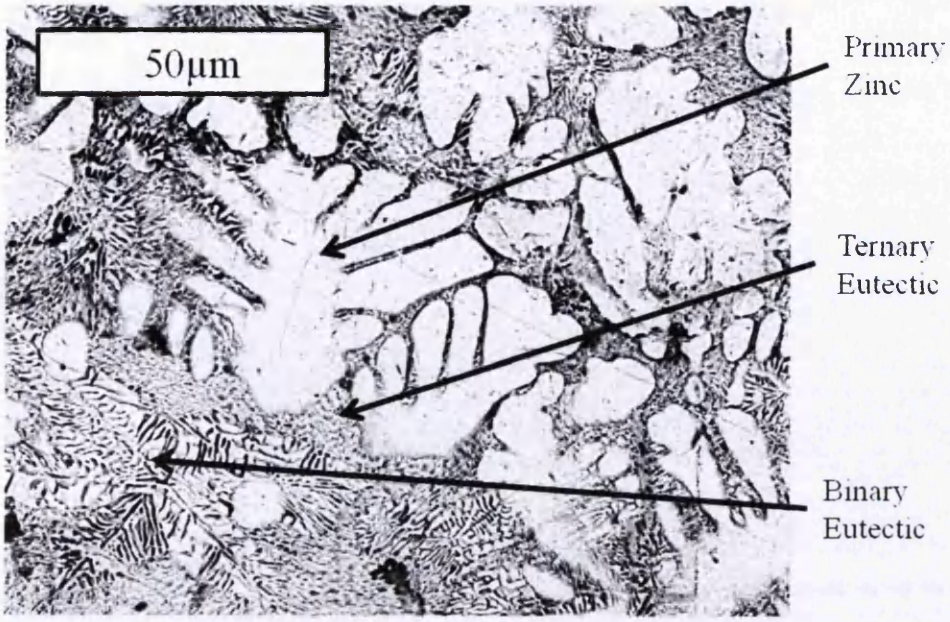


**Figure 3-1 :** SEM backscatter image showing the typical appearance and phases of Zn-Al(1.5wt%)-Mg(1.5wt%) hot dip coated steel. The three phases present are primary zinc, a binary eutectic composed of zinc and $MgZn_2$ and a Ternary eutectic composed of Zn-$MgZn_2$ and an Aluminium rich phase.

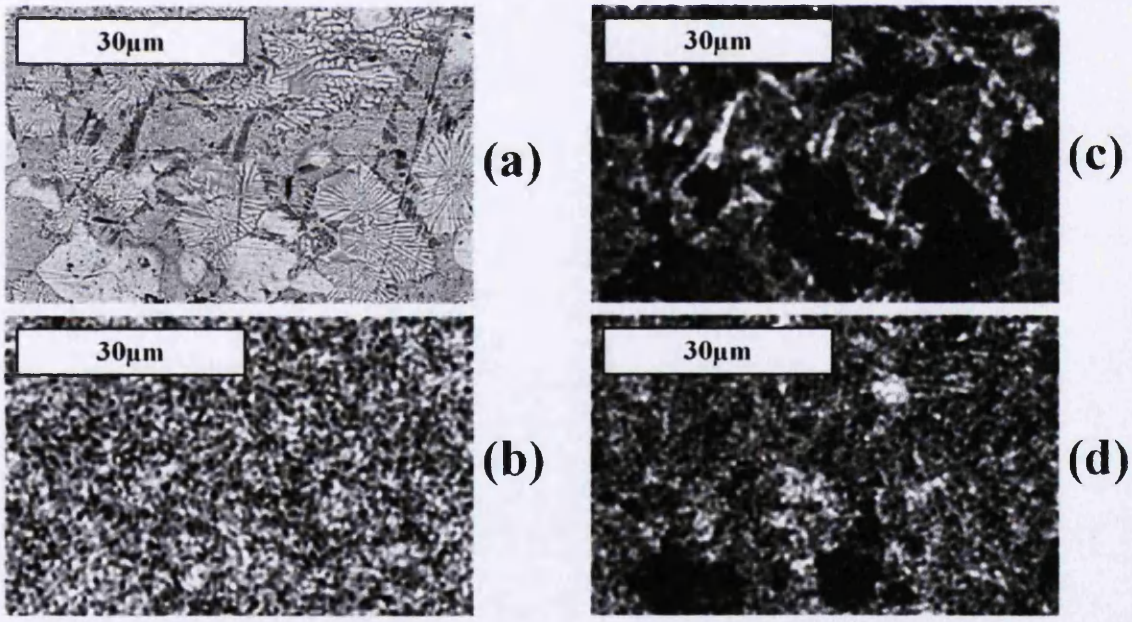


**Figure 3-2 : SEM and Energy Dispersive Spectroscopy (EDX); All images (a,b,c,d) are the same area and magnification on the sample surface (a)** Scanning Electron Microscope backscatter image of the surface of Zn-Mg-Al hot dip coated steel with a coating composition of Al 1.5wt% + Mg 1.5wt% and a coating weight of 140g/m$^2$ with a corresponding coating thickness of ~10µm **(b)** EDX elemental map showing the distribution of zinc on the sample surface **(c)** EDX elemental map showing the presence and distribution of aluminium on the Zn-Al-Mg surface **(d)** EDX elemental map showing the presence and distribution of magnesium on the sample surface.

| Element | Primary Zinc (wt%) | Binary Eutectic (wt%) | Ternary Eutectic (wt%) |
|---|---|---|---|
| Zinc | 99.7 | 96.42 | 93.33 |
| Aluminium | 0.23 | 0.86 | 3.53 |
| Magnesium | 0.07 | 2.72 | 3.14 |

**Table 3-2 :** The composition of each phase in Zn+Al *(1.5wt%)*+Mg*(1.5wt%)* hot dip steel coating measured using Quantax 70 EDX on a Hitachi TM3000 desktop SEM at an accelerating voltage of 15KeV. All values are calculated from K shell counts.

The surface area each phase on the Zn+Al*(1.5wt%*+Mg*(1.5wt%)* hot dip coating surface is measured using sigma scan digital image analysis of SEM backscatter images as described in section 2.3. It is found that primary zinc occupies ~30% of the surface area, the binary eutectic ~30% and the ternary eutectic makes up the remaining 40% of surface area. Primary zinc and binary eutectic are generally distributed in discreet regions of their respective phase, whilst the ternary eutectic makes up the remaining matrix and can often be continuously linked over the entire sample surface.

## 3.7 Corrosion Testing

### 3.7.1 Methodology

Corrosion is initiated using the standard test as described in section 2.1. A range of systematic concentrations and compositions of electrolyte as shown in *table 3-1* are used to initiate corrosion. Corrosion propagation occurs in a dessicator at a temperature of 22 degrees centigrade, and a relative humidity of 86%. Each composition of electrolyte is tested separately in a separate dessicator. This dessicator is spherical with a diameter of 0.25m and a resultant volume of $0.00818m^3$. For each experiment 2 samples are present, each with two defects, resulting in all results been reproduced over 4 defects. Digital image analysis as described in section 2.2 is used to study the corrosion morphology, filament length, and total corroded area in relation to time.

### 3.7.2 Results and discussion

After 5 weeks each electrolyte is found to produce its own distinct corrosion morphology on Zn-Al-Mg hot dip coated steel. HCl produces a ring of corrosion product around the defect. NaCl produces a form of pitting corrosion around the defect. The amount of pitting increases in correlation with the concentration of NaCl. $FeCl_2$ produces small amounts of red rust in the defect, but very little corrosion is seen on the intact Zn-Al-Mg hot dip coating surface regardless of concentration. The visual appearance after 5 weeks of HCl, NaCl and $FeCl_2$ is shown in figure 3-3.

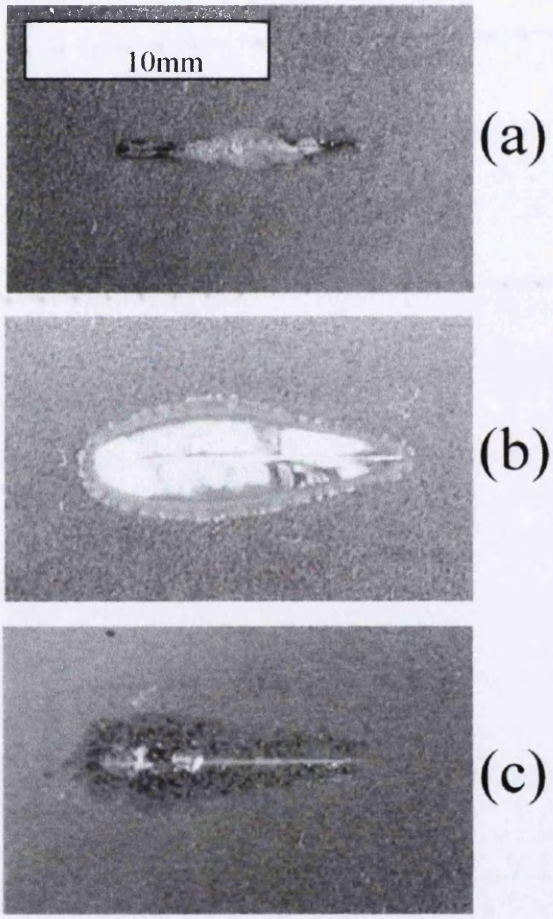


**Figure 3-3 :** Optical images taken with an optical stereo microscope of the corrosion morphology around the 1cm long penetrative defect on 140g/m$^2$ Al 1.5wt%+Mg 1.5wt% Zn-Al-Mg hot dip steel coating after initiation and a propagation time 5 weeks at a relative humidity of 86% and a temperature of 22°c **(a)** initiated with 2µl 2 molar $FeCl_2$, **(b)** initiated with 2µl of 2 molar HCl, **(c)** initiated with 2µl of 2 molar NaCl $FeCl_2$.

Acetic Acid *($CH_3COOH$)* reproducibly produces filiform corrosion, which initiates at the penetrative defect and propagates along the metal / organic coating interface. Filiform corrosion filaments also initiate and propagate from the cut edges of samples initiated with acetic acid. After a prolonged period of approximately 7 weeks, some filiform corrosion filaments also initiate on the seemingly intact Zn+Al+Mg coating surface. Initiation was seen to occur with concentrations of acetic acid electrolyte as low as 0.5mol/$dm^3$. The visual appearance after 1week, 2 weeks, 3week and 4 weeks and 5 weeks with 1.5mol/$dm^3$ acetic acid is shown in figure 3-4.

The relationship between acetic acid concentration, the total corroded area, and time is studied by analysing time separated images, using digital image analysis with sigma scan pro 5 as explained in section 2.3. All graphical data points are calculated by averaging the amount of corrosion measured around four 10mm penetrative defects, on two separate samples. The area measured includes both the area covered by filiform corrosion filaments, and the area of radial corrosion which is inherently found around the defect. The overall appearance of a test coupon after 8 weeks at 86%RH and initiation with 1.5mol/$dm^3$ acetic acid is shown in figure 3-5. The kinetics of filiform corrosion in the form of total area of corrosion by acetic acid strength is shown in the line graph in figure3-6. This shows a clear positive correlation between acid concentration and the amount of corrosion.

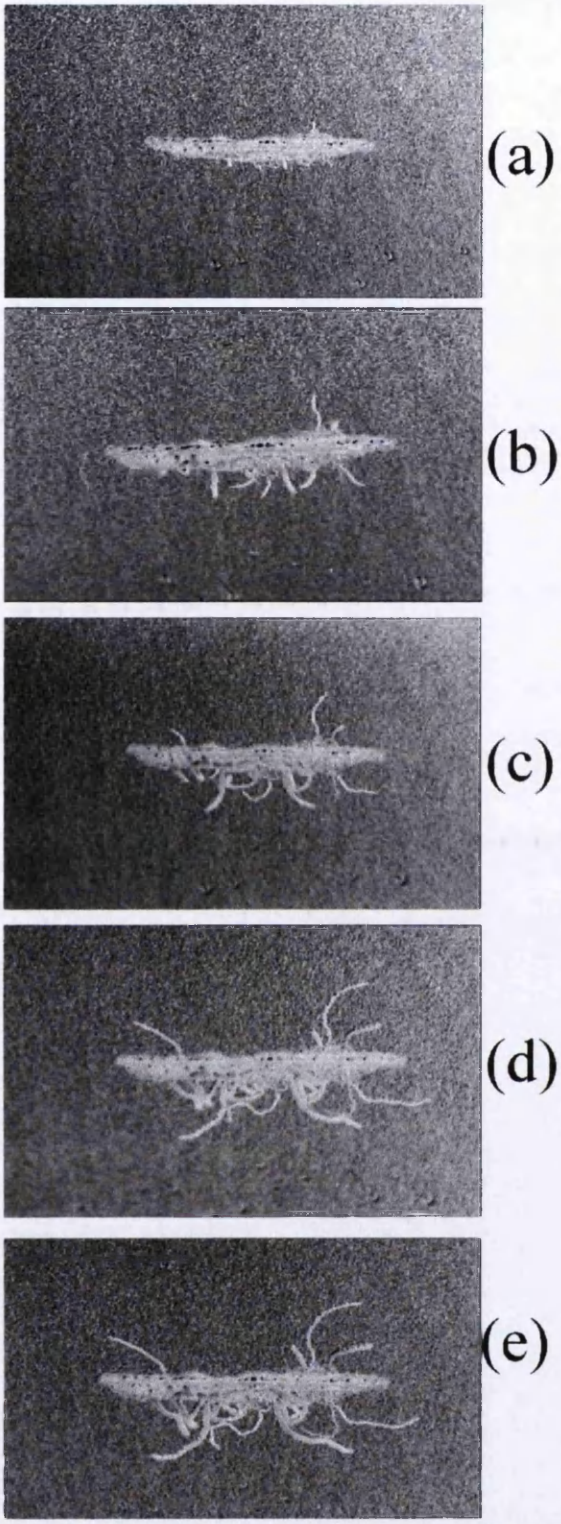


**Figure 3-4:** Optical images taken with an optical stereo microscope of the corrosion morphology around the 1cm long penetrative defect on 140g/m$^2$ Al 1.5wt%+Mg 1.5wt% Zn-Al-Mg hot dip steel coating after initiation with 2µl of 1.5 molar acetic acid, and propagation at a relative humidity of 86% and a temperature of 22°c. Propagation time is **(a)** 1 week **(b)** 2 weeks **(c)** 3 weeks **(d)** 4 weeks **(e)** 5 weeks

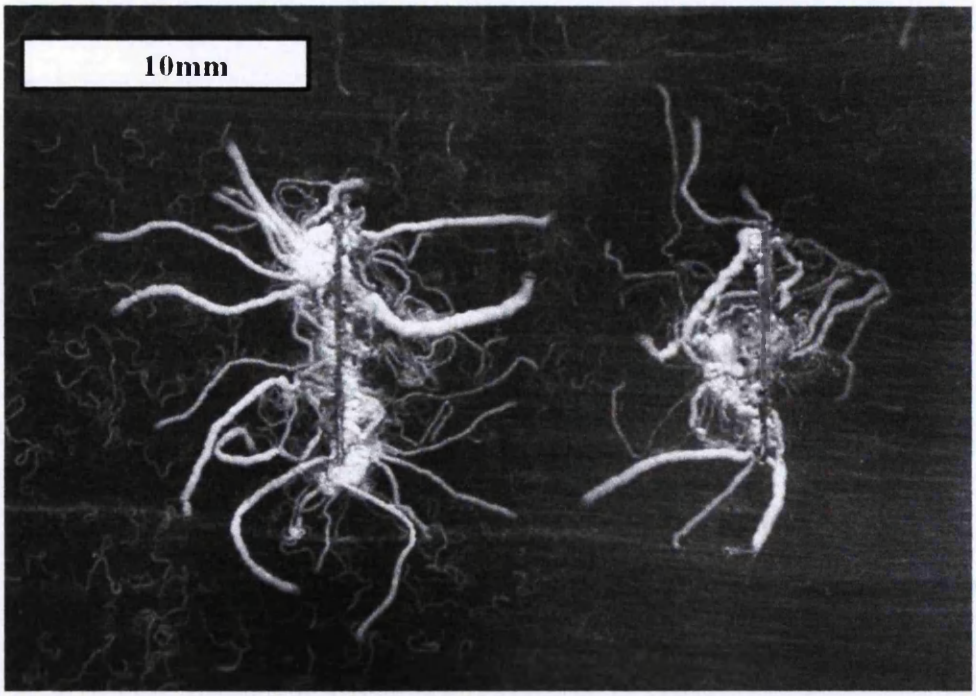


**Figure 3-5** : Appearance of Al*(1.5wt%)* Mg*(1.5wt%)* Zn-Al-Mg hot dip coated steel sample after initiation with 2µl of 1.5 mol/dm$^3$ acetic acid, and a propagation time of 8 weeks at 86%RH and a temperature of 22°c. Filiform corrosion filaments can be seen initiating and propagating and both 10mm long penetrative defects and on from the intact coating surface.

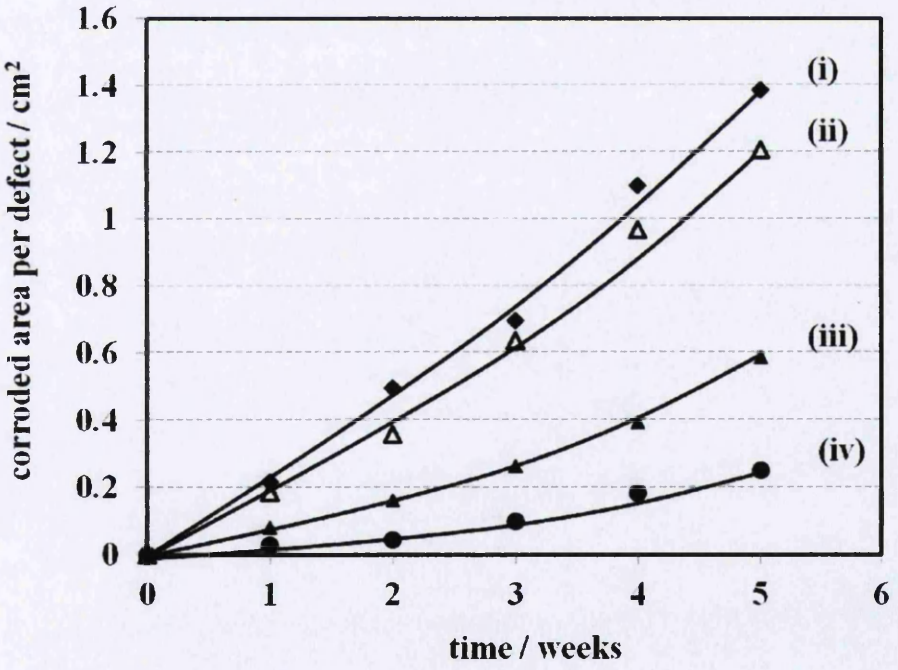


**Figure 3-6 :** The average total surface area covered in corrosion product around a 10mm penetrative defect averaged over 4 defects as measured using sigma scan digital image analysis. All samples are initiated with 2µl of relevant concentration acetic acid, and propagation occurs at a relative humidity of 86% and a temperature of 22°c. The corresponding concentrations on the initiate electrolyte are **(i)** 2 mol/dm$^3$ **(ii)** 1.5 mol/dm$^3$ **(iii)** 1 mol/dm$^3$ **(iv)** 0.5mol/dm$^3$

There is a slightly positive exponential trend for the kinetic relationship between the total area covered in corrosion product and time for all concentrations of acetic acid. The reason for this exponential curve is that the total area of corrosion encompasses both the areas covered by filiform filaments, which increases linearly with time, and an area of radial corrosion product around the defect, the area of which will increase by a square rule ($\pi r^2$) as the corrosion front propagates away from the defect. Also over time new filaments initiate and propagate, whilst the existing filaments continue to propagate. This also contributes to the positive parabolic trend over time in total corroded area. There is also a correlation between the total corroded area, and the concentration of acetic acid used to initiate corrosion. Higher concentrations of acetic acid are seen to produce more corrosion and therefore a larger corroded area, and a greater number of filiform corrosion filaments per defect are measured. This relationship is graphically represented in figure 3-7.

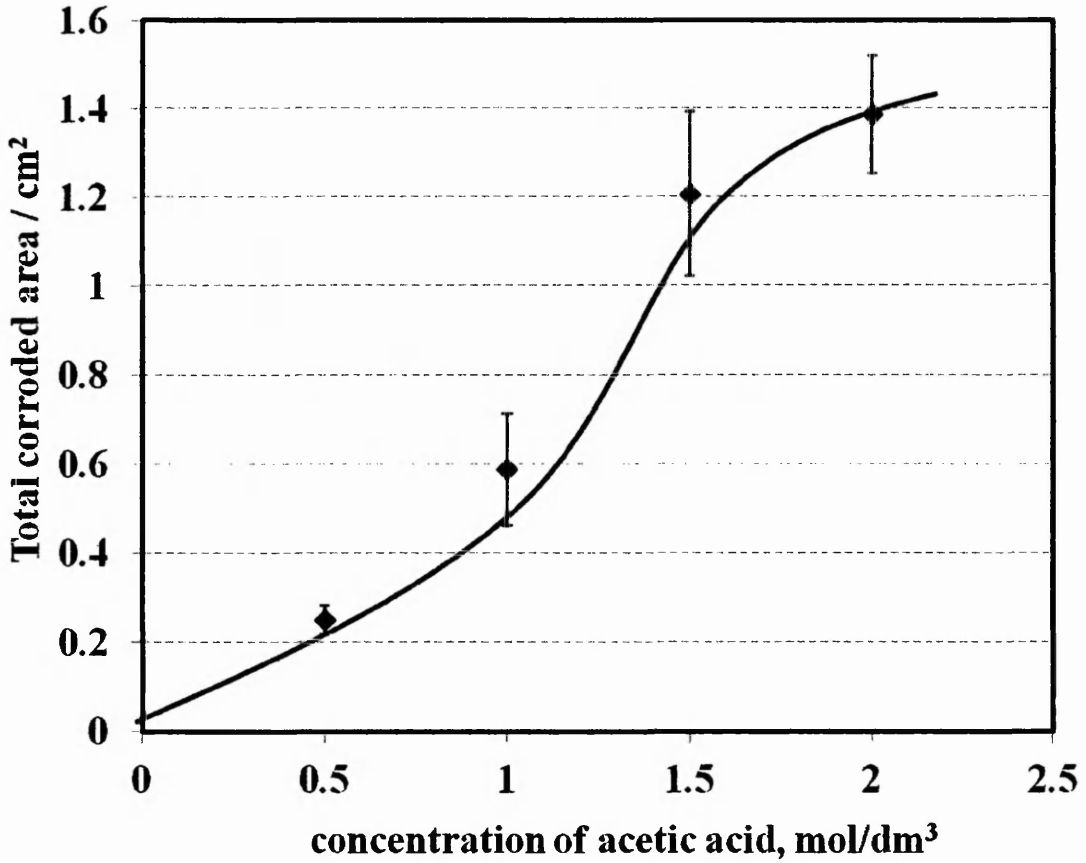


**Figure 3-7** – summary of the total corroded area in relation to acetic acid concentration around a 10mm penetrative defect, averaged over 4 defects. Corrosion is initiated with 2µl of acetic acid, and propagation conditions are 86% relative humidity and a temperature of 22°c.

In order to investigate the characteristics of filament propagation, the length of individual filiform filaments are measured in relation to time, using the technique described in section 2.3. All measurements are averaged over a total of 8 filaments, which is comprised of two filaments per defect, over a total of four defects. There is up to an order of magnitude variance in the length and width of individual filaments from a single defect, so the total filament length has not been analysed. However the propagation kinetics are more consistent over all filaments initiated with the same concentration of acid. The length of the filament depends largely on when the filament initiates. For this experiment the second and third "typical" filaments per defect are the filaments to be measured. The reason for this is because it represents the amount of time it takes for filaments to initiate, as well as a representation of growth rates. The average length of "typical" filiform corrosion filaments in relation to acetic acid concentration are shown in figure 3-8.

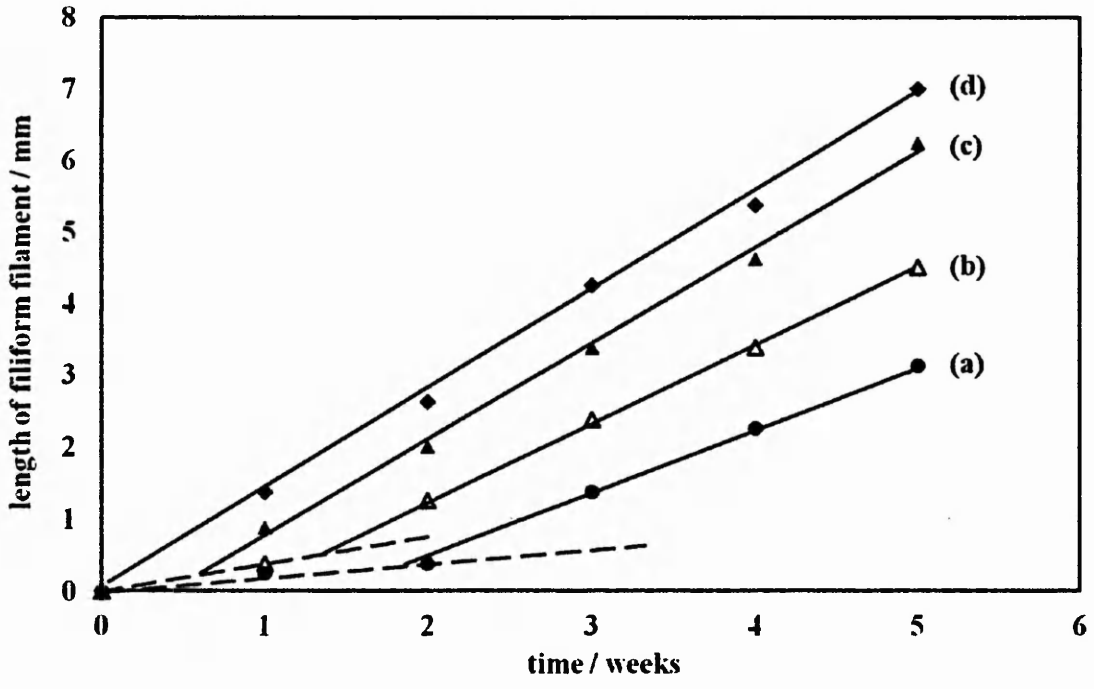


**Figure 3-8 :** The average length of filiform corrosion filaments initiating and propagating from a 10mm penetrative defect on a Zn-Al-Mg hot dip coated steel *(composition Al 1.5wt% + Mg 1.5wt%)* as measured using sigma scan digital image analysis. All measurements are an average of 8 *"normal"* filaments. All samples are initiated with 2µl of relevant concentration acetic acid, and propagation occurs at a relative humidity of 86% and a temperature of 22°c. The corresponding concentrations on the initiate electrolyte are **(a)** 0.5mol/dm$^3$ **(b)** 1 mol/dm$^3$ **(c)** 1.5 mol/dm$^3$ **(d)** 2 mol/ dm$^3$

Despite variance in the overall length of filiform filaments, the manner in which they initiate and propagate is consistent. An initiation period where no corrosion seems to occur is evident when the concentration of initiating acetic acid is below 1mol/dm$^3$. As a result of this, samples initiated with low concentrations of acetic acid (0.5mol/dm$^3$) may show no signs of filiform corrosion for up to 3 weeks. On samples initiated with 2µl of 1.5 or 2 mol/dm$^3$ acetic acid, this initiation period was not measurable as it was less than 1 week. On both of these samples, visible filiform corrosion had initiated within several days. When the length of an individual propagating filament is measured over time, its rate of growth was found to be linear. The maximum rate of growth measured is 1.4mm/week, when initiated with 2mol/dm$^3$ acetic acid, and a minimum of 0.83mm/week when initiated with 0.5mol/dm$^3$ acetic acid. Therefore, when corrosion is initiated with higher concentrations of acetic acid, the propagation rate of filaments is higher. However it must be noted that although higher concentrations of acid showed greater propagation rates, the range in filament length from a single defect was measured to be over 400%, and therefore by comparison this is a relatively small kinetic effect. However low concentrations of acetic acid also produce fewer filiform corrosion filaments per defect.

During propagation, the rate of filament growth is linear, meaning that the rate of the anodic and cathodic reaction is independent of filament length; and therefore the rate of the cathodic reaction is not limited by mass transport of oxygen through the tail to the head. It also indicates that filament length has no effect on the ionic conductivity between the anode and the cathode, and therefore the distance between the anode and the cathode is deduced to remain constant, regardless of filament length. At the anodic reaction site, the anodic dissolution reaction of the highly anodic $MgZn_2$ phase in the Zn-Al-Mg coating which will occur. The physical location of this site is at the front of the filament head. The cathodic reaction sites are most likely to be iron, either in the form of the substrate, or in the form of iron dross particles in the coating (91). Zinc and aluminium are more noble species than magnesium, however it is unlikely that these are very efficient at supporting a cathodic reaction due to the high over potentials that would be required.

## 3.6 Filament Morphology

Filiform corrosion filaments are composed of a head, filled with acetic acid, and a tail composed of corrosion product as described in section 1.7.6. On Zn-Al-Mg hot dip steel coatings the main corrosion product will be zinc oxide, which is highly porous in nature (5). As a result of this, oxygen can freely diffuse up the filament tail to the head. The morphology of filiform corrosion filaments was studied in further detail using an SEM. For SEM observations the organic coating is removed by immersing the sample in hexane for 15 minutes in an ultrasound bath. EDX studies show that the tail is depleted in zinc, and rich in iron in comparison to the un-corroded Zn-Al-Mg hot dip coating surface. These EDX elemental maps are shown in figure 3-10. There are also comparatively low levels of aluminium and magnesium present in the filament tail, indicating that the entire Zn-Al-Mg coating has been removed. In the head region levels of magnesium and aluminium are significantly depleted. There is also a reduction in the amount of zinc present; although some zinc will still remain. Increased levels of oxygen are also measured in the head region indicating that not all oxide has been removed during ultrasound cleaning. A potential reason for this may be that there is greater underlying topography in the Zn-Al-Mg coating as it has been partially etched, and therefore complete removal of oxide product proved to be more difficult. It may also be a different form of oxide to that found in the tail. A schematic diagram showing the proposed chemical reactions in the filament head is shown in figure 3-9.

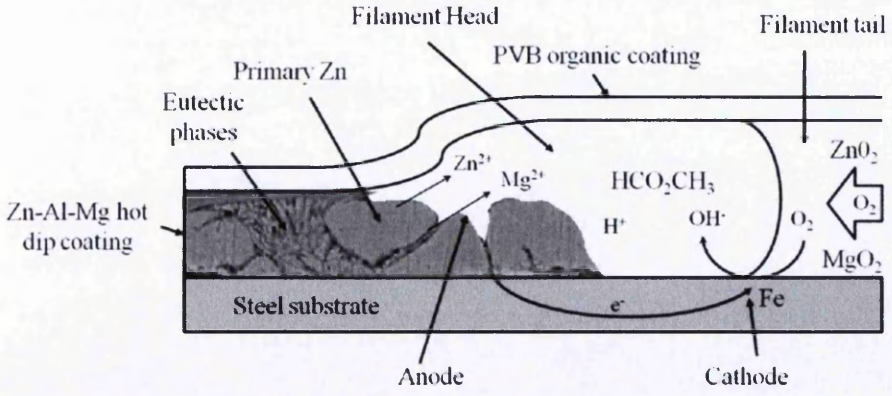


**Figure 3-9 :** Schematic diagram of filiform corrosion filament heat on ZN-Al-Mg hot dip coated steel. Anodic dissolution of the $MgZn_2$ phase exposed the steel substrate. This steel substrate then supports the cathodic reaction. Oxygen can diffuse to the reaction sites by diffusing up the tail of corrosion product.

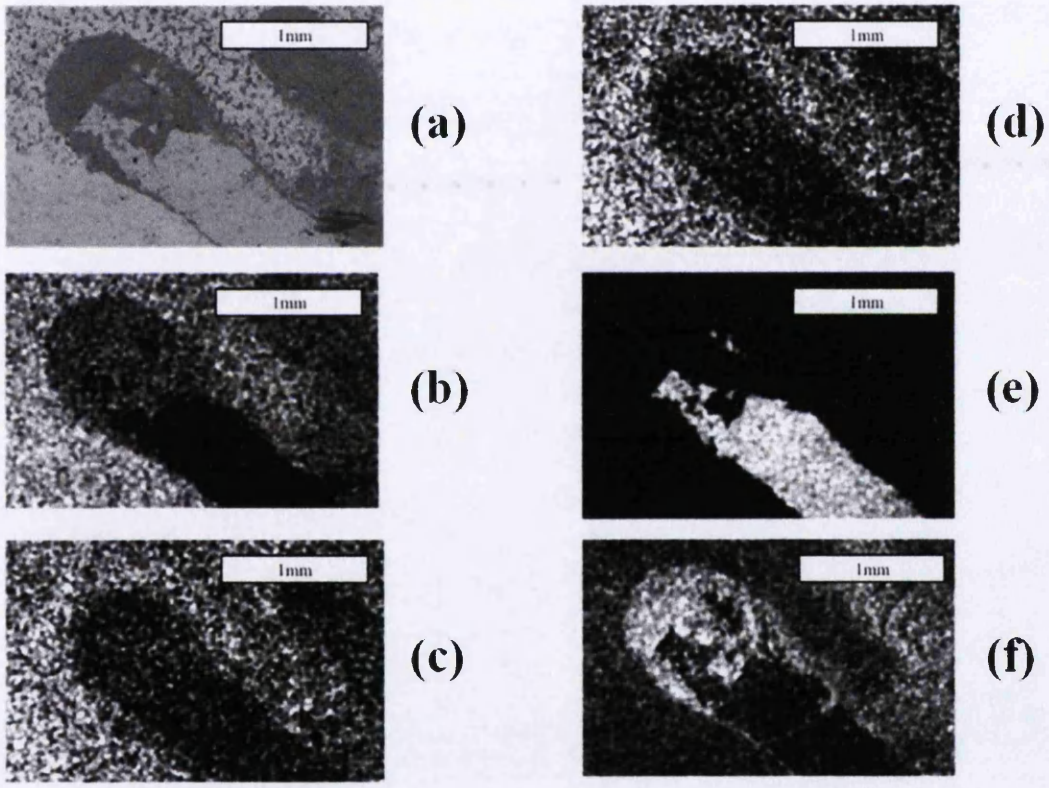


**Figure 3-10 : SEM and Energy Dispersive Spectroscopy (EDX); All images (a-f) are of the same area and magnification on the sample surface (a)** Scanning Electron Microscope backscatter image of a filiform corrosion filament on the surface of Zn-Mg-Al hot dip coated steel with a coating composition of Al 1.5wt% + Mg 1.5wt% and a coating weight of 140g/m$^2$ with a corresponding coating thickness of ~10µm. PVB organic coating and corrosion product have been stripped off by sample immersion in hexane, and unltrasonication for 10 minutes. **(a)** Backscatter SEM image showing a filiform corrosion filament. Images **(b-f)** are all EDX elemental maps showing the presence of **(b)** zinc **(c)** aluminium **(d)** magnesium **(e)** iron **(f)** oxygen.

Selective etching of the $MgZn_2$ eutectic phase by acetic acid can be visually seen on SEM backscatter images and EDX elemental maps focused at the front of a filiform filament. This is shown in figure 3-11. It is evident that initially in the corrosion process the primary zinc grains remain intact, however the eutectic phase around the grain is removed due to anodic dissolution. SEM EDX etching results are shown in figure 3-10, and the preferential etching of the eutectic to the front of a filiform corrosion filament is shown in figure 3-11.

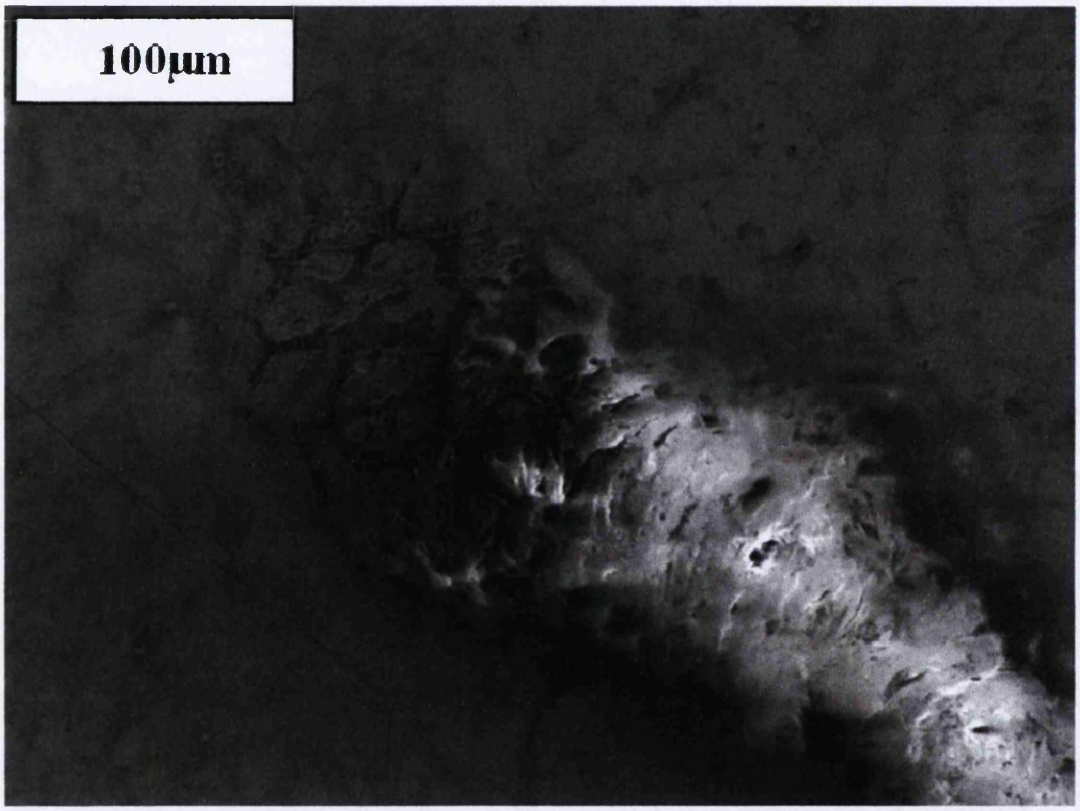


**Figure 3-11** SEM backscatter image taken with a Hitachi TM3000 desktop SEM showing the preferential anodic dissolution of the $MgZn_2$ rich eutectic phase in the binary eutectic in relation to the primary zinc grains

## 3.7 Acetic Acid Etching of Zn+Al+Mg hot dip coated steel

Anodic dissolution will preferentially occur in selected phases of the Zn-Al-Mg hot dip coating in acetic acid immersion conditions. This is studied using time dependant EDX analysis as described in section 2.6. Commercial hot dip coating systems are used for this study, rather than individual phases, in the form of separate homogenous phase samples, so that any galvanic effects between the different phases in the hot dip

coating, and in the underlying steel are taken in to account. It has been found that during immersion conditions, corrosion initiates in the $MgZn_2$ phase of the binary and ternary eutectics. Anodic dissolution rates of $MgZn_2$ are initially low until the point of exposing the underlying steel substrate. When the steel substrate is exposed the anodic dissolution rate of $MgZn_2$ increases dramatically. This can also be seen by the high rate of $MgZn_2$ dissolution localized to areas where the steel substrate is exposed, such as at cut edges and the penetrative defect. Initially the cathodic reaction sites are most likely to be iron dross particles on the surface on the Zn-Al-Mg coating, which means the current density of the cathodic reaction will be extremely high as iron dross particles occupy a very small percentage of the surface area of the Zn-Al-Mg hot dip coating. Some $MgZn_2$ in the binary eutectic is a continuous phase from surface of the coating, down to the iron substrate. As a result of this anodic dissolution of the $MgZn_2$ phase in the binary eutectic can expose iron in the steel substrate. Upon exposure the steel substrate will become the primary cathode, and as a result of the subsequent cathodic area increase, the cathodic current density will no longer be the limiting factor and therefore the rate of the cathodic reaction will increase by an order of magnitude, resulting in an increase in the overall rate of corrosion. Following this the entire Zn-Al-Mg hot dip coating undergoes rapid anodic dissolution. The SEM micrograph shown in figure 3-12 shows this mechanism in relation to time. Figure 3-13 also shows a cross section of Zn-Al-Mg hot dip coating which has been immersed in $0.1 mol/dm^3$ acetic acid. Preferential dissolution of the binary eutectic phase is visually apparent.

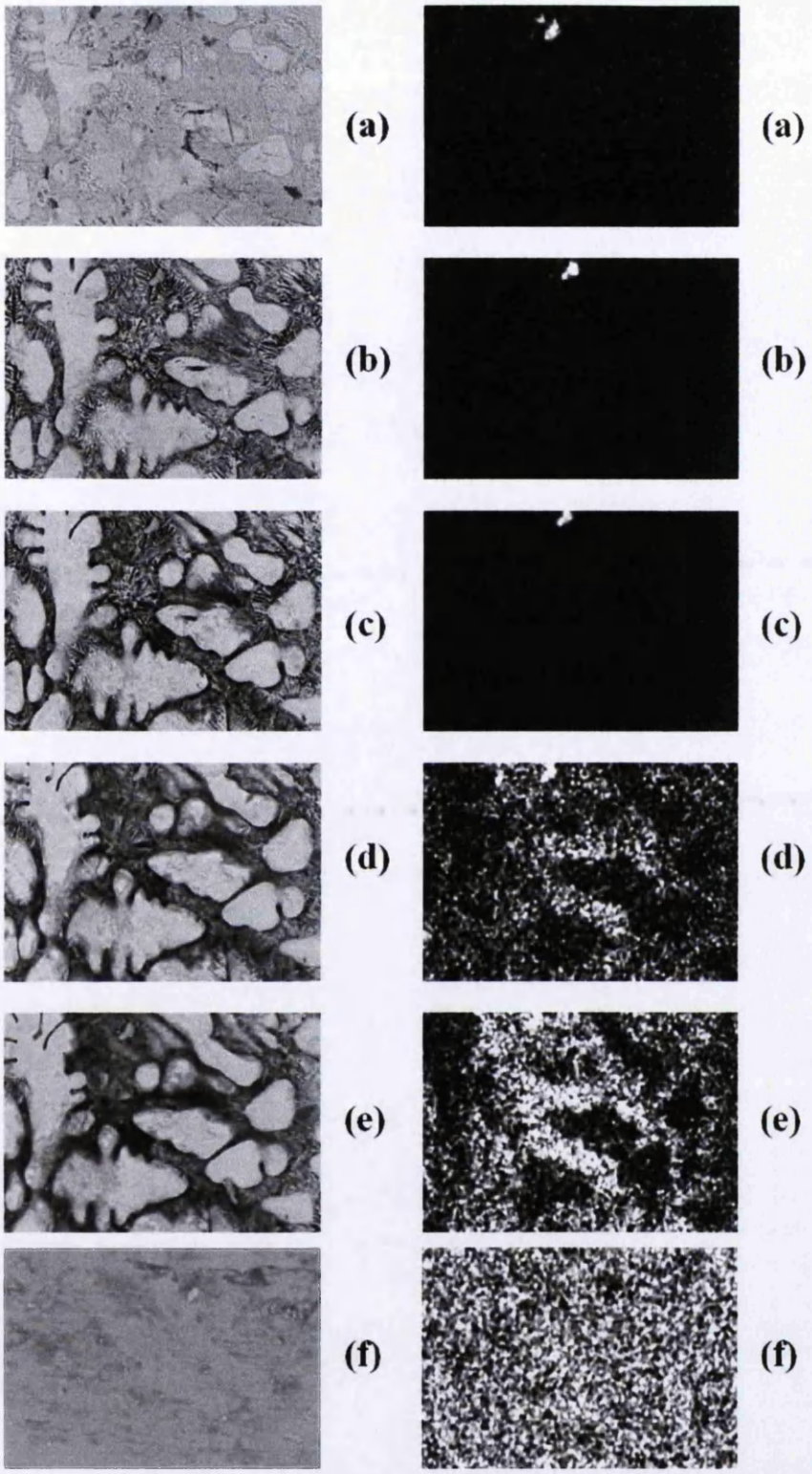


**Figure 3-12 :** SEM and Energy Dispersive Spectroscopy (EDX) images of a Al 1.5wt% + Mg 1.5wt% Zn-Al-Mg hot dip coated steel sample which has been immersed in 0.1mol/cm$^3$ acetic acid, and then the corrosion product has been removed by ultrasonication with hexane for 10 minutes. Images *left* are SEM backscatter and *right* are EDX elemental maps showing the corrososponding presence of surface iron. All images are at the same magnification, and of the same area. Immersion time for images are **(a)** 0 hours, **(b)** 1 hour, **(c)** 2 hours, **(d)** 3 hours, **(e)** 4 hours, **(f)** 5 hours

| time / hours | 1 | 2 | 3 | 4 | 5 |
|---|---|---|---|---|---|
| wt% iron | 0.71 | 0.91 | 4.79 | 6.22 | 52.68 |

**Table 3-3** : EDX measurement at 15KeV of iron over the entire imaged surface (*Figure 3-12*) in relation to time

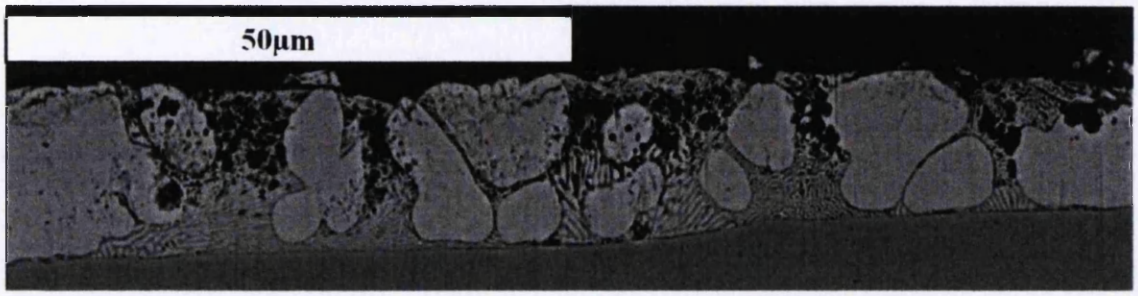


**Figure 3-13** : SEM backscatter image of a cross sectional micrograph of Al 1.5wt% + Mg 1.5wt% Zn-Al-Mg hot dip coated steel with a coating weight of 140g/m$^2$ after been etched with 0.1mol/dm$^3$ acetic acid for 2 hours. Preferential dissolution of the less noble eutectic phases can be seen between the larger homogeneous primary zinc grains

## 3.8 AFM

Atomic Force Microscope (AFM) topographical maps of Zn-Al-Mg hot dip coated steel samples have been composed to show the surface topography of Zn-Al-Mg hot dip coated steel after immersion in 0.1mol/dm$^3$ acetic acid for 1 hour. Topographical maps show a material has been removed around the grain boundaries of the primary zinc phase. It is in this region that the binary eutectic phase is found. The topography of material removal also shows a lamella structure indicating that one of the binary eutectic phases has been preferentially anodically dissolved at a higher rate. Topographical maps of Zn-Al-Mg hot dip coated steel after acetic acid immersion are shown in figure 3-14.

SKPFM studies were also carried out in order to investigate the potential contrast between the different phases in the Zn-Al-Mg coating. The potential of primary zinc

is shown to be homogeneous, and the potential of the zinc region of the binary eutectic is similar to the potential of primary zinc. The surface potential of the $MgZn_2$ phase of the binary is measured to be ~150 millivolts less than the potential of the surrounding zinc. The reason the full theoretical contrast is not observed is due to the AFM tip been 50nm from the surface of the Zn-Al-Mg hot dip coating, and this distance is too large to measure the full potential contrast (92) . Some contrast is also seen in the ternary eutectic phase. However this is unresolved due to resolution limitations of the experimental technique. However the average contrast of the ternary eutectic phase is still significantly less noble that the primary zinc grains. SKPFM surface potential maps are shown in figures 3-15 and 3-16.

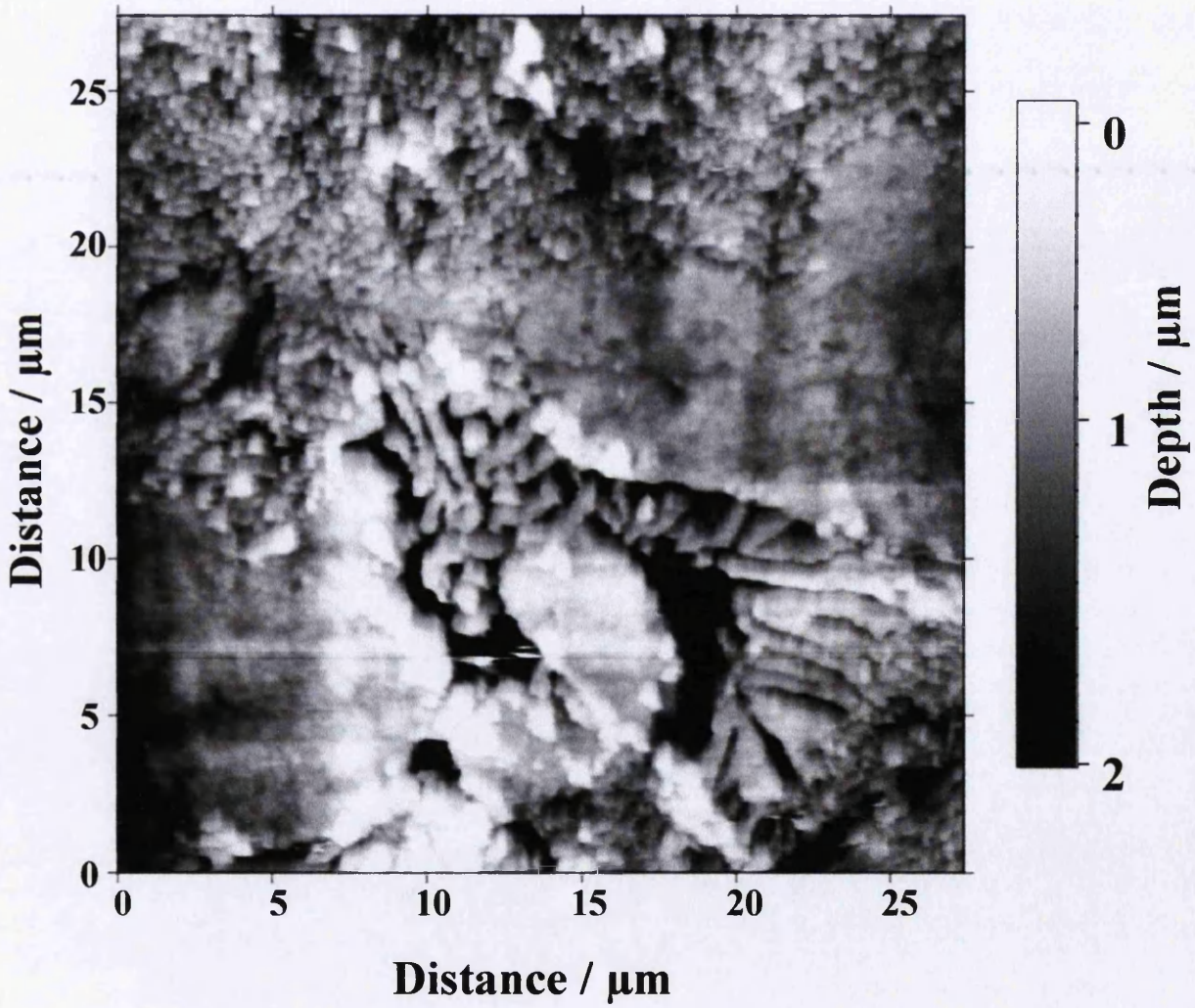


**Figure 3-14 :** Atomic force Microscope (AFM) topographical map (27µm x 27µm) of the surface of Al 1.5wt% Mg 1.5wt% Zn-Al-Mg hot dip coated steel after 1 hour of etching in 0.1mol/dm$^3$ acetic acid. Preferential dissolution of the less noble $MgZn_2$ in the binary eutectic can be observed.

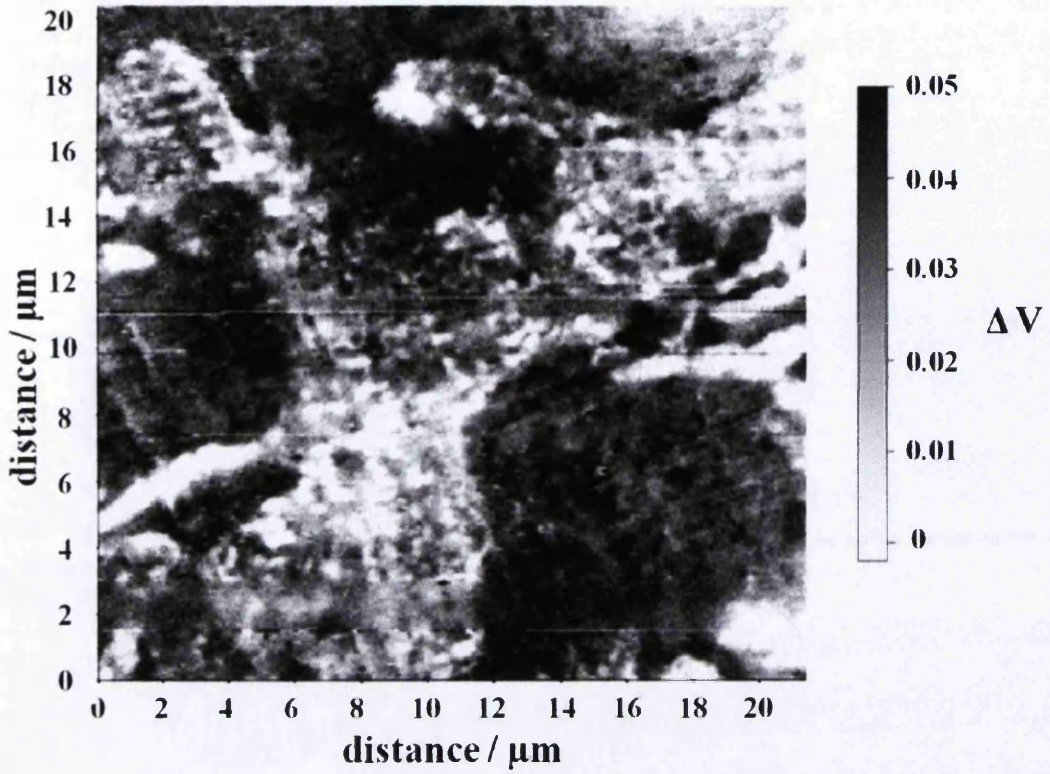


**Figure 3-15 :** SKPFM map (22µm x 22µm) of the surface of Al 1.5wt% Mg 1.5wt% Zn-al-Mg hot dip coated steel The light regions represent the more noble phase (primary zinc) and the light regions represent the less noble magnesium containing phases.

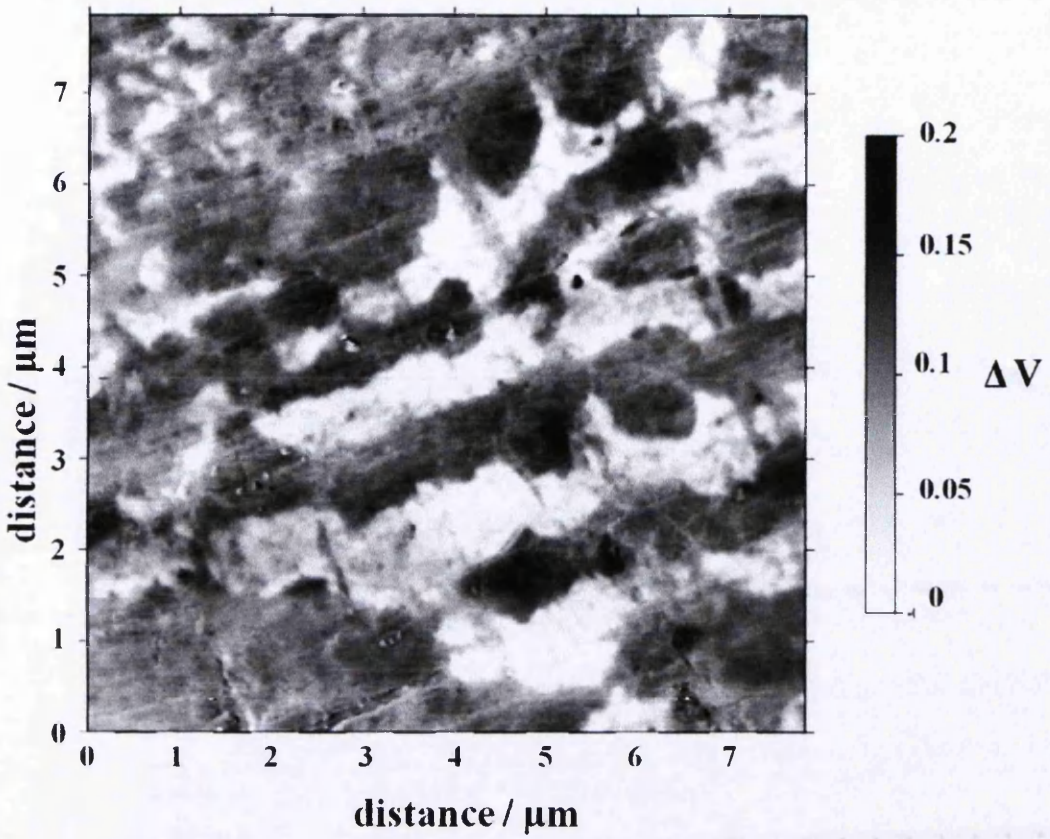


**Figure 3-16 :** SKPFM map (8µm x 8µm) of the binary eutectic on the surface of Al 1.5wt% Mg 1.5wt% Zn-Al-Mg hot dip coated steel The light regions represent the more noble phase (primary zinc) and the light regions represent the less noble $MgZn_2$ phase.

The AFM results show a correlation to the EDX results. The $MgZn_2$ phase is the least noble phase, and this phase supports the anodic reaction. This is seen both visually using EDX, and physically by topographical measurements with AFM. The SKPFM results show that the phase which is preferentially removed is the $MgZn_2$ phase.

## 3.9 Conclusion

The new generation of hot dip coatings containing magnesium and aluminium are susceptible to novel types of corrosion such as filiform corrosion. Of the tested electrolytes, acetic acid is the only electrolyte which has been found to initiate filiform corrosion reproducibly at a relative humidity of 86%. There is a large variance in the amount of filiform corrosion produced at each defect both in terms of total area

covered in corrosion, and the average number of filaments per defect. However a trend towards higher concentrations of acetic acid producing more corrosion can be seen. Concentrations of acid as low as 0.5mol/dm$^3$ were shown to produce filiform corrosion and higher concentrations such as 1.5mol/dm$^3$ produced approximately 5 times more corrosion. Due to the spread in data this has not been statistically analysed. However all future work in this thesis will use 1.5mol/dm$^3$ of acetic acid as this produced the most consistent and reliable results.

From EDX and AFM studies the mechanism of filiform initiation show that the $MgZn_2$ phase is the preferential site for the anodic reaction to occur. This can be visually seen during immersion etching experiments where this phase is preferentially removed. It can also be seen on images of filiform corrosion filaments where the binary eutectic has been removed ahead of the filiform filament. The resultant surface topography from $MgZn_2$ removal will also draw more electrolyte into the hot dip coating via an osmotic effect further promoting the removal of $MgZn_2$. The rate of $MgZn_2$ removal is dependent upon the concentration of acetic acid. Lower concentrations will remove $MgZn_2$ at a slower rate, and less $MgZn_2$ will be removed. This is the reason that filiform initiation times are much higher on samples with low concentrations of $MgZn_2$. Micrographs of Zn-Al-Mg hot dip coatings show that this binary eutectic phase is constant down to the steel substrate. As EDX results have shown when this phase is removed the amount of steel exposed at the surface is greatly increased. Where this underlying steel substrate is exposed, this area will become strongly cathodic promoting a pH gradient and the formation of localised anodic activity. The distance between the anodic dissolution of the $MgZn_2$ phase, and exposed steel substrate will remain equidistant with time, which is why the rate of filament propagation is constant regardless of filament length.

With regards to the filiform corrosion filament the anodic dissolution of $MgZn_2$ happens ahead of the filament head. This is visually shown in the SEM image figure 3-11. The filament head is composed of a droplet of electrolyte. When the $MgZn_2$ has been removed the underlying steel substrate is also exposed. The remaining phases of the hot dip coating are then removed. The hot dip coating is completely removed, and the tail is composed of exposed steel and corrosion product. This is shown in figure 3-10. Oxygen can freely diffuse up this tail to the head,

meaning that the rate of the redox reaction in the head is constant regardless of filament length.

# Chapter 4 : The effect of hot dip coating composition and thickness on filiform corrosion on Zn+Al+Mg hot dip coated steel

## 4.1 Introduction

The addition of magnesium and aluminium alloying additions to zinc based hot dip coatings has been shown to increase time to red rust by 4 to 10 times in salt spray tests as is discussed in more detail in chapter 1 (58). For this reason, most major steel companies globally are developing and commercializing their own versions of Zn-Al-Mg hot dip coated steel products. However there is a significant range in compositions of commercially available Zn-Al-Mg coatings, which is shown in table 4-1.

| Manufacturer | Product Name | Coating composition |
|---|---|---|
| Tata | Magizinc | Zn + Al*(1.5wt%)* + Mg*(1.5wt%)* |
| Arcelormittal | Magnelis | Zn + Al*(3.5wt%)* + Mg*(3wt%)* |
| Nippon Steel | Super Dyma | Zn + Al*(11wt%)* + Mg*(3wt%)* + Si*(0.2wt%)* |
| Nippon Steel | Super Zinc | Zn + Al*(4.5wt%)* + Mg*(0.1wt%)* |
| Nippon Steel | Dyma Zinc | Zn + Al*(0.2wt%)* + Mg*(0.5wt%)* |
| Nisshin Steel | ZAM | Zn + Al *(6wt%)* + Mg *(3wt%)* |
| Thyssenkrupp | Zn-ecoprotect | Zn + Al *(1wt%)* + Mg *(1wt%)* |

**Table 4-1** : Table of commercially produced Zn-Al-Mg hot dip galvanised steel coatings including the bath compositions and product names.

As has previously been reported in chapter 3, organically coated Zn-Al-Mg hot dip steel is susceptible to filiform corrosion, when exposed to acetic acid and an elevated relative humidity. The aim of this chapter is to study the filiform corrosion characteristics when initiated with acetic acid on a range of Zn-Al-Mg hot dip coating compositions.

## 4.2 Materials

The filiform corrosion properties of two sets of samples are tested in this chapter. The first is a set of hot dip Zn-Al-Mg samples have a fixed coating weight of 140g/m$^2$ *(10$\mu$ thickness)* and systematically varied hot dip coating compositions. The bath compositions of these samples are shown in table 4-2, and these samples are labelled (a-d). All samples are commercially produced on 0.7mm gauge mild steel substrate. Compositions given in table 4-2 are the target bath compositions provided by the Tata steel.

| | Zinc (wt%) | Aluminium (wt%) | Magnesium (wt%) |
|---|---|---|---|
| (a) | 98 | 1 | 1 |
| (b) | 97 | 1.5 | 1.5 |
| (c) | 94 | 3 | 3 |
| (d) | 91 | 6 | 3 |

**Table 4-2** Bath composition of hot dip coatings been studied in this paper. All samples are line produced hot dip coated, with a coating weight of 140g/m$^2$ giving an average coating thickness of ~10μm, Substrate is a 0.7mm gauge mild steel

The second experiment uses samples of a fixed bath composition of Zn+Al*(1.5wt%)*+Mg*(1.5wt%)*, and systematically varied coating weights. The coating weights for these samples are shown in table 4-3, and samples are labelled (A-F). Samples A-F are commercially produced on a 0.7mm gauge mild steel substrate.

| Sample id | Coating weight ($g/m^2$) | Coating thickness (μm) |
|---|---|---|
| (A) | 70 | 5 |
| (B) | 100 | 7 |
| (C) | 140 | 10 |
| (D) | 200 | 14 |
| (E) | 275 | 20 |
| (F) | 350 | 27 |

**Table 4-3 :** List of samples with systematically varied coating thicknesses and a fixed bath composition of Zn+Al*(1.5wt%)*+Mg*(1.5wt%)*. All samples are line produced on to 0.7mm mild steel substrate.

## 4.3 Methodology

Filiform corrosion is initiated using the technique described in section 2.1. Corrosion is initiated with 2μl of 1.5mol/$dm^3$ acetic acid per 10mm penetrative defect, and propagation conditions are 22°c and at a relative humidity of 86%. Corrosion measurements are carried out with digital image analysis using Sigma Scan Pro 5 as described in section 2.3. All other chemicals used are from the sigma chemical company in analytical grade purity.

## 4.4 Characterization of samples (a-d)

The microstructural phases and compositions of samples (a-d) are characterized using Energy dispersive x-ray spectroscopy (EDX) in a Hitachi TM3000 SEM. Samples are prepared by abrasive cleaning with an aqueous slurry of 4 μm alumina powder and deionised water, and organic residue is removed by immersing the sample in hexane in an ultrasound bath for 5 minutes. Samples are removed and rinsed with deionised water. No further preparation is carried out. Figures 4-1 to 4-4 show SEM backscatter images of the surface of Zn-Al-Mg hot dip coated steel samples (a-d). It must be noted that due to the rapid cooling conditions found in hot dip coatings, the microstructural

phases present are non-equilibrium phases, and therefore may not correspond to the phases predicted by the equilibrium ternary phase diagram. These images show a clear change in the physical appearance of the microstructure over the range of compositions tested. From studying these images it can be deduced that as the alloying additions of magnesium and aluminium are increased, greater levels of binary and ternary eutectic are seen, and the level of primary eutectic is reduced. This correlates with work carried out by Vlot *et al*[8] who stated that the average composition of the Zn-$MgZn_2$-Al ternary eutectic is Zn+Mg*(3.2wt%)*+Al*(3.2wt)*

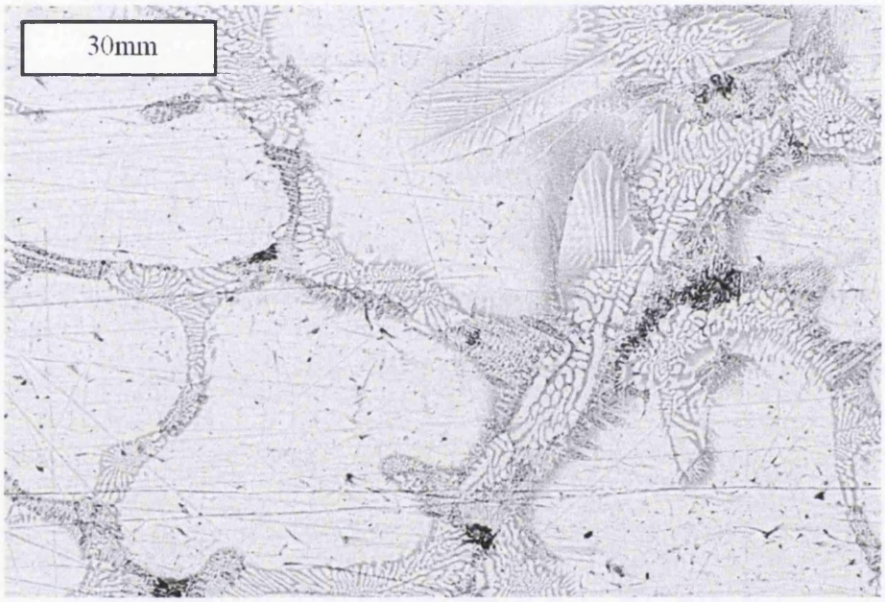


**Figure 4-1** SEM backscatter image of the surface of a Zn-Al-Mg hot dip steel coating (a) (composition Al 1wt% + Mg 1wt%) with a coating thickness of 140g/m$^2$ on a 0.7mm thick mild steel substrate.

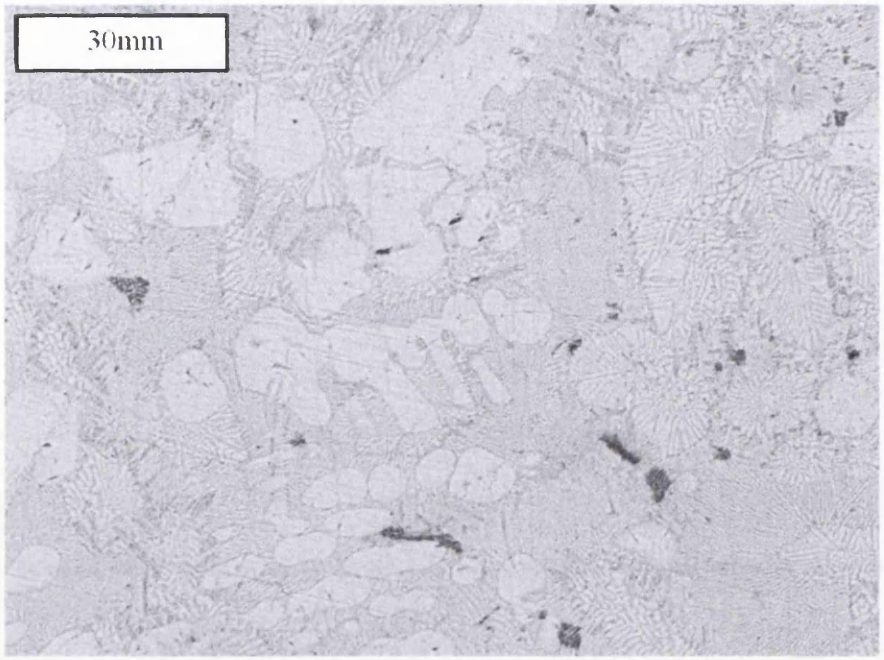


**Figure 4-2** SEM backscatter image of the surface of a Zn-Al-Mg hot dip steel coating (b) (composition Al 1.5wt% + Mg 1.5wt%) with a coating thickness of 140g/m$^2$ on a 0.7mm thick mild steel substrate. Sample is like produced commercial quality

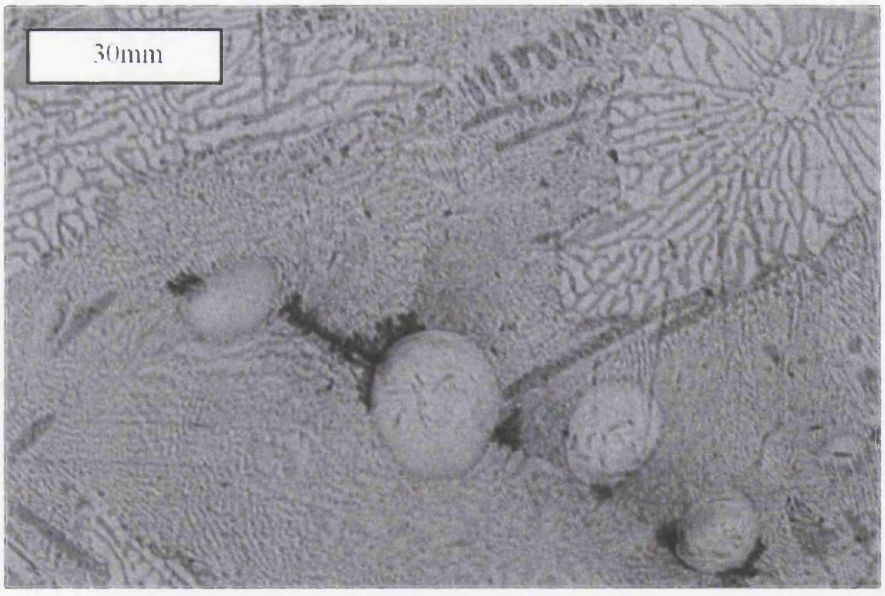


**Figure 4-3** SEM backscatter image of the surface of a Zn-Al-Mg hot dip steel coating (c) (composition Al 3wt% + Mg 3wt%) with a coating thickness of 140g/m$^2$ on a 0.7mm thick mild steel substrate. Sample is like produced commercial quality

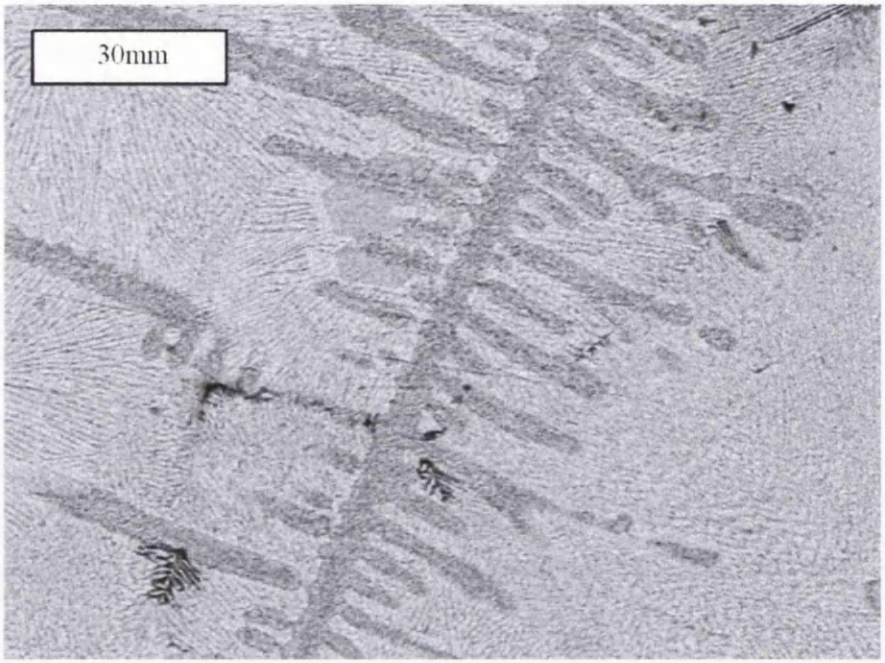


**Figure 4-4** SEM backscatter image of the surface of a Zn-Al-Mg hot dip steel coating **(d)**(composition Al 6wt% + Mg 3wt%) with a coating thickness of 140g/m$^2$ on a 0.7mm thick mild steel substrate. Sample is like produced commercial quality

### 4.4.1 Energy Dispersive X-Ray Spectroscopy elemental Mapping

In order to characterize samples (a-d) elemental mapping is carried out using the technique described in section 2.5 in a Hitachi TM3000 SEM using EDX. These maps show the physical location of zinc, aluminium and magnesium with respect to microstructural phases which can be visually observed with back scatter SEM images. Elemental maps for **(i)** Backscatter SEM image, **(ii)** zinc, **(iii)** aluminium and **(iv)** magnesium for samples (a-d) are shown in figures 4-5 to 4-8.

**Sample a (98wt%Zn, 1wt%Al, 1wt%Mg)**

The stated bath composition of sample (a) is 1wt% Mg ad 1wt% Al. The average surface composition measured over a 5x5mm region was 1.24wt% Mg and 1.65wt% Al. The reason for this differing from the bath composition may be due to fluctuation in the bath, or it may be due to surface enrichment of Mg an Al, or a combination of factors. The three main phases detected in sample a are primary zinc, which has an equaxed form, a course binary eutectic and a finer ternary eutectic. The primary zinc

phase is composed almost entirely of zinc (99.74wt%) with small amounts of aluminium (0.17wt%) and magnesium (0.09wt%). The aluminium and magnesium are most likely in solid solution with the zinc. The binary eutectic is visually much coarser than the ternary eutectic with a lamella spacing of approximately 500nm, although some lamella are up to two μm thick. The composition of this phase is 95.94 wt% zinc, 3.60wt% magnesium and 0.47wt% aluminium. This correlates to the literature where Vlot *et al* state that the binary eutectic is composed of zinc and $MgZn_2$. The ternary eutectic is much finer than the binary eutectic with a lamella spacing of approximately 200nm and the composition of this phase is 91.99wt% zinc, 4.04wt% aluminium and 4.08wt% magnesium. Again this correlates with Vlot *et al* who state that ternary eutectic is composed of Zinc, $MgZn_2$ and an Aluminium rich phase. The area of the surface was also measured by overlaying the image of the surface on to a grid and measuring the percentage of the grid which was covered by each phase. Percentages are rounded to the nearest 10% as there is a large variance depending on the area of the surface been measured. For sample (a) approximately 80% of the total surface area is primary zinc, and 10% is binary eutectic, and 10% is ternary eutectic.

**Sample b (978wt%Zn, 1.5wt%Al, 1.5wt%Mg)**

The microstructural phases seen in sample (b) are the same as the phases found in sample (a); primary zinc, binary eutectic and ternary eutectic. The composition of each phase is primary zinc, (99.64wt% zinc, 0.02wt% aluminium and 0.34wt% magnesium); binary eutectic (95.13wt% zinc, 0.66wt% aluminium and 4.21wt% magnesium) ; ternary eutectic (90.62wt% zinc, 4.02wt% aluminium and 4.36wt% magnesium). However the major difference between sample (a) and sample (b) is that on sample (b) with a higher wt% of aluminium and magnesium in the hot dip bath the total area covered by primary zinc is dramatically reduced. Primary zinc covers approximately 30% of the total surface area of sample (b) the binary eutectic occupies another 30% of the total surface area and the remaining 40% of the surface area is composed of ternary eutectic.

**Sample c (94wt%Zn,3wt%Al, 3wt%Mg)**

Sample (c) differs from samples (a) and (b) as virtually no primary zinc is observed. 50% of the sample surface is covered with a ternary eutectic. 30% of the surface is also covered by binary eutectic. A new aluminium rich phase is also observed which is not seen on samples (a) or (b), and this phase covers approximately 10% of the sample surface. The composition of phases found on the surface is as follows; primary zinc (99.45wt% zinc, 0.09wt% aluminium, 0.46wt% magnesium); binary eutectic (94.75wt% zinc, 0.51wt% aluminium, 4.74wt% magnesium); ternary eutectic (89.79wt% zinc, 7.39wt%aluminium, 0.12wt% magnesium), aluminium rich phase (80.56wt% zinc, 19.32wt% aluminium, 0.12wt% magnesium).

**Sample d (91wt%Zn,6wt%Al, 3wt%Mg)**

Sample d has no primary zinc phase at all, and a approximately 20% of the surface area is aluminium rich phase, which has a dendritic appearance. Virtually all of the remaining coating (approximately 70%) is ternary eutectic with only a small amount (10%) of binary eutectic present. The binary eutectic composition is (95.42wt% zinc, 0.45wt% aluminium, 4.13wt% magnesium) ; the ternary eutectic is (89.74wt% zinc, 3.90wt% aluminium and 6.36wt% magnesium). This shows a higher level of magnesium in the ternary eutectic than sample a,b and c. The composition of the aluminium rich phase is (79.24wt% zinc, 21.71wt% aluminium and 0.04wt% magnesium). This is consistent with sample c.

An overview of phase compositions and the total percentage of the surface area occupied by each phase is shown in tables 4-4 and 4-5 and EDX micrographs are shown in figures 4-5 to 4-8.

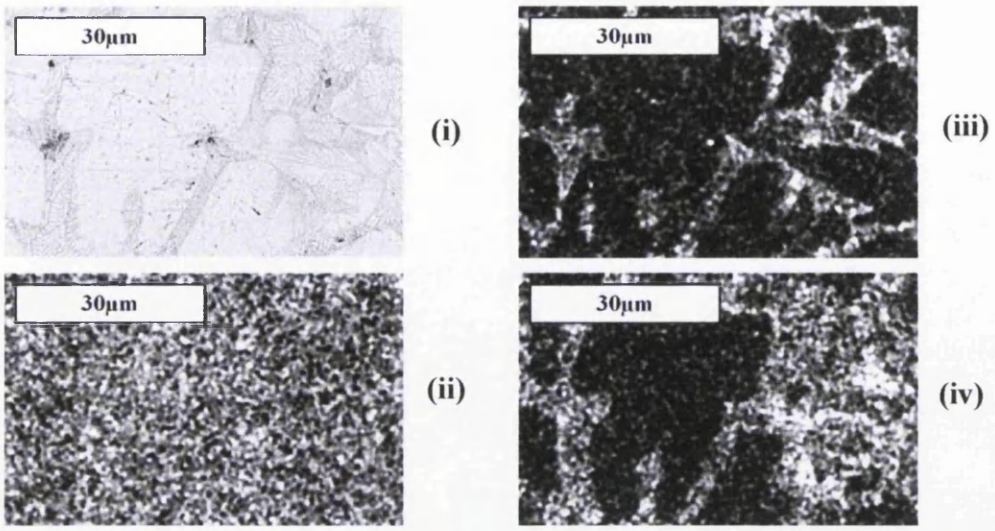


**Figure 4-5 : SEM and Energy Dispersive Spectroscopy (EDX); All images (i,ii,iii,iv) are the same area and magnification on the sample surface (i)** Scanning Electron Microscope backscatter image of the surface of Zn-Mg-Al hot dip coated steel with a coating composition of **Al 1wt% + Mg 1wt%** and a coating weight of 140g/m$^2$ with a corresponding coating thickness of ~10µm. Images **(ii-iv)** are EDX elemental maps showing elemental distributions on the sample surface of **(ii)** zinc **(iii)** aluminium **(iv)** magnesium

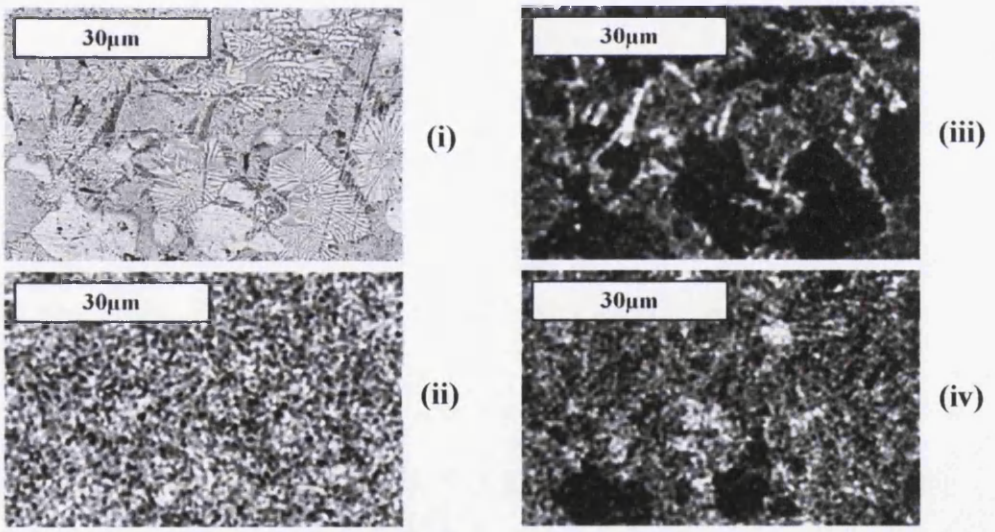


**Figure 4-6 : SEM and Energy Dispersive Spectroscopy (EDX); All images (i,ii,iii,iv) are the same area and magnification on the sample surface (a)** Scanning Electron Microscope backscatter image of the surface of Zn-Mg-Al hot dip coated steel with a coating composition of **Al 1.5wt% + Mg 1.5wt%** and a coating weight of 140g/m$^2$ with a corresponding coating thickness of ~10µm. Images **(b-d)** are EDX elemental maps showing elemental distributions on the sample surface of **(b)** zinc **(c)** aluminium **(d)** magnesium

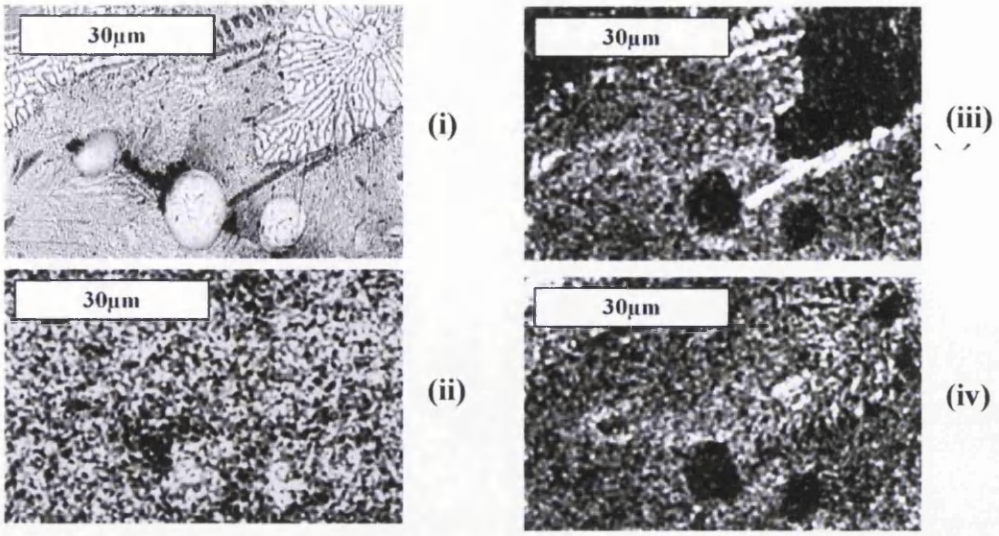


**Figure 4-7 : SEM and Energy Dispersive Spectroscopy (EDX); All images (i,ii,iii,iv) are the same area and magnification on the sample surface (i)** Scanning Electron Microscope backscatter image of the surface of Zn-Mg-Al hot dip coated steel with a coating composition of **Al 3wt%+ Mg 3wt%** and a coating weight of 140g/m$^2$ with a corresponding coating thickness of ~10µm. Images **(ii-iv)** are EDX elemental maps showing elemental distributions on the sample surface of **(ii)** zinc **(iii)** aluminium **(iv)** magnesium

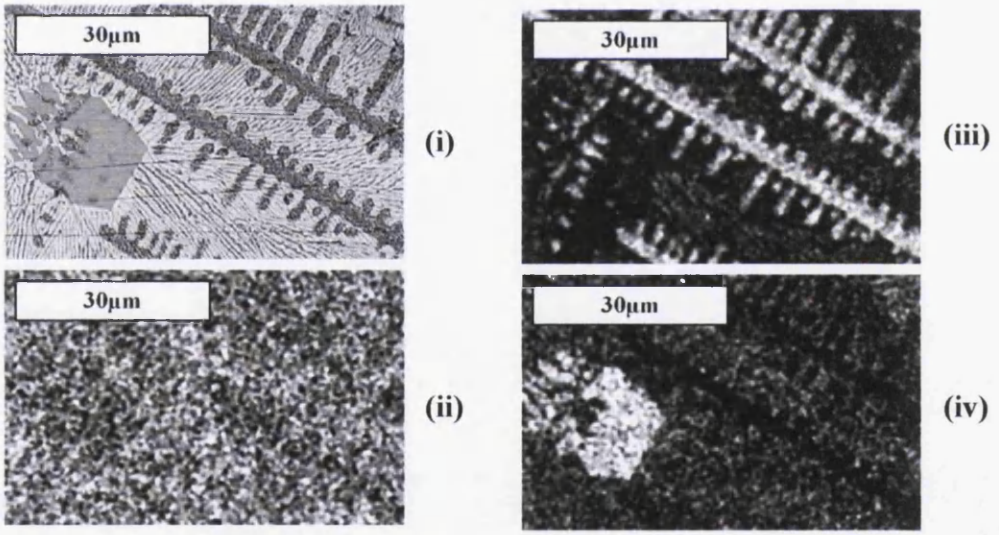


**Figure 4-8 : SEM and Energy Dispersive Spectroscopy (EDX); All images (i,ii,iii,iv) are the same area and magnification on the sample surface (i)** Scanning Electron Microscope backscatter image of the surface of Zn-Mg-Al hot dip coated steel with a coating composition of **Al 6wt% + Mg 3wt%** and a coating weight of 140g/m$^2$ with a corresponding coating thickness of ~10µm. Images **(ii-iv)** are EDX elemental maps showing elemental distributions on the sample surface of **(ii)** zinc **(iii)** aluminium **(iv)** magnesium

| Coating composition | Primary Zinc | Binary Eutectic | Ternary Eutectic | Zn/Al phase |
|---|---|---|---|---|
| Zn(99.9wt%) + Al(0.1wt%) | 100 | 0 | 0 | 0 |
| Zn + Al(1wt%) + Mg(1wt%) | 80 | 10 | 10 | 0 |
| Zn +Al(1.5wt%) + Mg(1.5wt%) | 30 | 30 | 40 | 0 |
| Zn + Al(3wt%) + Mg(3wt%) | 10 | 30 | 50 | 10 |
| Zn + Al(6wt%) + Mg(3wt%) | 0 | 10 | 70 | 20 |

**Table 4-4**: Approximate surface area covered by each phase as measured using EDX and Sigma scan image analysis found in Zn-Al-Mg hot dip coatings over tested range of compositions

| Sample | Phase | Zinc (wt%) | Aluminium (wt%) | Magnesium (wt%) |
|---|---|---|---|---|
| (a) | Primary zinc | 99.74 | 0.17 | 0.09 |
| (a) | Binary eutectic | 95.94 | 0.47 | 3.6 |
| (a) | Ternary eutectic | 91.88 | 4.04 | 4.08 |
| (b) | Primary zinc | 99.64 | 0.02 | 0.34 |
| (b) | Binary eutectic | 95.13 | 0.66 | 4.21 |
| (b) | Ternary eutectic | 90.62 | 4.02 | 4.36 |
| (c) | Primary zinc | 99.45 | 0.09 | 0.46 |
| (c) | Binary eutectic | 94.75 | 0.51 | 4.74 |
| (c) | Ternary eutectic | 89.79 | 7.39 | 3.82 |
| (c) | Zn-Al phase | 80.56 | 19.32 | 0.12 |
| (d) | Binary eutectic | 95.42 | 0.45 | 4.13 |
| (d) | Ternary eutectic | 89.74 | 3.90 | 6.36 |
| (d) | Zn-Al phase | 79.24 | 21.71 | 0.04 |

**Table 4-5** : Phase composition of each phase measured in normalised wt% on Zn-Al-Mg samples **(a-d)** using Quantax 70 EDX on a Hitachi TM3000 desktop SEM at an accelerating voltage of 15KeV

## 4.5 Filiform corrosion (sample a-d)

### 4.5.1 Methodology

Filiform corrosion is initiated using the technique described in section 2.1 using 2µl of 1.5mol/dm3 acetic acid per defect and propagation conditions of 86% relative humidity and a controlled temperature of 22°C. The total corroded area is analysed in relation to time for each sample using digital image analysis, described in section 2.2 and 2.3.

### 4.5.2 Results

**Sample a**

Sample **(a)** Zn+Al*(1wt%)*+Mg*(1wt%)* is found to have the least resistance to filiform corrosion of all samples tested, with filaments seen to be propagating from the penetrative defect 48 hours after initiation. Filaments are seen to initiate from the penetrative defect and cut edges after less than a week. After approximately 3 weeks filaments also initiate from the intact sample surface, which is a phenomenon not observed on samples b, c or d, where all observed filiform filaments initiate at either the penetrative defect, or the sample cut edge. Figure 4.9 to 4.15 show the kinetics of filiform corrosion over time. Sample (a) has virtually no initiation time, and then the total corroded area increases linearly over the measured test period of 5 weeks. It must be noted that filaments initiating from the intact surface are very fine, and were therefore not measurable with sigma scan digital image analysis. The appearance of these filaments can be seen in figure 4-12. After 10 weeks surface corrosion became so wide spread on sample (a) that significant levels of coating delamination occurred resulting in a total coating failure. After 12 weeks red rust was visible on the surface of the sample.

**Sample b**

Sample (b) with a composition of Zn + Al*(1.5wt%)* + Mg*(1.5wt%)* shows increased corrosion resistance to filiform corrosion, when compared to sample (a). Initially some white corrosion is seen around the defect, but no filiform corrosion filaments are observed. After a period of 1-2 weeks filaments start to initiate from the penetrative defects. After this initiation period, the total corroded area increases initially at a similar rate to sample (a). On sample (b) filiform filaments propagating from the defect have a similar morphology to the filaments on sample (a) with a filament width of 50μm to 250μm. When compared to sample (a) fewer filaments are seen per penetrate defect, and on the cut edge. No filament are seen to initiate from the intact coating.

**Sample c**

Sample (c) Zn + Al*(3wt%)* + Mg*(3wt%)* shows an increased initiation period of 3-4 weeks before filiform corrosion filaments are visually observed. Once filiform corrosion has initiated the kinetics of the total corroded area are significantly slower than the propagation kinetics of samples (a) and (b) with total corroded area per defect increasing by an average of 0.494cm$^2$ per week. The morphology of filaments also appears to be different when compared to samples (a) and (b). The widest filaments seen on samples (a) and (b) are approximately 250μm wide. There are also a significant number of filaments with widths below 50μm seen on both sample (a and b). Filaments that initiate from the intact surface always have a width of less than 50μm on sample (a). On sample (c) there are far fewer filaments, and filaments have a width of up to 1mm. Furthermore very few thin filaments form, whilst on sample (a) and (b) the majority of filaments are in the 50 -200μm region.

**Sample d**

Sample (d) showed no filiform corrosion after the entire test period, and only a small amount of white corrosion is present around the penetrative defect. The visual appearance of samples with relation to time can be seen in figures 4-9 to 4-11) and the appearance of samples after the 12 week test can be seen in figures 4-12 to 4-15. Figure 4-16 shows the corrosion kinetics of the different samples graphically, showing the total corroded area in relation to time. Again the variance across the four defects is significant, but general trends can still be analysed. It is seen the level of aluminium in the sample is increased. On samples a,,b and c there is an initiation period. From chapter 3 it is most likely that this period correlates to the amount of time it takes to expose the underlying steel substrate. This theory is tested by etching the sample in 0.1mol/dm$^3$ acetic acid.



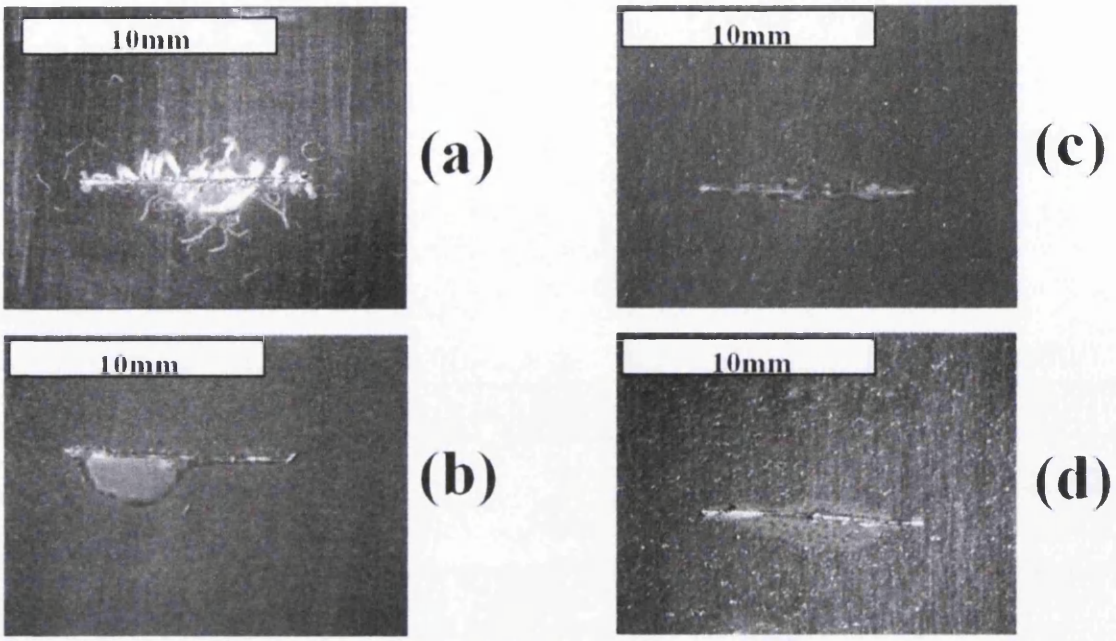


**Figure 4-9 :** Optical images taken with an optical stereo microscope of filiform corrosion around the 1cm long penetrative defect after **1 week**. Corrosion is initiated with 2µl of 1.5 molar acetic acid, and propagation occurs at a relative humidity of 86% and a temperature of 22°c. The coating composition of Zn-Al-Mg hot dip coating is **(a)** Zn+Al*(1wt%)*+Mg*(1wt%)* **(b)** Zn+Al*(1.5wt%)*+Mg*(1.5wt%)* **(c)** Zn+Al*(3wt%)*+Mg*(3wt%)* **(d)** Zn+Al*(6wt%)*+Mg*(3wt%)*

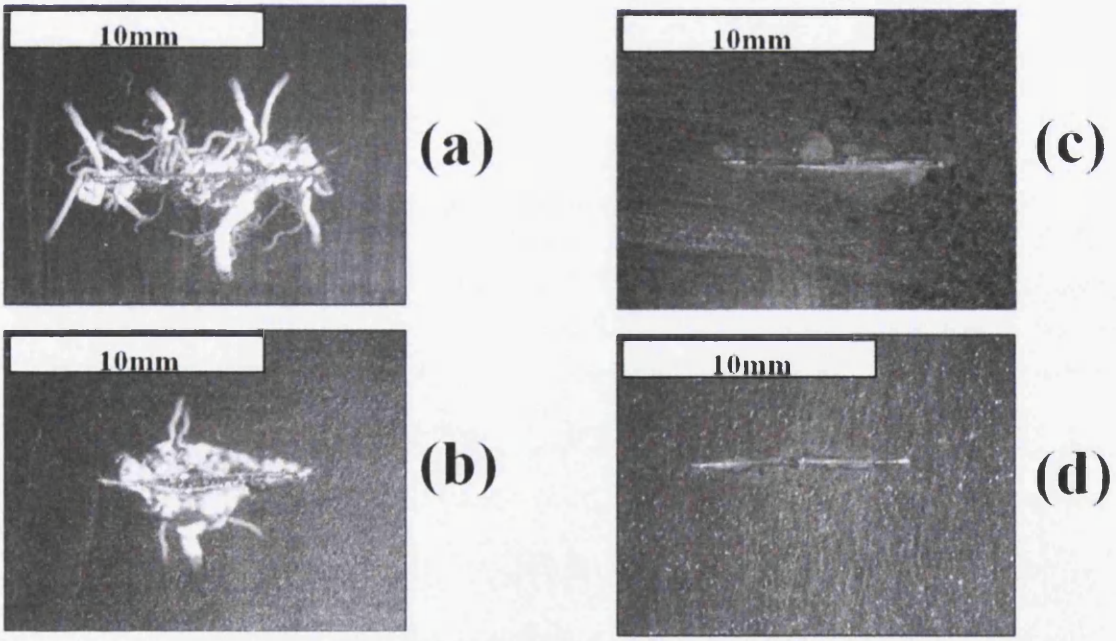


**Figure 4-10 :** Optical images taken with an optical stereo microscope of filiform corrosion around the 1cm long penetrative defect after **4 weeks**. Corrosion is initiated with 2µl of 1.5 molar acetic acid, and propagation occurs at a relative humidity of 86% and a temperature of 22°c. The coating composition of Zn-Al-Mg hot dip coating is **(a)** Zn+Al*(1wt%)*+Mg*(1wt%)* **(b)** Zn+Al*(1.5wt%)*+Mg*(1.5wt%)* **(c)** Zn+Al*(3wt%)*+Mg*(3wt%)* **(d)** Zn+Al*(6wt%)*+Mg*(3wt%)*

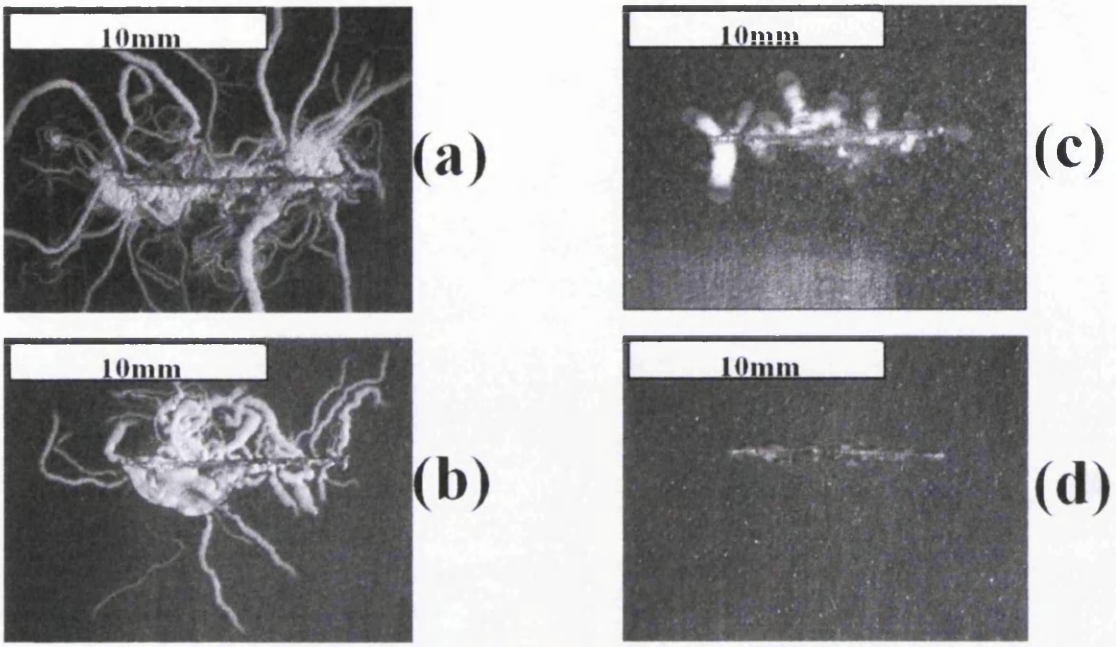


**Figure 4-11 :** Optical images taken with an optical stereo microscope of filiform corrosion around the 1cm long penetrative defect after **8 weeks**. Corrosion is initiated with 2µl of 1.5 molar acetic acid, and propagation occurs at a relative humidity of 86% and a temperature of 22°c. The coating composition of Zn-Al-Mg hot dip coating is **(a)** Zn+Al*(1wt%)*+Mg*(1wt%)* **(b)** Zn+Al*(1.5wt%)*+Mg*(1.5wt%)* **(c)** Zn+Al*(3wt%)*+Mg*(3wt%)* **(d)** Zn+Al*(6wt%)*+Mg*(3wt%)*

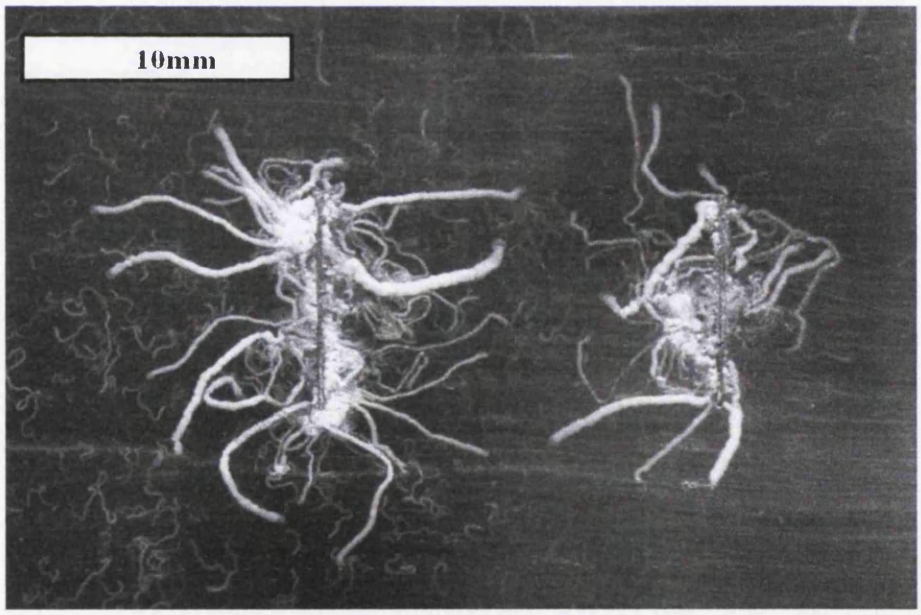


**Figure 4-12 :** Optical image of sample **(a)** Zn + Al*(1wt%)* + Mg*(1wt%)* hot dip coated mild steel sample after filiform corrosion initiation with 2µl of 1.5mol/dm$^3$ acetic acid per penetrative defect. Sample has been stored at a relative humidity of 86%, and a temperature of 22°c in a dessicator for 12 weeks. Significant levels of filiform corrosion can be seen to propagate from both the penetrative defects and the intact coat

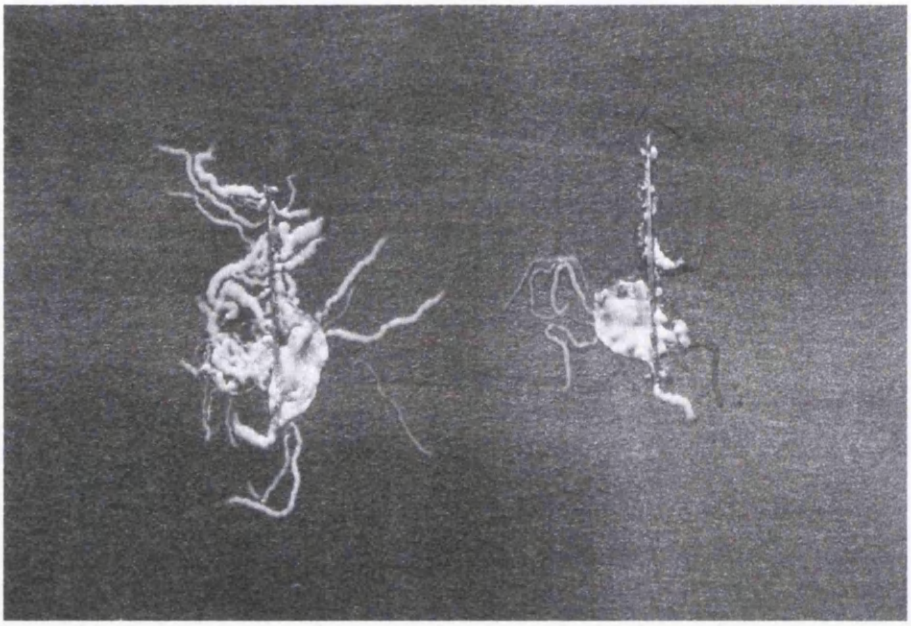

**Figure 4-13 :** Optical image of sample **(b)** Zn + Al*(1.5wt%)* + Mg*(1.5wt%)* hot dip coated mild steel sample after filiform corrosion initiation with 2µl of 1.5mol/dm$^3$ acetic acid per penetrative defect. Sample has been stored at a relative humidity of 86%, and a temperature of 22°c in a dessicator for 12 weeks. Filiform corrosion can be seen to propagate from both the penetrative defects and a small amount of filiform corrosion seems to initiate from the intake coating surface.

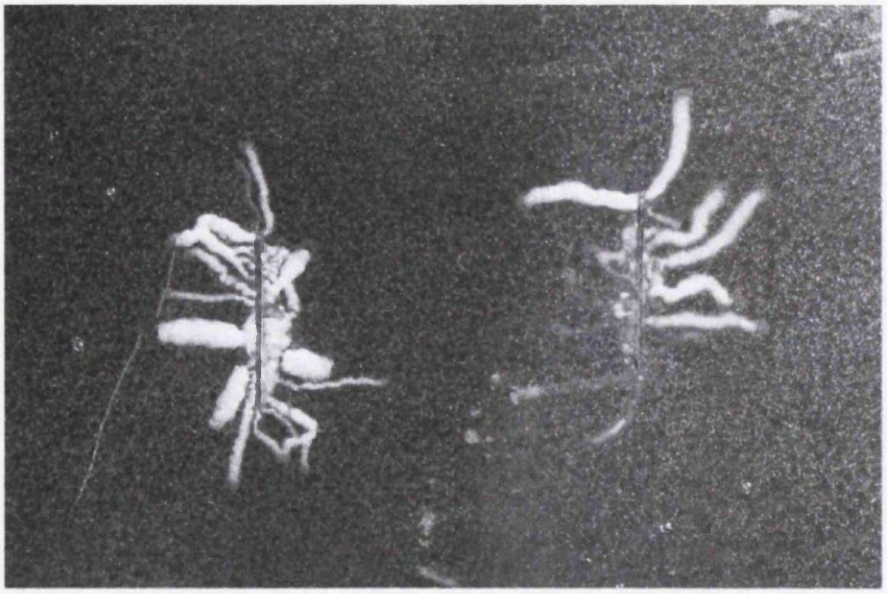

**Figure 4-14 :** Optical image of sample **(c)** Zn + Al*(3wt%)* + Mg*(3wt%)* hot dip coated mild steel sample after filiform corrosion initiation with 2µl of 1.5mol/dm$^3$ acetic acid per penetrative defect. Sample has been stored at a relative humidity of 86%, and a temperature of 22°c in a dessicator for 20 weeks. No filiform corrosion is seen to initiate in the intact sample surface. The defect filaments are also significantly thicker than those seen on samples **(a)** and **(b)**.

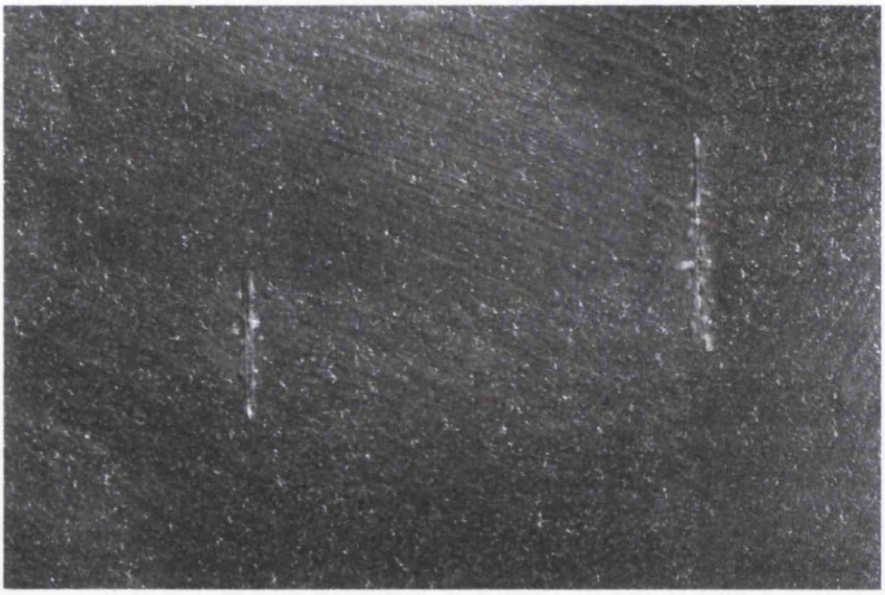

**Figure 4-15 :** Optical image of sample **(d)** Zn + Al*(6wt%)* + Mg*(3wt%)* hot dip coated mild steel sample after filiform corrosion initiation with 2µl of 1.5mol/dm$^3$ acetic acid per penetrative defect. Sample has been stored at a relative humidity of 86%, and a temperature of 22°c in a dessicator for 20 weeks. No filiform corrosion is visible after 12 weeks.

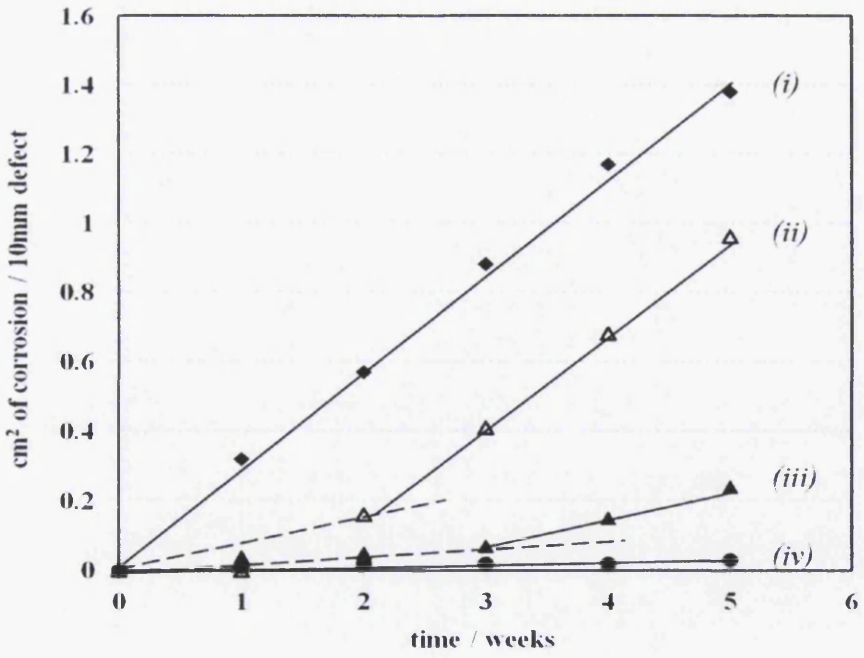


**Figure 4-16 :** The average total surface area covered in corrosion product around a 10mm penetrative defect averaged over 2 defects as measured using sigma scan digital image analysis. All samples are initiated with 2µl of 1.5mol/dm$^3$ aqueous acetic, and propagation occurs at a relative humidity of 86% and a temperature of 22°c. Lines represent Zn-Al-Mg hot dip coating compositions of **(i)** Zn+Al*(1wt%)*+Mg*(1wt%)* **(ii)** Zn+Al*(1.5wt%)*+Mg*(1.5wt%)* **(iii)** Zn+Al*(3wt%)*+Mg*(3wt%)* **(iv)** Zn+Al*(6wt%)*+Mg*(3wt%)*

## 4.6 Etching experiments (methodology)

If exposed, the steel substrate will form a highly efficient cathode with a large surface area as described in chapter 3. As a result of this time to iron exposure may be a critical variable in understanding the susceptibility of a hot dip coating composition to filiform corrosion.

Hot dip Zn-Al-Mg coated steel samples (samples a to d) are immersed in aqueous 0.1mol/dm$^3$ acetic acid. The experiment is carried out using the technique described in section 2.6. The sample is removed from the acetic acid every 30 minutes with PTFE tweezers, and rinsed in ethanol before SEM backscatter imaging and EDX elemental mapping analysis.

## 4.7 Results

The filiform corrosion resistance of the tested Zn-Al-Mg hot dip coatings (a to d) shows a strong correlation to the time to iron exposure during the etching experiments. On sample **(a),** which is highly susceptible to filiform corrosion, significant levels of iron are detected on the sample surface after 3 hours of immersion, in 0.1mol/dm$^3$ acetic acid. Furthermore after 4 hours immersion the entire hot dip coating has been removed. When the coating has been removed the only elements detected on the surface are iron and aluminium, all zinc and magnesium has been removed. Coatings with a greater resistance to filiform corrosion, such as sample **(c)** start to show increased levels of iron on the sample surface after 6 hours, and the coating has been completely removed after 8 hours. The time to iron exposure for samples a-d is shown in figure 4-24.

The corrosion mechanism of all coatings (samples a-d) when immersed in 0.1mol/dm$^3$ acetic acid show a similar trend. Within the first hour practically all of

the elemental magnesium has been removed from the surface of the coating as is shown in the EDX results. The proportion of surface aluminium also increases over time for all samples. This shows that magnesium is anodically dissolved very rapidly. Surface enrichment of aluminium is due to aluminium not been anodically dissolved by acetate.

After the first hour of immersion when surface magnesium is depleted, the resultant aluminium content on the surface of the coating has a large effect on the further corrosion resistance of the coating. It is proposed that on samples (c and d), with high aluminium content, 3 and 6wt% respectively, the surface concentration of aluminium is sufficiently high to form a continuous protective passive aluminium film. As a result of this film, the sample has a high resistance to further corrosion. On samples (a and b) with low alloying additions of aluminium this passivation layer does not form or is discontinuous, and therefore the coating is susceptible to further corrosive attack. It is proposed that the aluminium content of the coating, and the resultant protective film is the main reason for the difference in corrosion performance between the different compositions of coating.

As previously mentioned the rate of coating dissolution in etching experiments correlates to the filiform corrosion performance of the coating. For example coatings where the time to iron exposure is low during etching experiments are also highly susceptible to filiform corrosion. Coating etching experiments on samples a to d are visually shown in figures 4-17 to 4-20. Figure 4-21 graphically shows the amount of surface magnesium measured on samples (a to d) with regards to time. It can be seen that on all samples the amount of magnesium measured on the surface reduces over immersion time in acetic acid. Figure 4-22 shows the amount of surface aluminium measured with regards to time. Samples c and d both plateau at approximately 25wt% surface aluminium. Samples a and b do not have enough aluminium to reach this amount to the level of surface aluminium increases until the coating has been removed. Figure 4-23 shows the amount of iron exposure in relation to time for samples a-d. This time to iron exposure time directly correlated to the filiform corrosion resistance of the sample. Samples which showed the highest levels of filiform corrosion also show the shortest time to iron exposure during etching experiments. Figure 4-24 gives a summary of the time to 10wt% iron exposure. This again highlights this correlation between time to iron exposure and filiform corrosion resistance.

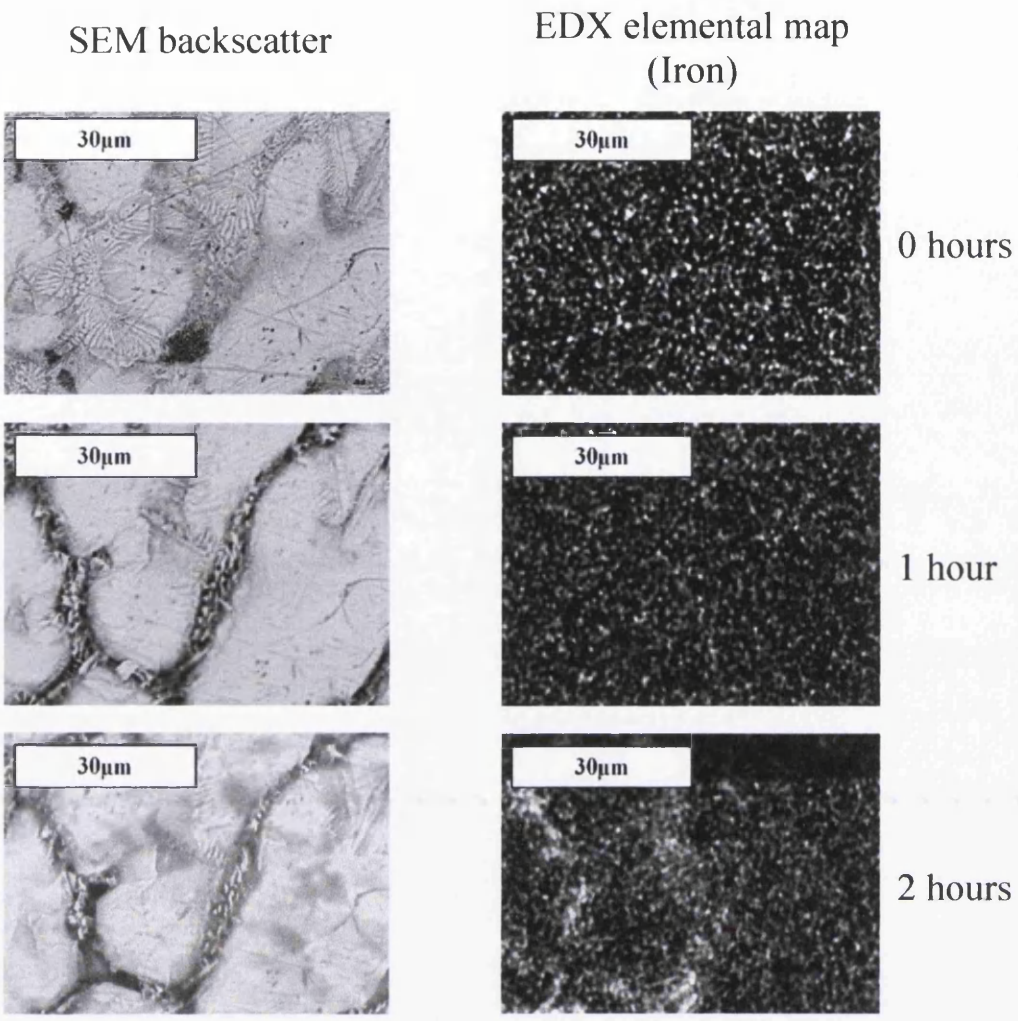


**Figure 4-17 :** SEM and Energy Dispersive Spectroscopy (EDX) images of a sample (a) Zn+Al*(1wt%)*+ Mg*(1wt%)* hot dip coated steel sample which has been immersed in 0.1mol/dm$^3$ acetic acid and images and EDX mapped every hour. Prior to imaging and mapping the corrosion product is been removed by ultrasonication in hexane for 10 minutes. Images *left* are SEM backscatter and *right* are EDX elemental maps showing the corrososponding presence of surface iron. All images are at the same magnification, and of the same area.

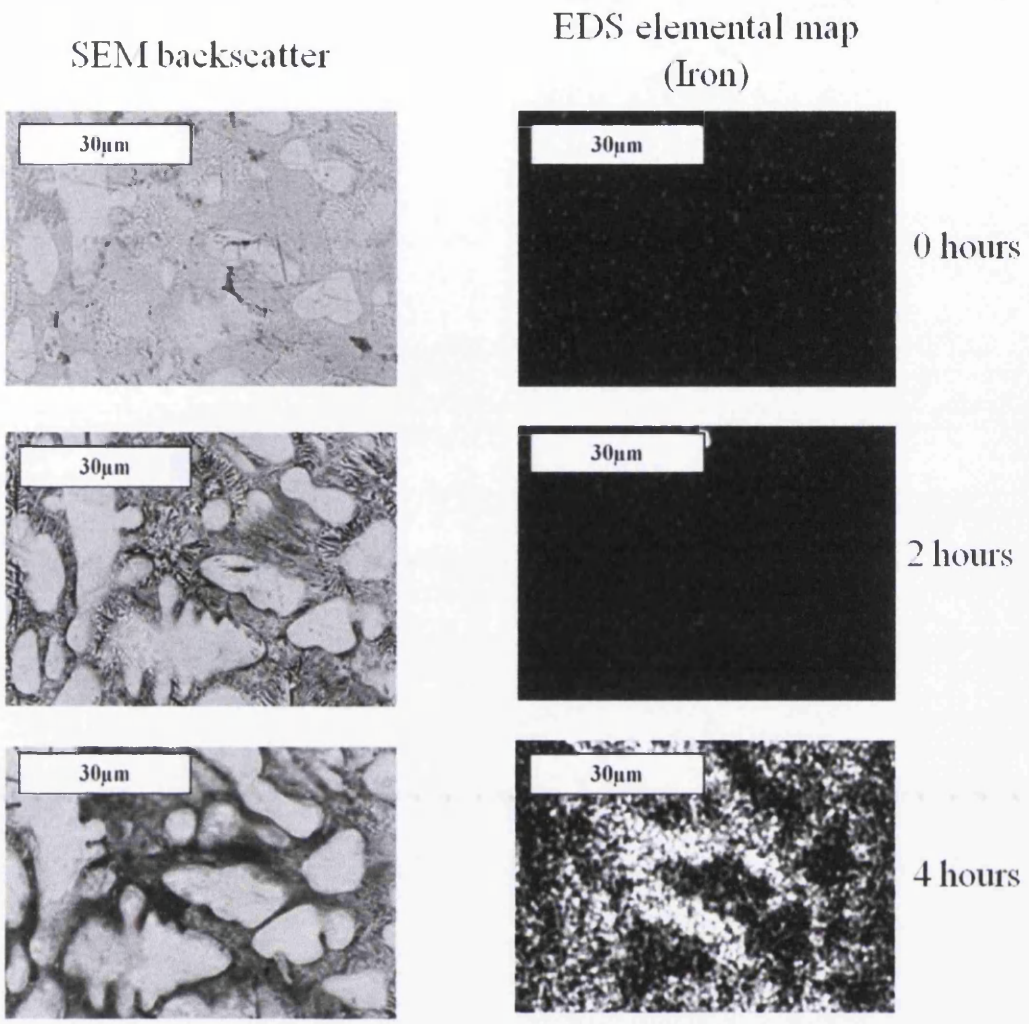


**Figure 4-18 :** SEM and Energy Dispersive Spectroscopy (EDX) images of a sample (b) Zn+Al*(1.5wt%)*+ Mg*(1.5wt%)* hot dip coated steel sample which has been immersed in 0.1mol/dm$^3$ acetic acid and images and EDX mapped every hour. Prior to imaging and mapping the corrosion product is been removed by ultrasonication in hexane for 10 minutes. Images *left* are SEM backscatter and *right* are EDX elemental maps showing the corresponding presence of surface iron. All images are at the same magnification, and of the same area.

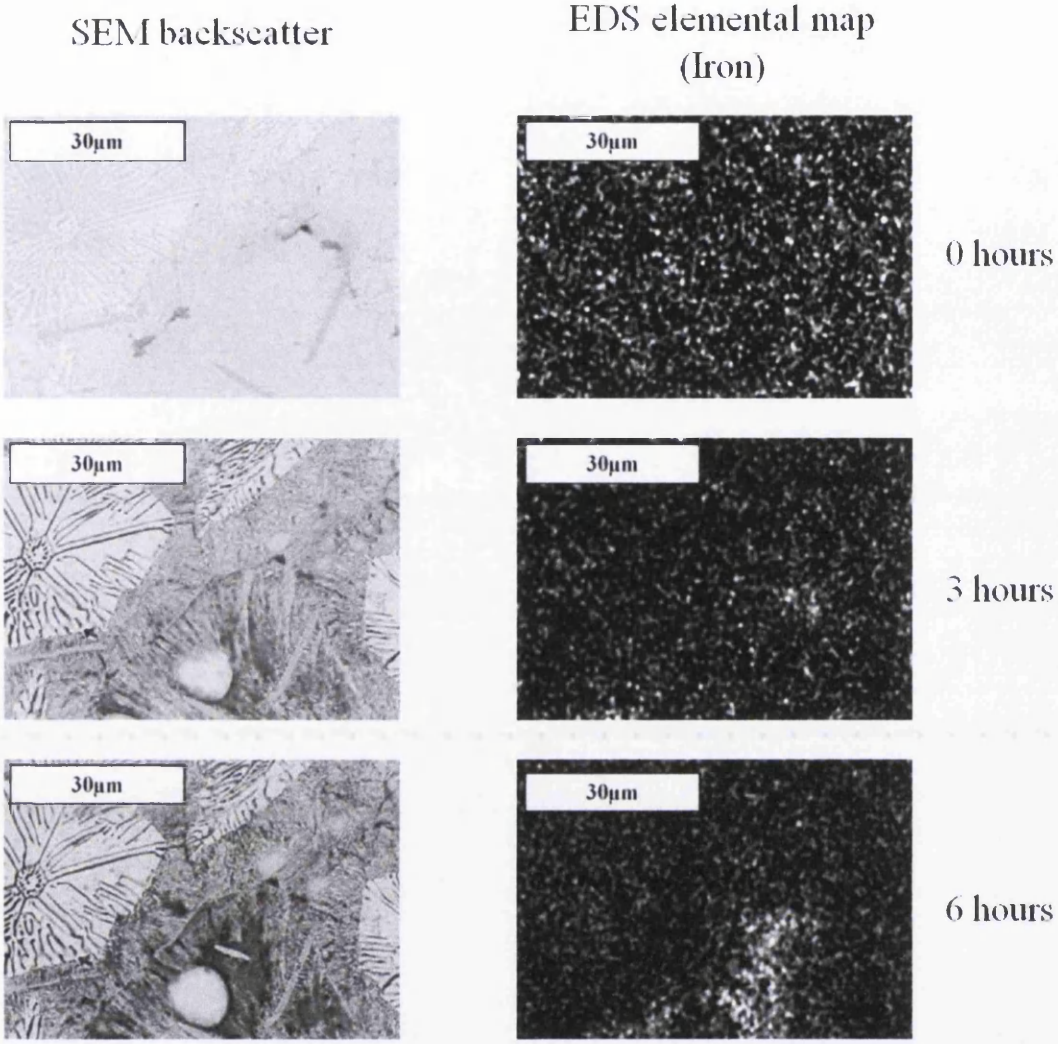


**Figure 4-19 :** SEM and Energy Dispersive Spectroscopy (EDX) images of a sample (c) Zn+Al*(3wt%)*+ Mg*(3wt%)* hot dip coated steel sample which has been immersed in 0.1mol/dm$^3$ acetic acid and images and EDX mapped every hour. Prior to imaging and mapping the corrosion product is been removed by ultra-sonication in hexane for 10 minutes. Images *left* are SEM backscatter and *right* are EDX elemental maps showing the corresponding presence of surface iron. All images are at the same magnification, and of the same area.

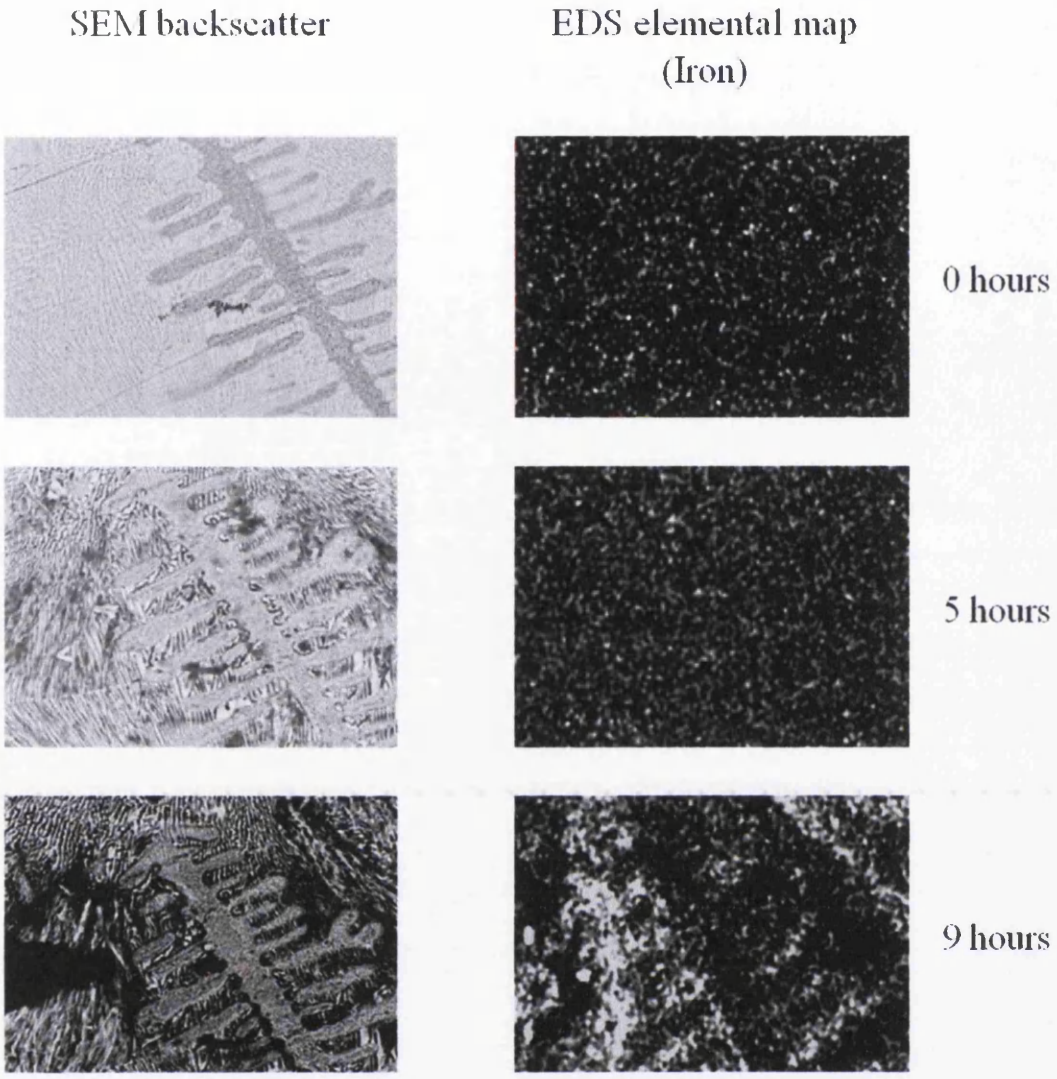


**Figure 4-20 :** SEM and Energy Dispersive Spectroscopy (EDX) images of a sample (d) Zn+Al*(6wt%)*+ Mg*(3wt%)* hot dip coated steel sample which has been immersed in 0.1mol/dm$^3$ acetic acid and images and EDX mapped every hour. Prior to imaging and mapping the corrosion product is been removed by ultrasonication in hexane for 10 minutes. Images *left* are SEM backscatter and *right* are EDX elemental maps showing the corresponding presence of surface iron. All images are at the same magnification, and of the same area.

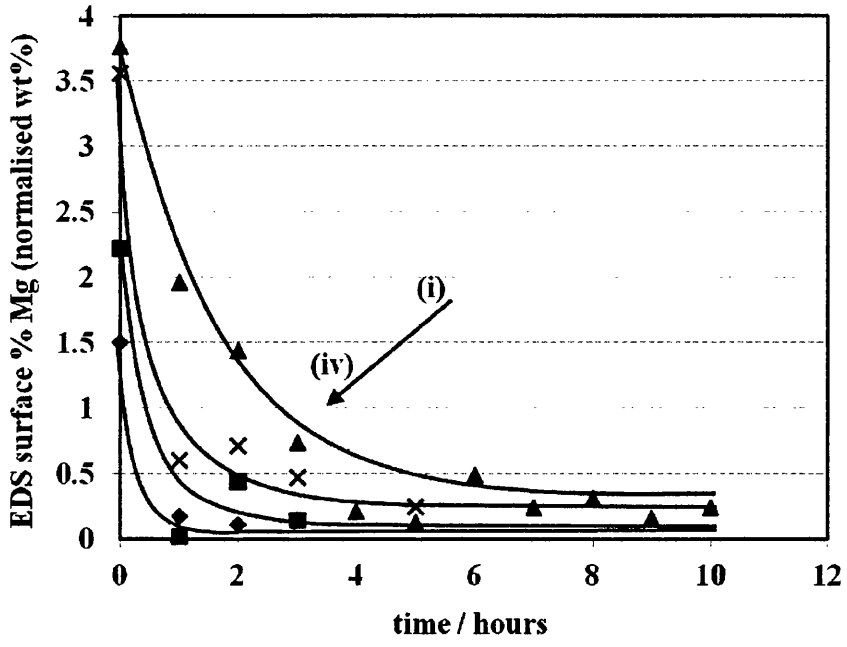


**Figure 4-21** : EDX surface composition plots for a 200 x 100µm sample surface area showing the normalised wt% of magnesium *(when normalised in relation to zinc, aluminium and iron)* in relation to etching time in 0.1mol/dm3 acetic acid **(i)** represents *Zn+Al(6wt%)+Mg(3wt%)* sample (d). **(ii)** *Zn + Al(3wt%)+Mg(3wt%)* sample (c), **(iii)** *Zn+Al(1.5wt%)+Mg(1.5wt%)* sample (b), **(iv)** *Zn+Al(1wt%)+Mg(1wt%)* sample (a)

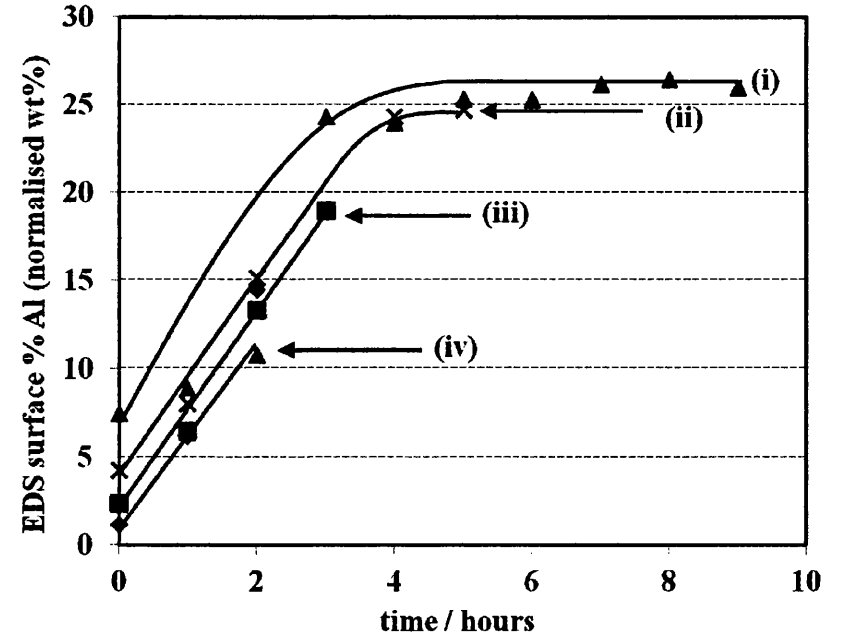


**Figure 4-22** : EDX surface composition plots for a 200 x 100µm sample surface area showing the normalised wt% of aluminium *(when normalised in relation to zinc, aluminium and iron)* in relation to etching time in 0.1mol/dm3 acetic acid. The reason for the gradient change in lines i and ii is due to the hot dip coating been completely removed **(i)** represents *Zn+Al(6wt%)+Mg(3wt%)* sample (d). **(ii)** *Zn + Al(3wt%)+Mg(3wt%)* sample (c), **(iii)** *Zn+Al(1.5wt%)+Mg(1.5wt%)* sample (b), **(iv)** *Zn+Al(1wt%)+Mg(1wt%)* sample (a).

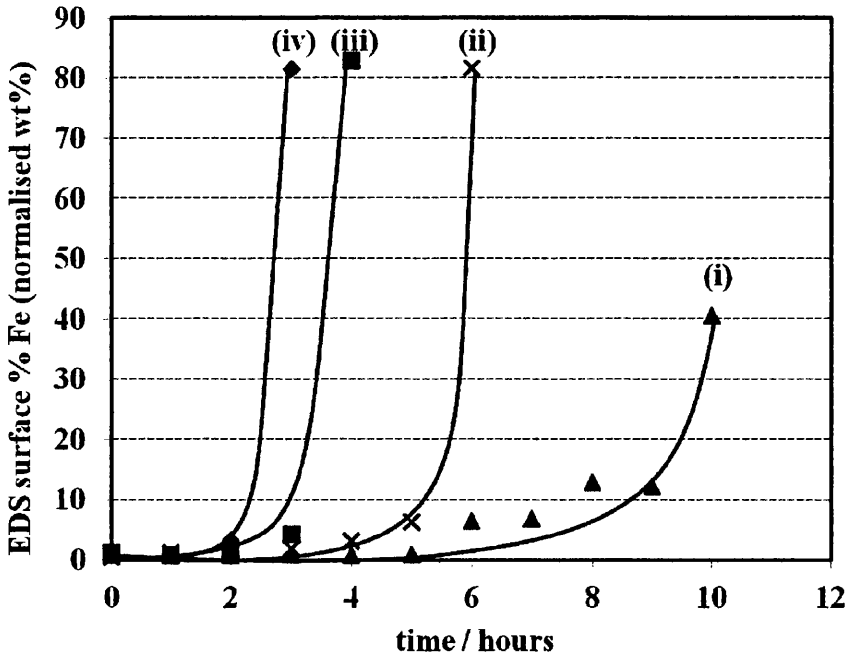


**Figure 4-23** : EDX surface composition plots for a 200 x 100μm sample surface area showing the normalised wt% of aluminium *(when normalised in relation to zinc, aluminium and iron)* in relation to etching time in 0.1mol/dm3 acetic acid **(i)** represents *Zn+Al(6wt%)+Mg(3wt%)* sample (d). **(ii)** *Zn + Al(3wt%)+Mg(3wt%)* sample (c), **(iii)** *Zn+Al(1.5wt%)+Mg(1.5wt%)* sample (b), **(iv)** *Zn+Al(1wt%)+Mg(1wt%)* sample (a)

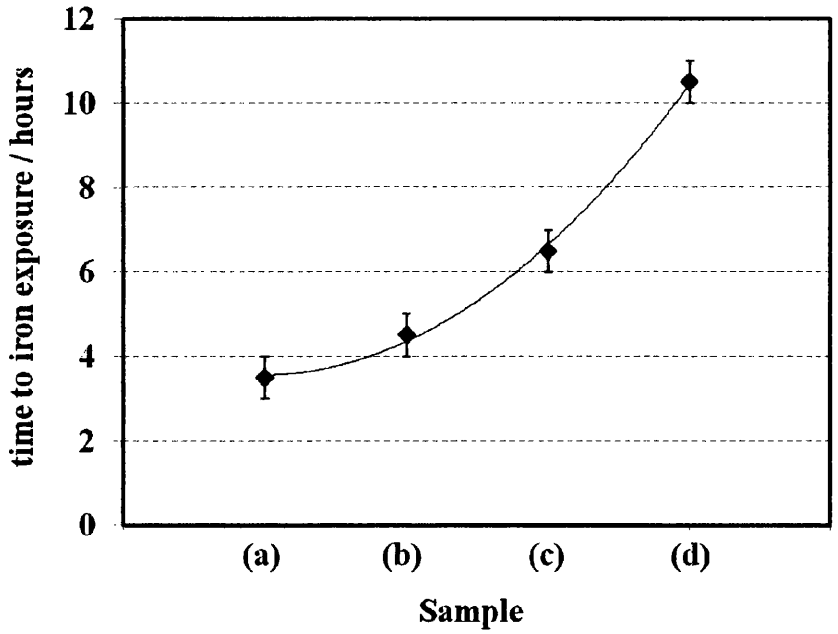


**Figure 4-24** Time till measured iron exposure exceeds 10wt% during etching experiment in relation to sample id. Until aluminium content of the sample increased the amount of time to iron exposure increases. Etching conditions 10mol/dm$^3$ acetic acid, coating weights 140g/m$^2$, coating thickness 10µm

## 4.8 Coating thickness

In order to further investigate the effect of iron exposure time on filiform corrosion kinetics, hot dip coatings of a fixed composition of Zn-1.5wt%Mg-1,5wt%Al were studied. The time to iron exposure is measured using the etching experiment described in section 2.6 and filiform corrosion tests are carried out using the standard filiform corrosion experiment described in section 2.1. A description of samples A to F is given in section 4.1 and table 4-3.

**Sample characterization (samples A-F)**

Samples A-F have a bath composition of 1.5wt% Aluminium and 1.5wt% Magnesium, with the remainder of the coating is made of zinc. This makes these samples the same composition as sample b. Coating thickness is verified by using a SEM micrograph of each coating and measuring the coating thickness. SEM Backscatter images of these micrographs are shown in figure 4-25. It can be seen from these micrographs

that composition, and microstructural phases remain constant and consistence with sample b which is analysed in section 4.4. Also all samples are on a 0.7mm mild gauge steel substrate so the only variable is the coating thickness.

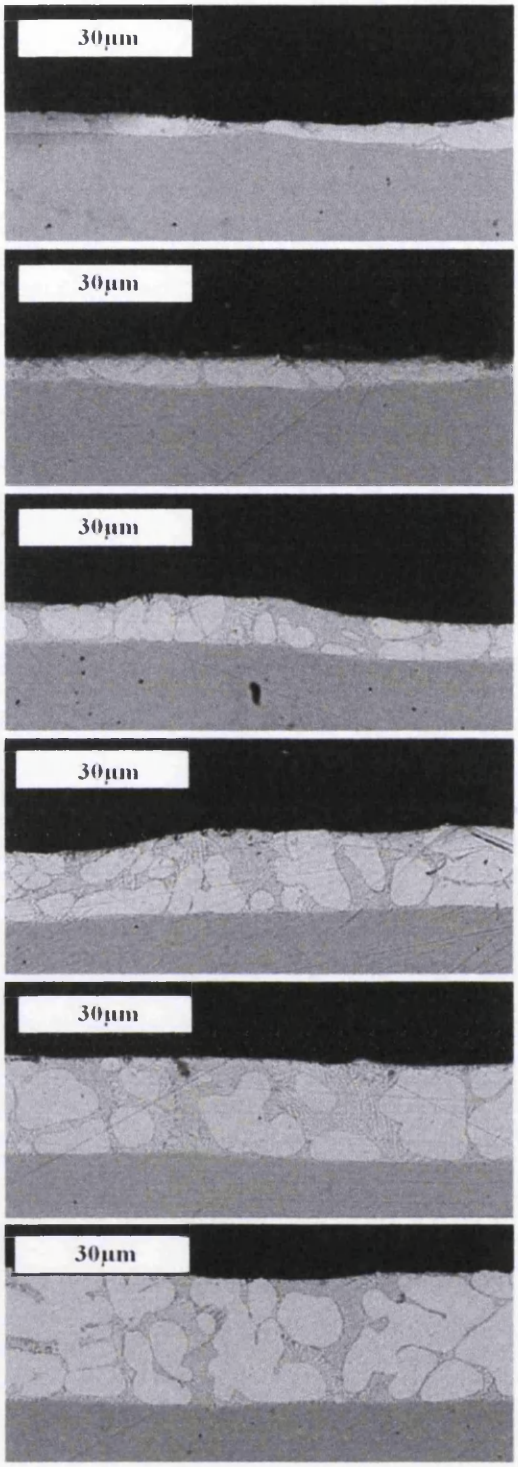


**Figure 4-25** : SEM Micrographs showing cross sections of samples A-F and there corresponding coating thicknesses. All hot dip coatings (A-F) have the same bath composition and the same microstructural phases are present.

## 4.9 Results

### EDX etching on coating thickness

All samples A-F are immersed in 0.1mol/dm$^3$ acetic acid. Samples are removed every 30 minutes, rinsed and placed in an SEM for backscatter imaging and elemental mapping. This technique is described in section 2.6. The corrosion mechanism of samples A-F is the same as sample b. Initially magnesium is removed from the surface. This is followed by the removal of the binary and ternary eutectic phases. When the underlying steel substrate is exposed the remaining primary zinc phase is rapidly corroded leading to an overall coating failure. Time to 10% iron exposure is shown in figure 4-26. It can be seen that thicker coating weights have a longer time to iron exposure.

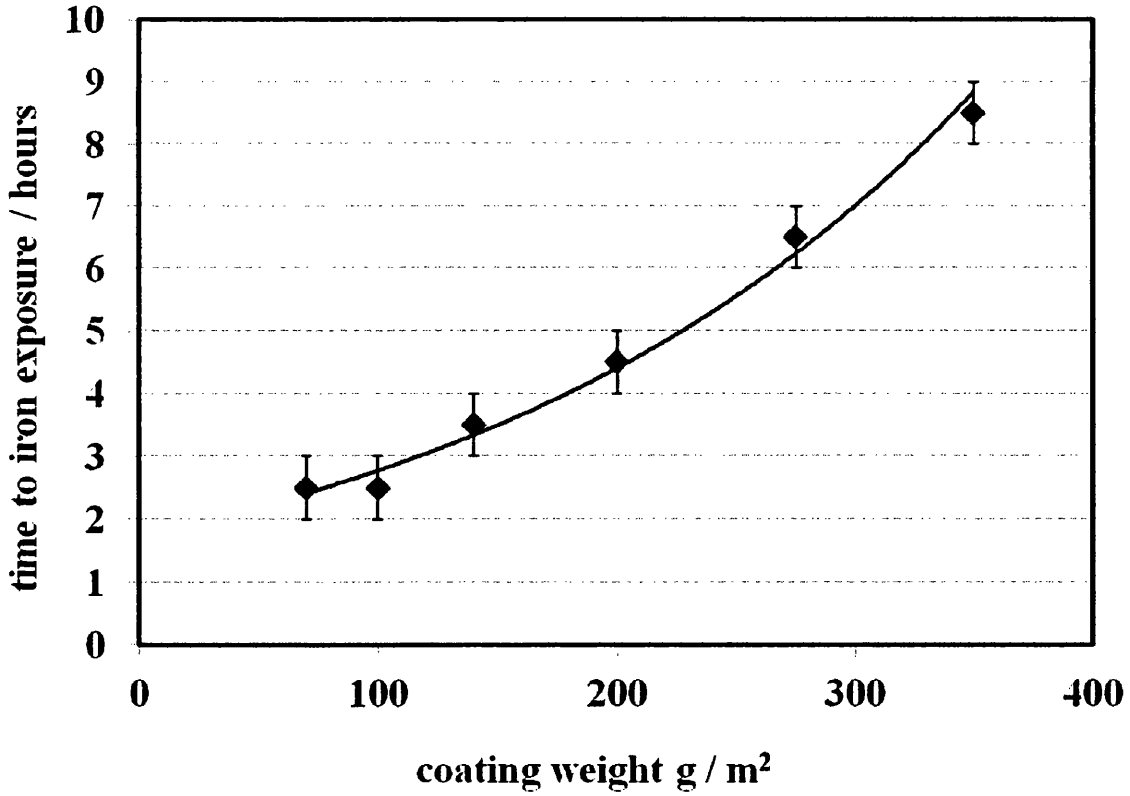


**Figure 4-26** : The time required in hours to for a systematic variation of coating thicknesses to expose the iron substrate when a Zn+Al*(wt%1.5)*+Mg*(1.5wt%)* coating is corroded in immersion conditions with 0.1mol/dm$^3$ acetic acid at a temperature of 20°c

The mechanism of filiform corrosion in this case is the same as the mechanism described in chapter 3 and on sample b in chapter 4. By studying the kinetics of filiform corrosion when the Zn+Al*(1.5wt%)*+Mg*(1.5wt%)* hot dip coating thickness is systematically varied it can be seen that the initiation period for filiform corrosion to initiate is proportional to the thickness of the coating. Thinner coatings, such as coating A have a very short initiation periods, whilst thicker coatings have a much longer initiation period. This correlated to the time to expose the steel substrate shown in etching experiments and reinforces the theory that filament propagation relies on the underlying steel substrate to be exposed to support the cathodic reaction.

The propagation rate for filiform corrosion also reduces with coating thickness, eg filiform corrosion propagates at a slower rate on thicker coatings. There are several potential reasons for this. It may potentially be due to more corrosion product been deposited on the sample surface of a thicker coating. This corrosion product will reduce the efficiency of transfer of species to the cathode, and acting as a mass transport barrier. Another reason for the reduced propagation rate may be because there is physically more hot dip coating to be anodically dissolved, which is a time dependant process and will therefore take more time, or a combination of both factors. Finally the net amount of aluminium in a thicker coating is greater. As a result of this when magnesium and zinc have been removed there is greater potential for aluminium enrichment on the surface which has previously been demonstrated to have a passivation effect. The total corroded area in relation to time and coating weight is shown in Figure 4-27.

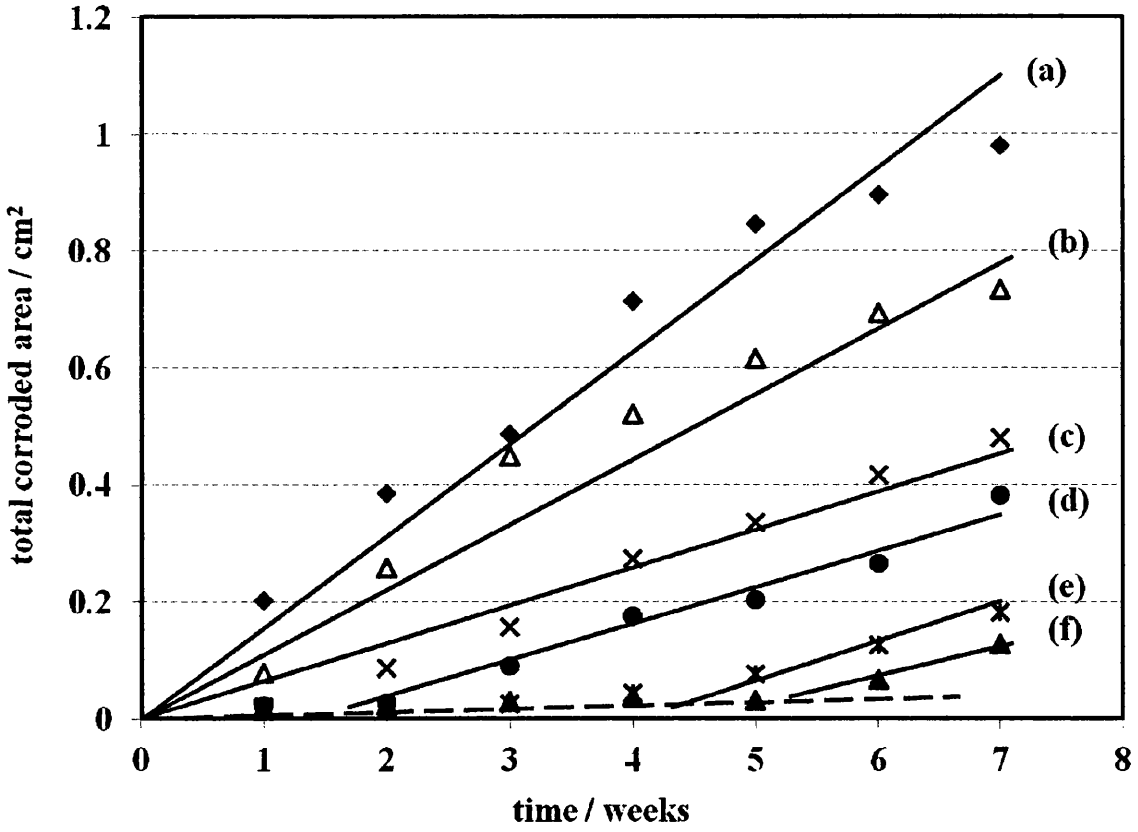


**Figure4-27 :** The average total surface area covered in corrosion product around a 10mm penetrative defect averaged over 2 defects as measured using sigma scan digital image analysis. All samples are initiated with 2µl of relevant concentration acetic acid, and propagation occurs at a relative humidity of 86% and a temperature of 22°c. Each data series corresponds to a coating weight off **(a)** 70g/m² **(b)** 100g/m² **(c)** 140g/m² **(d)** 200g/m² **(e)** 275g/m² **(f)** 350g/m²

## 4.10 Conclusion

The first section of this chapter investigated the role of alloying additions to the hot dip coated steel. It has been shown that increased levels of aluminium greatly increase the corrosion resistance of the coating when exposed to acetic acid. Coating (a) which has the lowest level of aluminium (1wt%) underwent rapid anodic dissolution in acetic acid immersion conditions, and the steel substrate was exposed within 2.5 hours. As the aluminium content of coatings increased, the time to iron exposure also increased. This is due to aluminium forming a passive oxide film on the surface of the sample. Samples with above 3wt% aluminium form a continuous passive aluminium oxide film and show slower rates of coating dissolution. These results also correlate to the filiform corrosion kinetics of the coating. Samples with high aluminium content are

much less susceptible to filiform corrosion when compared to samples with a low aluminium content.

The second part of this chapter investigates the effect of coating weight on a sample with a fixed composition. Thicker coatings show an increased time to iron exposure during etching experiments, and again this correlates to thicker coatings having a higher resistance to filiform corrosion.

Commercially one of the driving forces behind the development of Zn-Al-Mg hot dip coatings is the ability to use reduced coating weights, and therefore reduce costs. As a result of this the use of thicker coatings is not a economically viable option to improve the filiform corrosion resistance of the coating. It does however highlight that time to iron exposure is critical for the filiform corrosion resistance of coatings, and it has been shown that time to iron exposure can be increased by increasing the alloying addition of aluminium.

# Chapter 5 : Inhibition of filiform corrosion with phenylphosphoic acid inhibitors

## 5.1 Introduction

As has been previously discussed the market for organically coated hot dip coated galvanised steel products is of global importance for both the automotive and construction industries. An integral component of these organic coating systems is the primer layer, which often provides corrosion protection to the underlying steel substrate via the inclusion of corrosion inhibiting pigments. Traditionally the most conventional corrosion inhibiting pigments have been chromium (VI) anions, such as zinc or strontium chromate. However there is significant legislative pressure to find chromium free corrosion inhibiting pigments as chromium (VI) as it has been shown to be toxic and carcinogenic (93).

One potential alternative to $Cr^{6+}$ is to incorporate chromium free inhibitors into organic coatings in the form of disperse pigments that form sparingly soluble salts such as zinc phosphate into the organic coating system (94-97). A second method is to incorporate smart release pigments into an organic coating system such as hydrotalcite clays. In these systems stored inhibitor species are released, and the sequestration of aggressive ions occurs when contact is made between the ion exchange clay and the aggressive electrolyte (98) (99). This method is discussed in chapter 6. In this chapter a different approach is used, where the inhibitor in its acid form is directly dissolved into a solution of the polymer. This approach is similar to etch primers where some components of the organic coating, primer solution cause a reaction with the metal surface and lead to the formation of a protective layer at the metal organic coating interface (100).

In this study systematic variations of phenylphosphonic acid ($H_2PP$) are incorporated into polyviynal butyral coatings (PVB) and the effect on filiform corrosion in relation to time is measured using digital image analysis. It has been previously demonstrated by Williams *et al* (97) that $H_2PP$ additions to PVB coatings inhibit filiform corrosion on aluminium substrates (101). Williams *et al* also

demonstrated that polyaniline doped with $H_2PP$ dispersed within a PVB coating effectively decreases the rate of cathodic disbondment on iron surfaces by up to 99% with increasing volume fractions (102). The mechanism suggested by Williams *et al* is that PPA will form an insoluble salt film on the metal surface which will act as a barrier to electron transfer and therefore reduce the rate of corrosion (78).

## 5.2 Methodology

Filiform corrosion is initiated using the technique described in section 2.1. Corrosion is initiated with 2µl of 1.5mol/dm$^3$ acetic acid per 10mm penetrative defect, and propagation conditions are 22°c and at a relative humidity of 86%. Relative humidity is controlled using a saturated salt solution of potassium chloride in a dessicator. Corrosion is allowed to propagate for 6 weeks, and measurements are taken on a weekly basis. Corrosion measurements are carried out using digital image analysis using Sigma Scan Pro 5 as described in section 2.2 and section 2.3. Filament length is measured using the technique described in section 2.4 All chemicals are ordered from the sigma chemical company in analytical grade purity. All tests are repeated 4 times on 2 separate samples, with each sample containing 2 defects. The volume of the dessicator is 0.008m$^2$ and 4 samples are stored in each dessicator.

## 5.3 Sample preparation

All samples used in this chapter are commercially produced Zn+Al+Mg hot dip coated steel, with a bath coating composition of Zn+Al*(1.5wt%)*+Mg*(1.5wt%)*. The gauge of the mild steel substrate is 0.7mm as measured using a micrometre screw gauge, and the hot dip coating weight is 140g/m$^2$ resulting in an average coating thickness of 10µm. This sample is described in more detail in section 3.4. All other chemicals are supplied from the Aldrich Chemical Company in analytical grade purity. Systematic levels of phenylphosphonic acid (PPA) are added to the PVB organic coating, and the effect of the corrosion inhibition of PPA is studied. The levels of PPA that is added to the PVB coating are: (a) 0wt%, (b) 2wt%, (c) 4wt%, (d) 6wt%, (e) 8wt% and (f) 10wt%.

## 5.4 Results and Discussion

Filiform corrosion filaments are observed on uninhibited PVB coated Zn-Al-Mg hot dip coated steel after just one week. Initially a few filaments grow from the penetrative defect, and as the propagation time increases these become the larger wider filaments. Over this propagation period new filaments also start to initiate at the penetrative defect. The typical appearance of a PVB coated Zn-Al-Mg hot dip coated steel sample after 5 weeks is shown in figure 5-1 (a). When low levels of PPA are added to the PVB coating (2-4wt%) a similar mechanism is seen to the uninhibited sample, apart from the size and number of filaments are reduced in correlation to the amount of PPA that is added. Levels of PPA above 6wt% show only small sporadic amounts of filiform corrosion. The typical appearance of penetrative defects after 5 weeks is shown in figure 5-1.

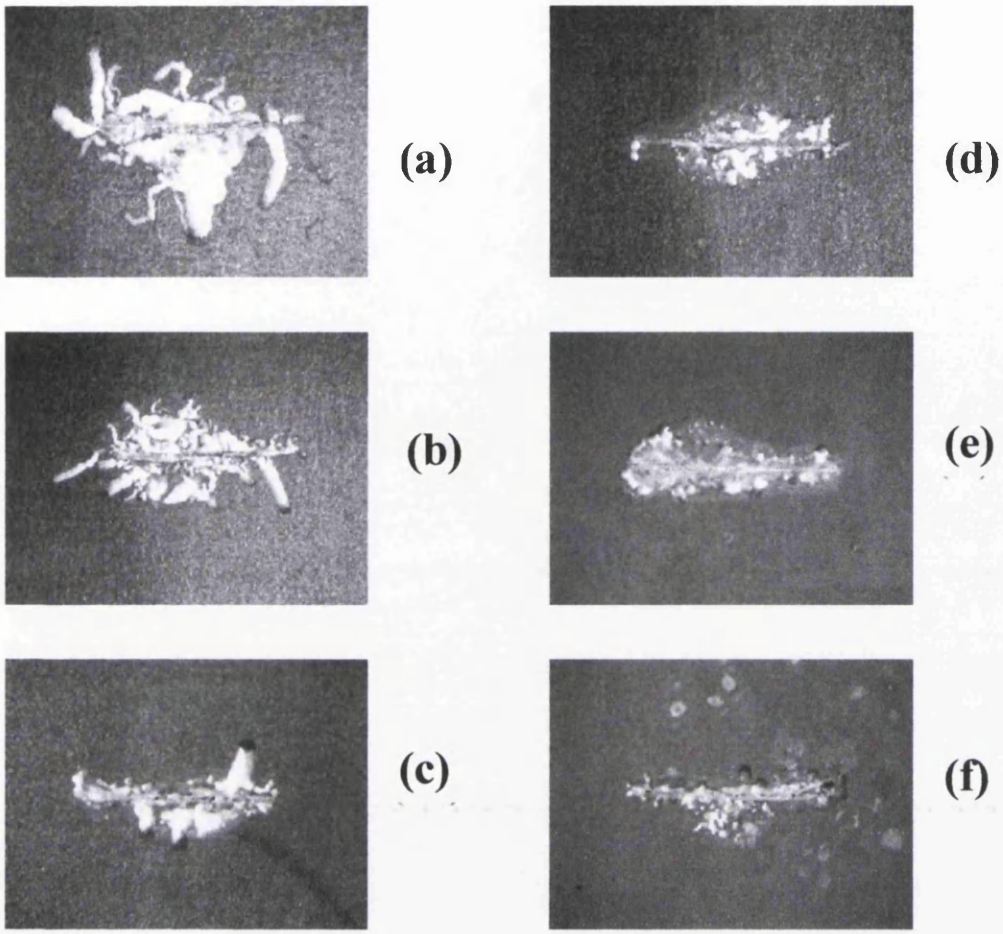


**Figure 5-1 :** Appearance of Zn+Al*(1.5wt%)*+Mg*(1.5wt%)* hot dip coated steel samples with a coating weight of 140g/m$^2$ after 5 weeks at 86%RH and 22°c. Corrosion is initiated with 2µl of 1.5mol/dm$^3$ acetic acid per 10mm penetrative defect. Sample (a) 0wt% PPA, (b) 2wt%PPa, (c) 4wt% PPA, (d) 6wt%PPA, (e) 8wt% PPA, (f) 10wt% PPA.

The rate of filiform corrosion follows a positive parabolic relationship with time. Initially corrosion rates are low, but as more filaments start to propagate from the defect the total corroded area increases at a higher rate over time. Unlike hydrotalcite (chapter 6) there is not such a defined initiation and propagation period when using PPA as a corrosion inhibitor. In the case of PPA the corrosion rate gradually increases over time. The addition of PPA does however result in a large decrease in the total corroded area. Figure 5-2 shows a time dependant plot of the total area covered in corrosion product in relation to the amount of PPA added to the PVB coating. A summary of the total corroded area after 5 weeks is also shown in figure 5-3. These results show a significant decrease in the total corroded area when PPA is added to the PVB coating, and a systematic decrease in the corroded area when the amount of PPA is increased. After a 5 week propagation period samples containing 10wt% PPA show

approximately an 80% reduction in the total corroded area compared to an uninhibited sample.

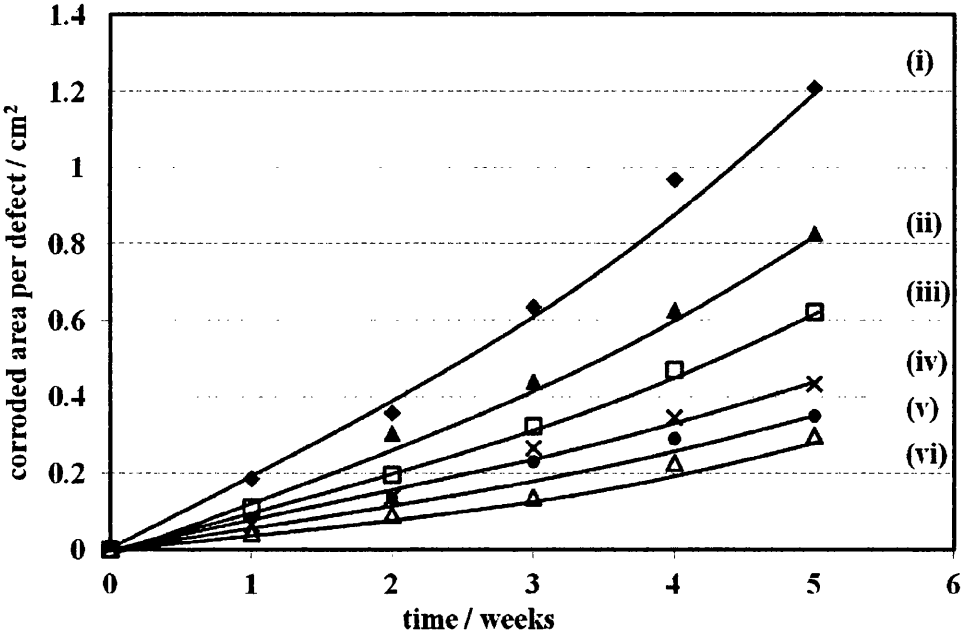


**Figure 5-2** The total area covered in corrosion product around a 10mm penetrative defect in relation to time when corrosion is initiated with 1.5µl of 1.5mol/dm$^3$ aqueous acetic acid on a Zn+Al*(1.5wt%)*+Mg*(1.5wt%)* hot dip zinc sample. Propagation conditions are 86%RH and a temperature of 22°c. Systematic amounts of phentylphosphonic acid are mixed with the PVB coating as is represented by **(i)** 0wt% PPA, **(ii)** 2 wt% PPA, **(iii)** 4 wt% PPA, **(iv)** 6wt% PPA, **(v)** 8 wt% PPA, **(vi)** 10wt% PPA

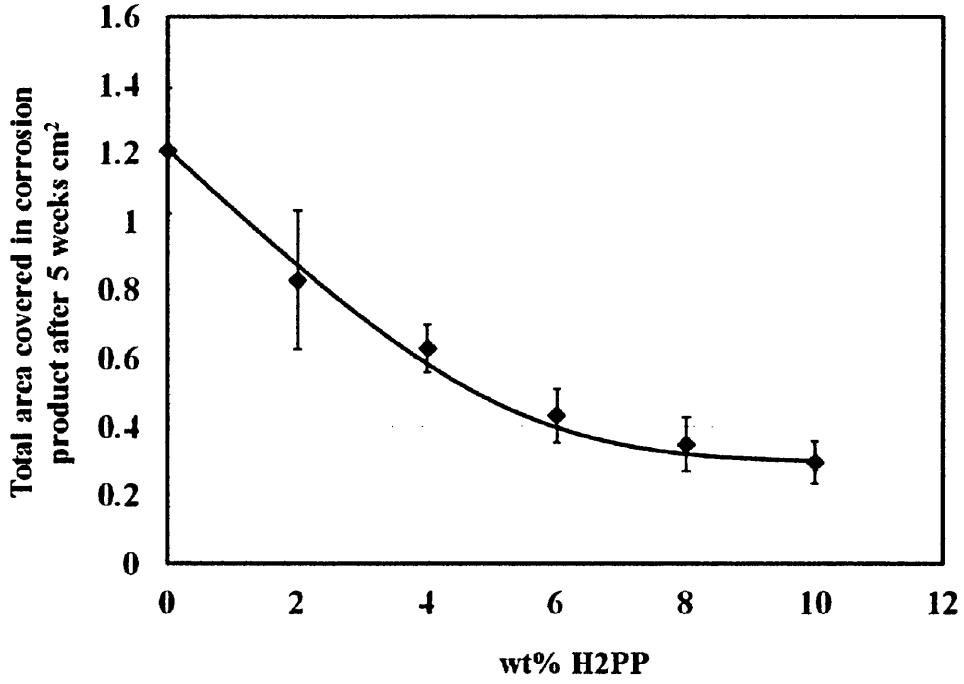


**Figure 5-3** : A summary of the of the total area covered in corrosion product around a 10mm penetrative defect after 5 weeks in relation to the wt% of PPA additions to the PVB organic coating. Corrosion is initiated with 1.5µl of 1.5mol/dm$^3$ aqueous acetic acid on a Zn+Al*(1.5wt%)*+Mg*(1.5wt%)* hot dip zinc sample. Propagation conditions are 86%RH and a temperature of 22°c

The appearance of defects in relation to time is shown in figure 5-4 (2wt% PPA) and figure 5-5 (10wt% PPA). Uninhibited samples, and sample containing low levels of PPA show filiform corrosion filaments with a typical morphology. Corrosion on samples where the PPA additions are higher (>6%) some corrosion can start to resemble pitting rather than mobile filaments. The reason for this is most likely because the filaments are static. The rate of filament growth is shown in figure 5-6.

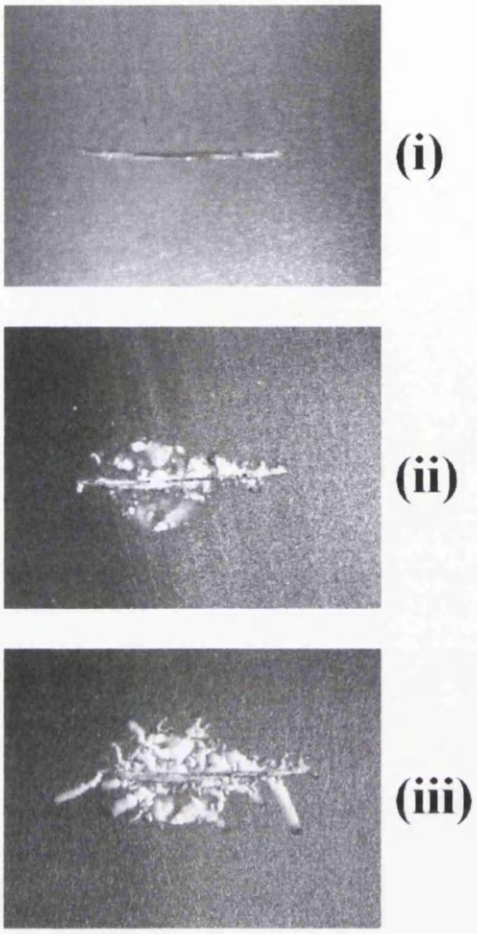


**Figure 5-4** : surface appearance of 10mm penetrative defect on sample **(b)** (2wt% PPA) after initiation with 1.5µl of 1.5mol/dm$^2$ aqueous acetic acid. Propagation conditions are 86%RH and 22°c. Propagation time is (i) 1 week, (ii) 3 weeks, (iii) 5 weeks.

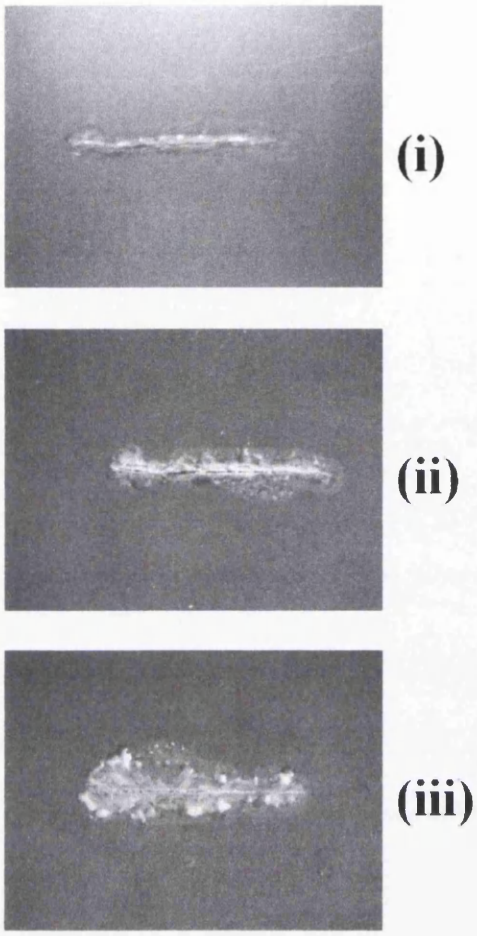


**Figure 5-5** : surface appearance of 10mm penetrative defect on sample **(e)** after initiation with 1.5µl of 1.5mol/dm$^2$ aqueous acetic acid. Propagation conditions are 86%RH and 22°c. Propagation time is (i) 1 week, (ii) 3 weeks, (iii) 5 weeks.

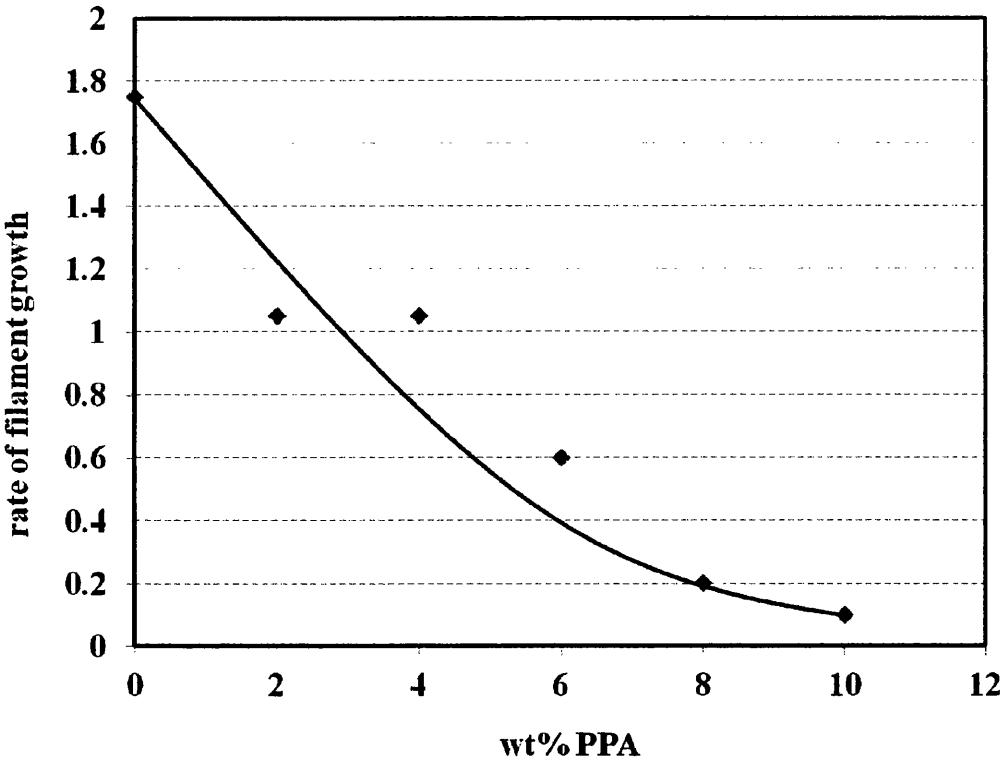


**Figure 5-6 :** The average rate of filament growth during the propagation stage in relation to the wt% of PPA added to the PVB coating. All filiform corrosion is initiated with 2μ of 1.5mol/dm$^3$ aqueous acetic acid per defect on PVB + PPA coated Zn+Al*(1.5wt%)*+Mg*(1.5wt%)* hot dip coated steel, and propagation occurs at a relative humidity of 86% and a temperature of 22°c

Although corrosion is initiated at the cut defects, filiform corrosion is also observed to be initiating from the cut edges of the samples, most likely initiated due to volatile acetic acid in the dessicator atmosphere. The amount of corrosion, both in terms of filament length and number of filaments observed at the cut edges is highly dependent on the amount of PPA within the PVB coating. On samples containing no PPA significant amounts of edge filiform corrosion can be seen. As the amount of PPA increases the amount of edge filiform corrosion decreases. No edge filiform corrosion was observed on samples containing above 6wt% PPA. The appearance of edge filiform corrosion is shown in figures 5-7. The number of filaments per cm of edge and the average length of filament per is shown in figure 5-8.

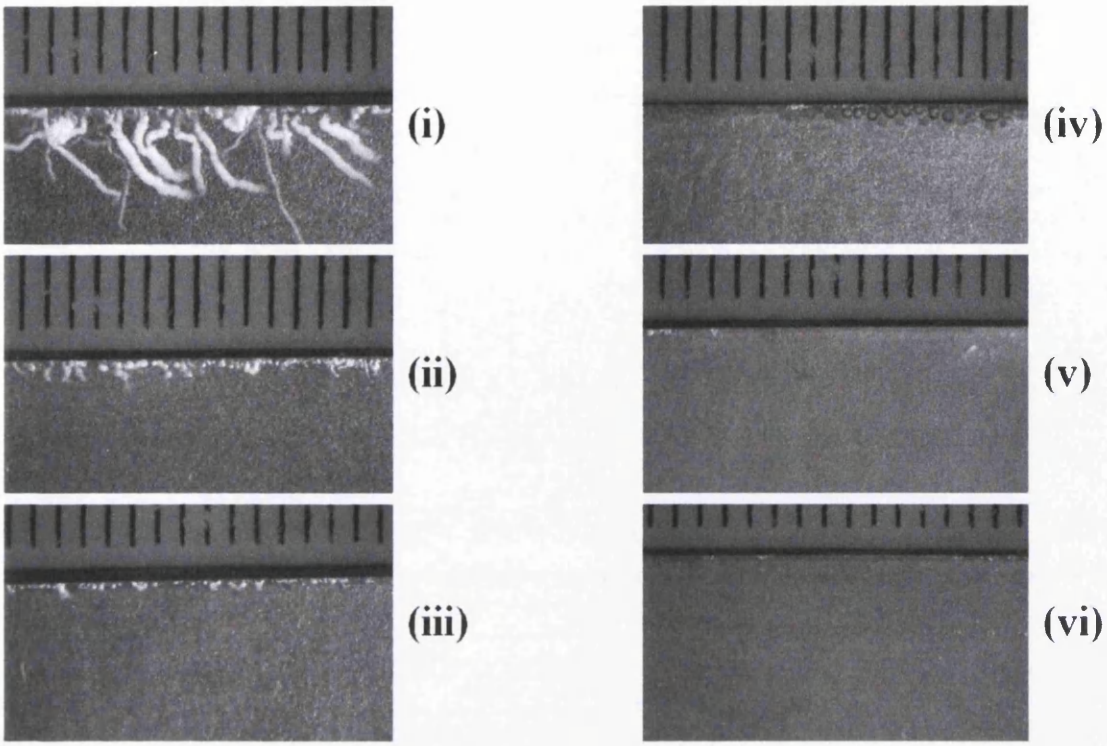


**Figure 5-7** : Appearance of the sample cut edge after 5 weeks propagation time at 86% RH .and 22°c on Zn+Al*(1.5wt%)*+Mg*(1.5wt%)* hot dip coated steel. Corrosion is initiated with gaseous acetic acid from the defect experiment. Samples are (i) 0wt% PPA, (ii) 2wt% PPA, (iii) 4wt% PPA, (iv) 6wt% PPA, (v) 8wt% PPA and (vi) 10wt% PPA

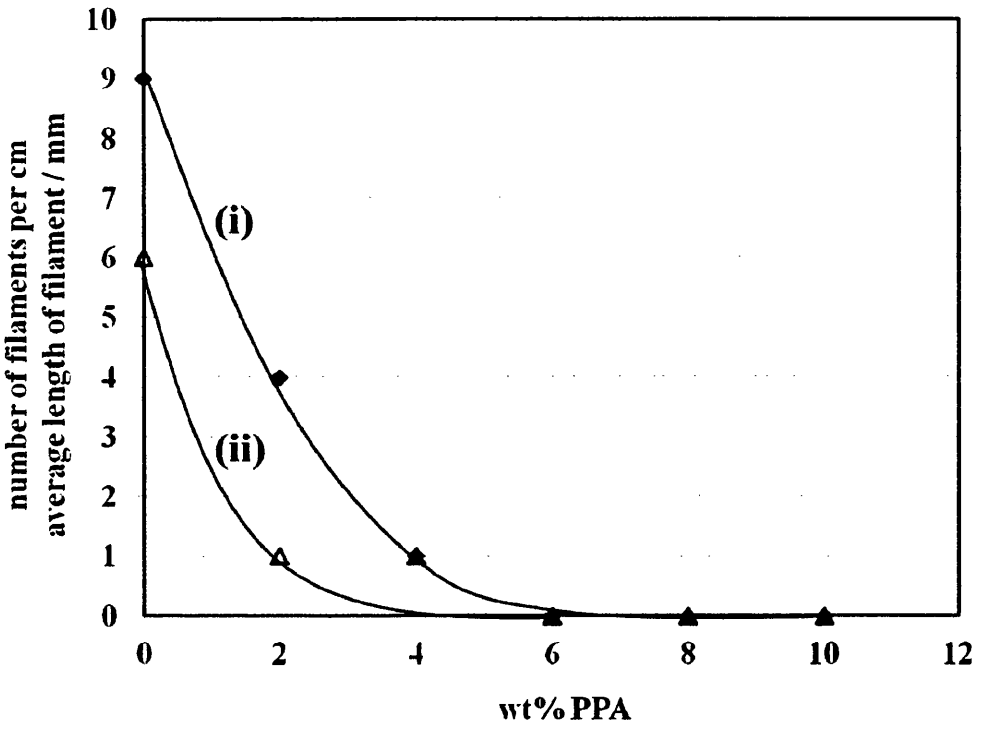


**Figure 5-8**. Graph showing the number of filament per cm for edge filiform filaments, and the average length of edge filiform corrosion filaments on Zn+Al(1.5wt%)+Mg(1.5wt%) hot dip coated steel after 5 weeks at 86%RH at 22°c (i) The number of edge corrosion filaments per cm of cut edge which are over 1mm in length after 5 weeks. (ii) The average length of edge filaments after 5 weeks

## 5.5 Discussion

Increasing additions of PPA to PVB organic coatings on Zn-Al-Mg hot dip coated steel results in an increase in filiform corrosion resistance. The reason for this inhibition is attributed to the ability of $H_2PP$ to form an insoluble salt film on the metal surface. This insoluble salt reduced the efficiency of electron transfer to cathodic reaction sites. The formation of this insoluble salt layer will start as soon as the PVB/$H_2PP$ ethanolic solution is applied to the metal surface. The dissociation of $H_2PP$ dissolved in the ethanol will produce $H^+$ cations. These cations will react with the zinc on the surface, causing an acid etch, which will generate $Zn^{2+}$ cations at the coating, metal interface. The following equilibrium reactions illustrate the de/protonation of $H_2PP$.

$$H_2PP_{(aq)} \leftrightarrow HPP^-_{(aq)} + H^+_{(aq)} \ (pK_{a1} = 2.3) \qquad (5.1)$$

$$HPP^-_{(aq)} \leftrightarrow PP^{2-}_{(aq)} + H^+_{(aq)} \ (pK_{a2} = 7.8) \qquad (5.2)$$

When $H_2PP$ is added to PVB, there will initially be a low pH produced at the coating / hot dip interface when the coating is first applied. The pH will slowly increase due to the progressive removal of excessive $H^+$ by neutralisation with $OH^-$. This $OH^-$ is produced by the reaction shown in reaction 5.3.

$$O_2+2H_2O+4e^- \leftrightarrow 4OH^- \quad (5.3)$$

The electrons that drive this reaction are produced by the anodic reaction on the zinc surface

$$Zn \leftrightarrow Zn^{2+}+2e^- \quad (5.4)$$

Low pH will also favour the disassociation of $H_2PP$ to form HPP and $PP^{2-}$ as shown in equations 5.1 and 5.2. When sufficiently high concentration of $PP^{2-}$ builds up it will react with the under film $Zn^{2+}$ to form a solid insoluble layer of $Zn^{2+}PP^{2-}$ on the coating interface.

$$Zn^{2+} + PP^{2-} \leftrightarrow Zn^{2+}PP^{2-}_{(s)} \quad (5.5)$$

It is proposed that the formation of this solid, continuous insoluble salt film on the hot dip Zn-Al-Mg surface forms a barrier to electron transfer. This subsequently blocks and oxygen reduction reactions from taking place on the metal surface (103). The thickness, and continuous nature of this salt film most probably correlates to the amount of $H_2PP$ added to the PVB coating, e.g. more $H_2PP$ will produce a thicker, more continuous salt film resulting in higher levels of corrosion resistance.

As has been previously demonstrated in chapter 3 the most reactive phase of Zn-Al-Mg hot dip coatings is the $MgZn_2$ eutectic phase. With the addition of PPA to the organic coting it is hypothesised that the $MgZn_2$ phase is chemically etched due to the low pH conditions and this phase will be replaced with insoluble zinc phosphate

## 5.6 Conclusion

The addition of phenyl phosphinic acid $H_2PP$ dissolved in a 30 μm thick poly viynal butyral (PVB) HDG organic coating system, has been shown to result in a significant increase in the filiform corrosion resistance of Zn-Al-Mg hot dip coated steel when

initiated with acetic acid. Reductions in total corroded area of over 80% were observed after a 5 week corrosion period when 10wt% $H_2PP$ is added to the PVB coating. Furthermore there was a reduction in both the number, and size of filiform corrosion filaments.

The proposed mechanism for this increase in corrosion resistance is due to the disassociated $PP^{2-}$ deriving from the $H_2PP$, reacting with $Zn^{2+}$ to form an insoluble layer of $Zn^{2+}PP^{2-}$ on the under film Zn-Al-Mg metal surface. This salt layer is insoluble and will act as a barrier for electron transfer for the cathodic reaction to take place on the metal surface. Increased levels of PPA in the organic coating resulted in increased levels of filiform corrosion resistance. This is potentially due to the insoluble salt layer becoming thicker and more continuous, and therefore acting as a more efficient barrier. Further work is needed to characterize this salt layer on the surface of Zn-Al-Mg hot dipped coating, in order to understand if this is a continuous homogenous layer of zinc phosphate, or if this is a heterogeneous salt layer composed of a variety of zinc, aluminium and magnesium phosphates. PPA however is a viable nontoxic method of increasing the filiform corrosion resistance of Zn-Al-Mg hot dip coated steel in an acetic acid environment.

# Chapter 6 : Inhibiting Filiform Corrosion on Zn+Al+Mg hot dip coated steel with anion exchange pigments

## 6.1 .Introduction

One of the main challenges facing the steel industry is finding corrosion inhibiting alternatives to chromium VI on organically coated hot dip steel. One potential method is to incorporate ion exchange clays into the primer layer of the organic coating (104). Ion exchange clays can either be an anion exchange clay such as hydrotalcite, or a cation exchange clay such as bentonite. Both anion and cation exchange pigments have been shown to be effective overall corrosion inhibitors by reducing the number of aggressive anions or cations present at the coating / metal interface respectively (105,106). Furthermore Williams *et al* have demonstrated that anion exchange pigments incorporated in to organic coatings, in the form of hydrotalcite incorporates with a PVB lacquer can be used to inhibit filiform corrosion initiated with acetic acid on an AA2024 aluminium substrate (106).

It has been shown in previous chapters that organically coated Zn+Al+Mg hot dip coated steel is susceptible to filiform corrosion when exposed to acetic acid and high relative humidity. In this chapter systematic variations of hydrotalcite will be incorporated with a model PVB organic coating, and the amount and the influence on filiform corrosion will be measured using digital image analysis. This technique has previously been successfully used by Williams *et al* to inhibit filiform corrosion aluminium alloys and magnesium alloys (107). Crystalline hydrotalcite is a clay with a layered structure consisting of adjacent positive and negatively charged layers. Anions in the negatively charged layer can be exchanged for anions from an external medium. As a result of this, aggressive anions present in the electrolyte can be exchanged for selected anions which are incorporated into the anion exchange clay. Hydrotalcite clays are described in further detail in section 1.11.4. The aim of the work in this chapter is to incorporate hydrotalcite into a model organic coating on hot dipped Zn-Al-Mg coated steel, and study the effect this has on filiform corrosion when initiated with acetic acid.

## 6.2. Methodology

Filiform corrosion tests as described in section 2.1 are carried out on line produced hot dip Zn-Al-Mg coated mild steel samples. The substrate has a gauge of 0.7mm, and the hot dip coating has a bath composition of 1.5wt%Mg + 1.5wt%Al and the remainder is zinc. The coating thickness is $140g/m^2$ which translates to an average coating weight of approximately 10 μm. This sample is described in more detail in section 3.4.

Filiform corrosion is initiated using the technique described in section 2.1 using $1.5mol/dm^3$ of acetic acid per 10mm penetrative defect. Samples are stored in a dessicator, and propagation occurs at a controlled relative humidity of 86% at a temperature of 22°c. The volume of the dessicator is of $0.008m^2$ and it contains 4 samples, each with 2 defects. The amount of surface corrosion around each defect is measured weekly for 6 weeks, using digital image analysis (Sigma Scan Pro 5) as described in section 2.3. All other chemicals are sourced from the sigma chemical company in analytical grade purity. Filiform corrosion tests are repeated on a total of 4 defects per scenario on two samples, each sample containing two separate defects.

All organic coating systems tested in this chapter are bar cast model ethanolic PVB coatings (Poly vinyl butyral-co-vinyl alcohol-co-vinyl acetate) (Aldrich order number 418439) with systematic additions of synthetic hydrotalcite (HT) (Aldrich order number 652288). Preparation techniques for these coatings are described in more detail in section 2.1. Of special note for this chapter is the importance of homogeneous dispersion of the hydrotalcite clay. This is ensured by first mixing the HT and PVB with ethanol separately, forming two separate viscous liquids. Each of these liquids is mixed for 3 hours, first manually and then with a magnetic stirrer bar. Before further mixing both liquids are visually inspected for a homogeneous appearance. The two liquids are then mixed and stirred with a glass rod for 10 minutes. They are further mixed using a magnetic stirrer bar for 24 hours. The reason for mixing in this way is to ensure that the HT is completely dispersed with the PVB coating. If HT is simply added to the PVB ethanolic solution, the HT will agglomerate, and the HT dispersion in the coating will be inconsistent and therefore

result in inconsistent properties. After mixing the coating is stored in a sealed glass container for 24 hours before use to reduce the number of air bubbles in the coating. Five systematic volume fractions (VF) of HT PVB coatings are mixed and tested. The compositions are shown in table 6-1. The volume fraction of HT in relation to PVB is calculated using the equation shown in equation 6-1:

$$M_{pig} = Ø \cdot M_{pol} \cdot P_{pig} / (1 - Ø) \cdot P_{pol} \quad (6\text{-}1)$$

Where $M_{pig}$ is the "Mass of pigment", in this case HT; $M_{pol}$ is the "Mass of polymer" which is PVB; $P_{pig}$ is the "density of pigment"; $P_{pol}$ is the "density of polymer", and Ø represents the volume fraction of pigment (HT). For all calculations the density of PVB is assumed to be 0.8g/cm$^3$ and the density of hydrotalcite is 2.06g/cm$^3$. All synthetic hydrotalcite used is sourced from the Sigma Aldrich chemical company, and is a synthetic Mg-Al hydrotalcite clay with a chemical composition of $Mg_6Al_2(OH)16CO_3 \cdot 4H_20$

| Sample id | VF hydrotalcite | Substrate composition |
|---|---|---|
| (a) | 0 | Zn+Al(1.5wt%)+Mg(1.5wt%) |
| (b) | 0.05 | Zn+Al(1.5wt%)+Mg(1.5wt%) |
| (c) | 0.1 | Zn+Al(1.5wt%)+Mg(1.5wt%) |
| (d) | 0.15 | Zn+Al(1.5wt%)+Mg(1.5wt%) |
| (e) | 0.2 | Zn+Al(1.5wt%)+Mg(1.5wt%) |
| | | Zn+Al(1.5wt%)+Mg(1.5wt%) |

**Table 6-1 :** List of samples with systematic variations in the VF of HT contained in the PVB organic coating. Substrate composition remains fixed, and the hot dip coating weight is fixed at 140g/m$^2$. All coatings are applied to 0.7mm gauge steel.

## 6.3 Results and Discussion

On the control samples containing no HT (sample a) the first signs of filiform corrosion filaments are visually observed 1-2 weeks after initiation. This is consistent with the results in chapter 3. After 5 weeks the average number of filaments per defect is 9, and the rate of filament length growth over the entire 5 week measured propagation period is constant / linear. The total corroded area then increases over

time with positive parabolic relationship. After 5 weeks the total average corroded are per defect for a sample coated with a PVB coating containing no HT is 1.2cm$^2$.

Samples containing 0.05volume fraction HT (sample b) again show visual signs of filiform corrosion after approximately 2 weeks. However there is a reduction in the number and length of these filaments after a 5 week period when compared to sample a. Also after 5 weeks the total corroded area per defect is an average of 0.58cm$^2$.

When 0.1volume fraction HT is added to the PVB organic coating (sample c), filiform corrosion filaments can be visually seen to initiate within 2 weeks. 5 weeks after initiation, digital image analysis shows a reduction in the total corroded area when compared to samples (a) and (b), with an average total corroded area of 0.41cm$^2$ per defect for sample c after 5 weeks. Furthermore sample (c) shows a reduction in the average number of filiform corrosion filaments, and the average length of individual filiform corrosion filaments when compared to samples a and b. With further increases in the volume fraction of HT incorporated in to the PVB (samples d and e) these trends / correlations are continued within this sample range.

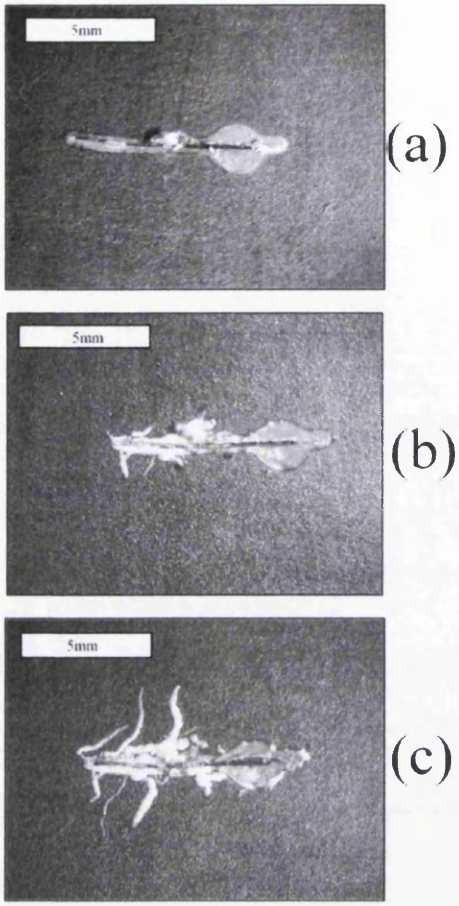


**Figure 6-1** : The surface appearance of the 10mm penetrative defect after **(i)** 1 week, **(ii)** 3 weeks, and **(iii)** 6 weeks on PVB coated Zn+Al(1.5wt%)+Mg(1.5wt%) 140g/m$^2$ hot dip coating with the PVB coating containing a volume fraction of 0.1hydrotalcite. Initiation is with 2µl of 1.5mol/dm$^3$ acetic acid, and propagation conditions of 22°c and 86% relative humidity

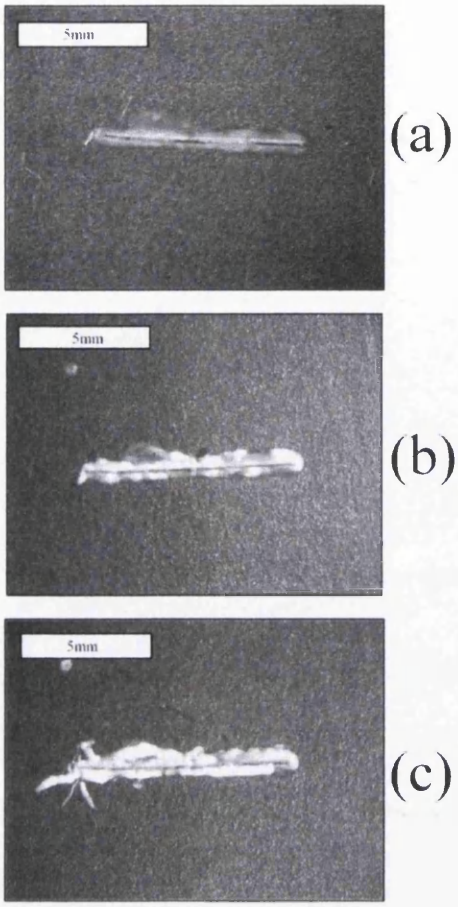


**Figure 6-2** : The surface appearance of the 10mm penetrative defect after **(i)** 1 week, **(ii)** 3 weeks, and **(iii)** 6 weeks on PVB coated Zn+Al(1.5wt%)+Mg(1.5wt%) 140g/m2 hot dip coating with the PVB coating containing a volume fraction of 0.2 hydrotalcite. Initiation is with 2µl of 1.5mol/dm$^3$ acetic acid, and propagation conditions of 22°c and 86% relative humidity

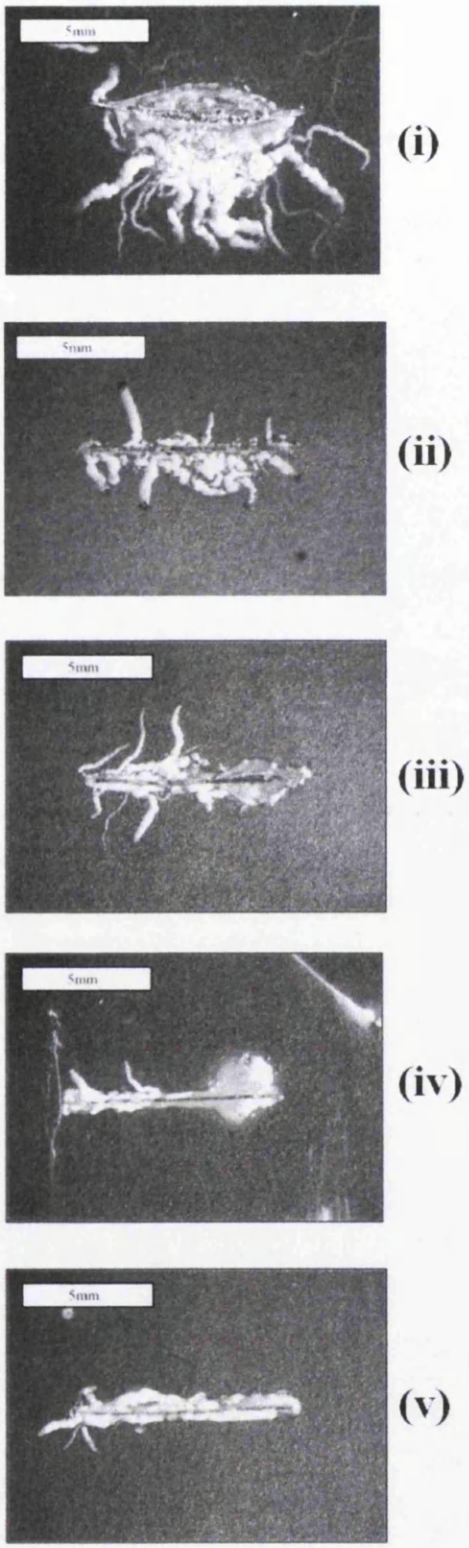


**Figure 6-3** : The surface appearance of the 10mm penetrative defect on PVB organically coated Zn+Al*(1.5wt%)*+Mg*(1.5wt%)* hot dip steel samples after 5 weeks after filiform corrosion initiation with 2µl of 1.5mol/dm$^3$ acetic acid, and propagation conditions of 22°c an 86%. Samples contain a systematic variation in the volume fraction (VF) of hydrotalcite (HT)in the PVB organic coating **(i)** 0 VF HT, **(ii)** 0.05 VF HT, **(iii)** 0.1 VF HT, **(iv)** 0.15 VF HT, **(v)** 0.2 VF HT.

When the propagation kinetics in relation to time of individual filiform corrosion filaments on uninhibited PVB coated Zn+Al+Mg hot dip coated steel are studied; linear filament growth rates are found to be linear after initiation The kinetics of filiform corrosion in relation to total areas corroded and HT volume fraction in the coating is shown in figure 6-4. The filament length in relation to HT volume fraction in the coating is shown in figure 6-5 and rates of filament growth are shown in figure 6-6. The addition of HT has been shown to reduce the rate of filament propagation with regards to time after initiation, resulting in a negative parabolic kinetic trend. On samples containing 0.2VF HT, filament propagation has completely stopped after 4 weeks. Increasing VF of HT also results in a reduction in the average number of filiform filaments. This is shown in figure 6-7. The reason for this is that the hydrotalcite will scavenge acetic acid via the anion exchange reaction, reducing acetate anions to form water and carbon dioxide via a reversible equilibrium reaction. Although this reaction is reversible, the carbon dioxide reaction product will diffuse through the organic coating in to the atmosphere, meaning that the concentration of $CO_2$ required for the reversible reaction is diminished, and therefore the two reactions will not be in kinetic equilibrium. As a result of this, the concentration of aggressive acetic acid anions in the filament head is reduced, and an excess of water is formed in the filament head as is shown equation 6-2.

$$2HAc_{(aq)} + C0_{3\,(HT)}^{2-} \leftrightarrow 2Ac_{(HT)}^{-} + H_2CO_{3\,(aq)} \rightarrow H_2O_{(l)} + CO_{2\,(g)} \qquad (6\text{-}2)$$

Excess $H_2O$ in the filament head will dilute the electrolyte, reducing the relative excess of aggressive anions per volume of electrolyte, causing an increase in electrolyte pH.

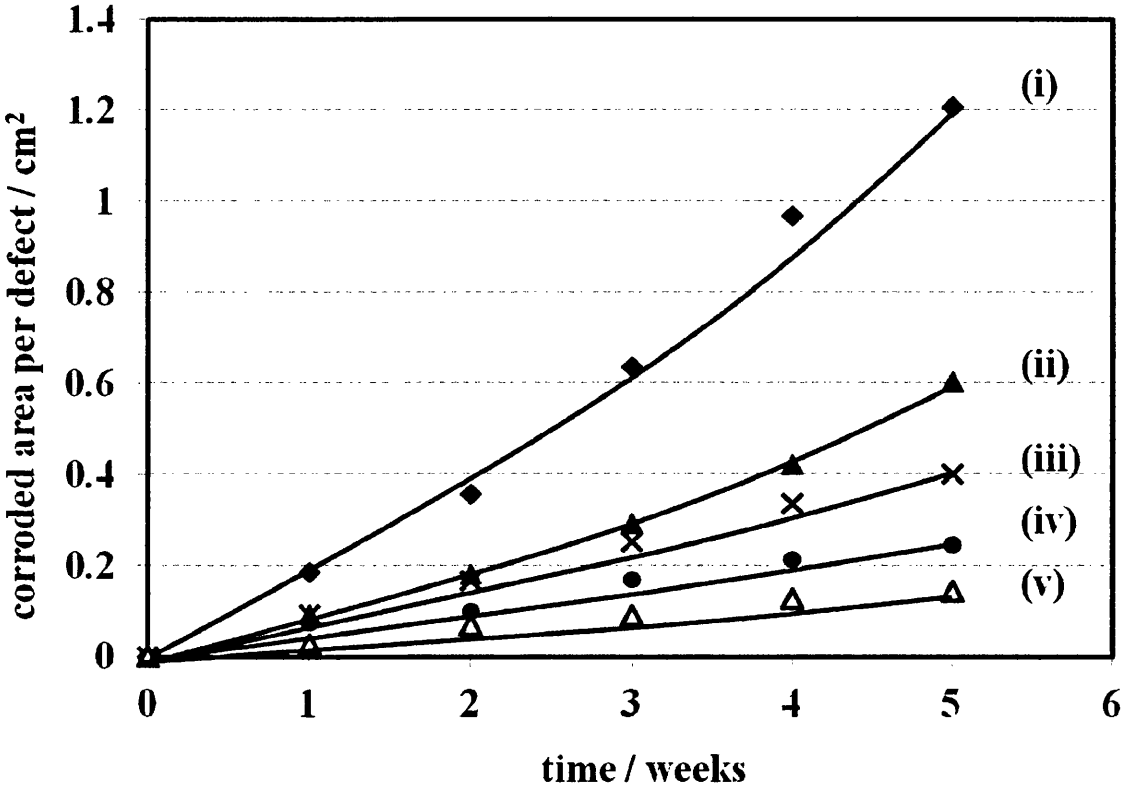


**Figure 6-4 :** The average total surface area covered in corrosion product around a 10mm penetrative defect on PVB coated Zn+Al*(1.5wt%)*+Mg*(1.5wt%)* hot dip coated steel, averaged over 4 defects as measured using sigma scan digital image analysis. All filiform corrosion is initiated with 2µl of 1.5mol/dm$^3$ acetic acid per defect, and propagation occurs at a relative humidity of 86% and a temperature of 22°c. Volume fraction (VF) of hydrotalcite (HT) in the PVB organic coating is systematically vaired and this is shown in data sets **(i)** 0 VF HT, **(ii)** 0.05 VF HT, **(iii)**, 0.1VF HT, **(iv)** 0.15 VF HT, **(v)** 0.2 VF HT

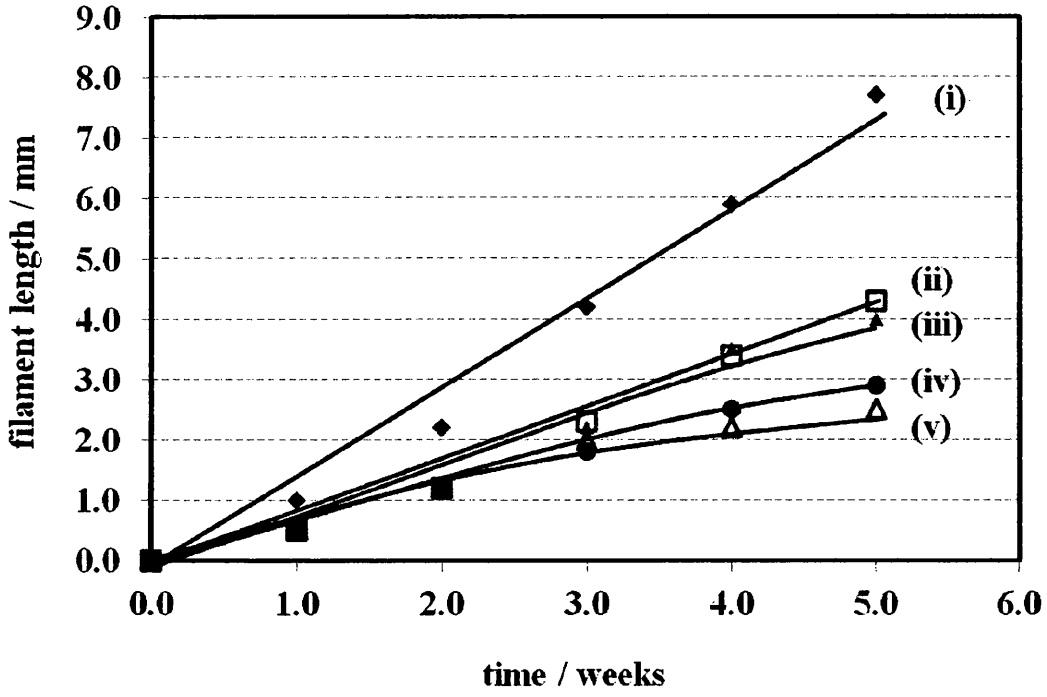


**Figure 6-5 :** Filament length averages over 4 typical filaments to show the propagation kinetics of a filiform filament from a 10mm penetrative defect on PVB coated Zn+Al*(1.5wt%)*+Mg*(1.5wt%)* hot dip coated steel. All filiform corrosion is initiated with 2µl of 1.5mol/dm$^3$ acetic acid per defect, and propagation occurs at a relative humidity of 86% and a temperature of 22°c. Volume fraction (VF) of hydrotalcite (HT) in the PVB organic coating is systematically varied and this is shown in data sets **(i)** 0 VF HT, **(ii)** 0.05 VF HT, **(iii)**, 0.1VF HT, **(iv)** 0.15 VF HT, **(v)** 0.2 VF HT

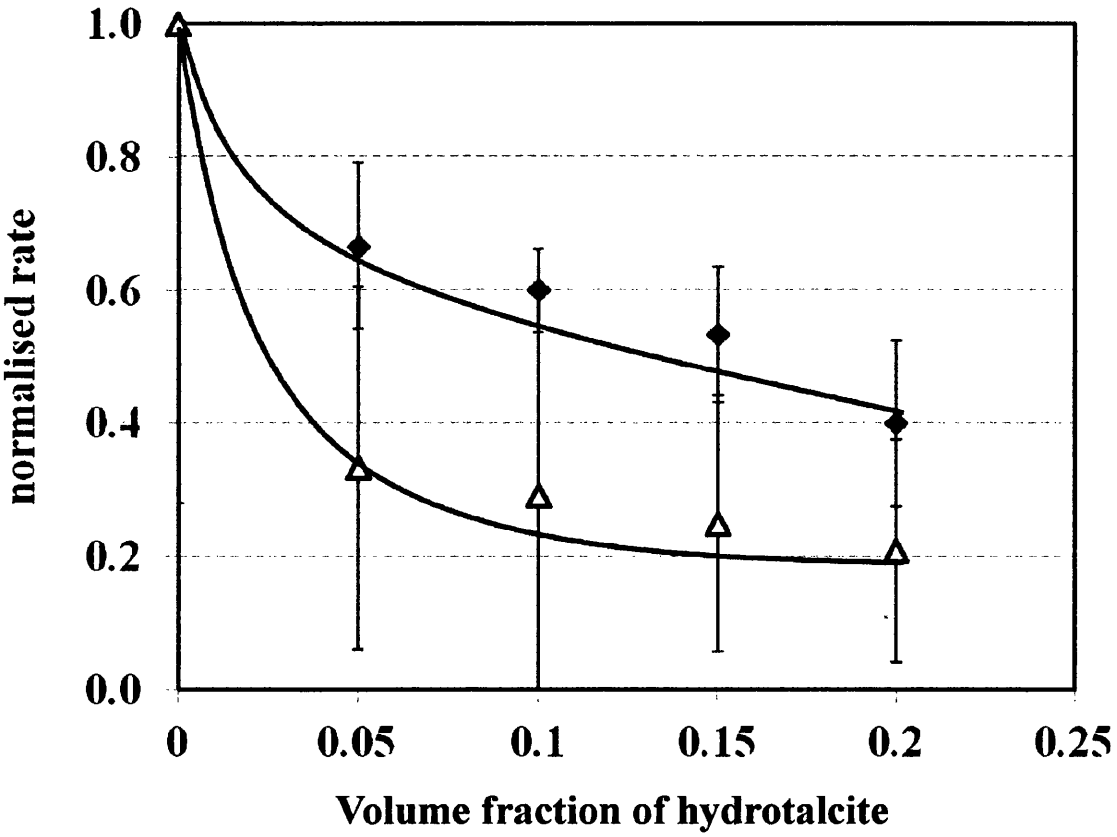


**Figure 6-6** The average rate of filament length growth between **(i)** 1 and 2 weeks, and **(ii)** 4 and 5 weeks. Higher levels of hydrotalcite can be seen to reduce the rate of growth by a greater amount, as the hydrotalcite has scavenged more acid from the filament head. Experiment is carried out on PVB coated Zn+Al*(1.5wt%)*+Mg*(1.5wt%)* hot dip coated steel. All filiform corrosion is initiated with 2µl of 1.5mol/dm$^3$ acetic acid per defect, and propagation occurs at a relative humidity of 86% and a temperature of 22°c

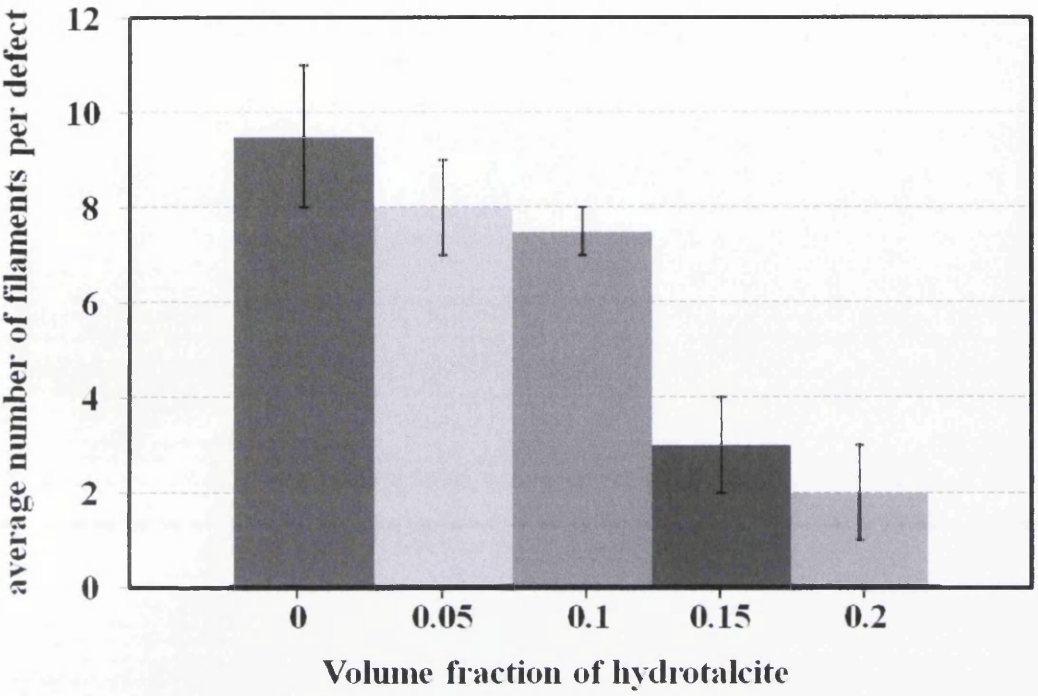


**Figure 6-7** : The average number of filaments averaged over 4 10mm penetrative defects on PVB coated Zn+Al*(1.5wt%)*+Mg*(1.5wt%)* hot dip coated steel. All filiform corrosion is initiated with 2µl of 1.5mol/dm$^3$ acetic acid per defect, and propagation occurs at a relative humidity of 86% and a temperature of 22°c

The morphology of filiform corrosion filaments when HT is present also differs from uninhibited filaments. When no HT is present the width of filiform filaments remain constant along their entire length. This is due to the filament head having a constant composition and electrolyte volume. When HT is added the filaments have a conical morphology, as in the filament width reduces with filament length. This is shown in SEM backscatter images in figures 6-8 and 6-9.

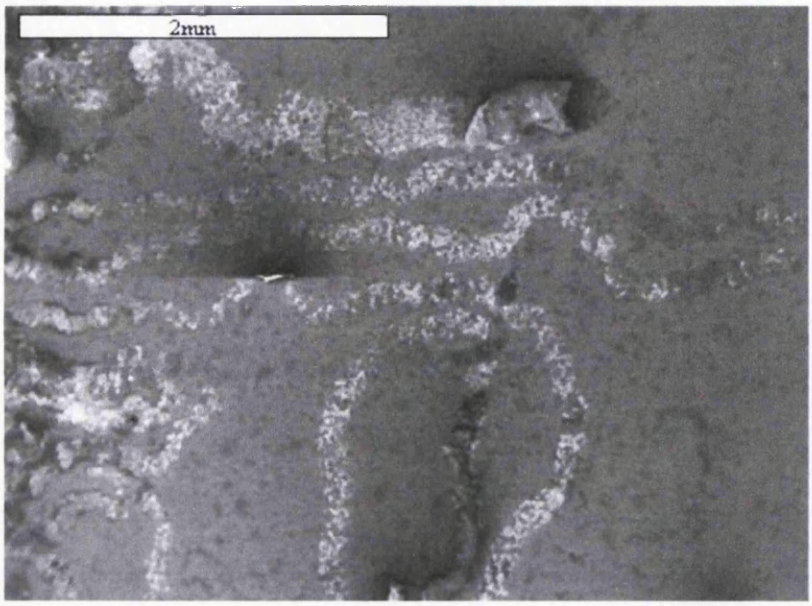


**Figure 6-8** : SEM image of filiform corrosion filaments on a Zn+Al*(1.5wt%)*+Mg*(1.5wt%)* hot dip coated steel sample after 6 weeks of propagation at 86%RH at 22°c. When no hydrotalcite is present the rate of filament propagation, and the thickness of the filament remain constant over time as the amount of electrolyte in the head is conserved.

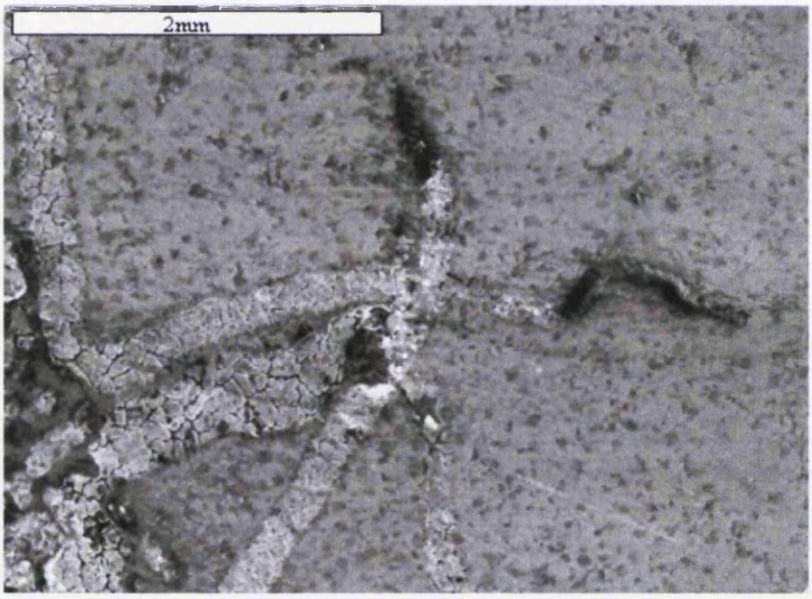


**Figure 6-9** : SEM image of filiform corrosion filaments on a Zn+Al*(1.5wt%)*+Mg*(1.5wt%)* hot dip coated steel sample after 6 weeks of propagation at 86%RH at 22°c. 0.1 volume fraction hydrotalcite is present in the PVB coating. This HT has reduced the amount of electrolyte in the filament head over time, and as a result of this the rate of filament propogation reduces. The filaments can also be seen to have a conical shape, as there width is also reduced over time due to the reduction in electrolyte volume.

## 6.5 Conclusion

The addition of HT to PVB model organic coatings on Zn-Al-Mg hot dip coated steel leads to a reduction in the total corroded area per defect after 5 weeks, the average length of filiform corrosion filaments, and the average number of filiform corrosion filaments per defect. The magnitude of this reduction correlates to the amount of HT addition (more HT results in a smaller total corroded area, and fewer smaller filiform corrosion filaments).

The HT mechanism for corrosion inhibition is the scavenging of acetate anions in the filament head, and subsequent anion exchange for carbonate anions from the HT converting the acetic acid to aqueous carbonate anions. These carbonate anions are then further reduced to carbon dioxide, which will diffuse through the organic coating in to the atmosphere creating non equilibrium condition for the reversible reaction, reducing the rate of the reverse reaction and favouring the permanent removal of acetate from the filament head. The overall efficiency of the reaction is governed by the HT exchange capacity. There is a finite amount of HT present in the coating, and therefore a finite number of exchange reactions can occur. If the amount of acetic acid exceeds the HT capacity, then the HT capacity will be exhausted, and some acetic acid will remain, and corrosion will continue. Where there is an excess of acetic acid this will happen at a local level. As the corroded area increased acetate is exposed to un-exhausted areas of coating which will enable more anion exchange reactions to occur. HT is a viable, not toxic method of reducing the susceptibility of organically coated Zn-Al-Mg hot di

# Chapter 7 Overview and Future work

**Overview of findings**

Zn-Al-Mg hot dip steel coatings are currently in development globally for commercial uses in automotive and construction sectors. Most traditional corrosion testing methods such as salt spray test the cathodic disbondment performance of coatings. The addition of magnesium has been shown to dramatically improve the resistance of these coatings to cathodic disbondment and for this reason these coatings regularly outperform conventional zinc based coatings in salt spray tests by as much as 10x. However the addition of anodic phases potentially also makes these coatings vulnerable to anodic forms of attack such as pitting corrosion and filiform corrosion.

In this thesis it has been shown that organically coated Zn-Al-Mg hot dip coatings are susceptible to filiform corrosion when initiated with acetic acid. The mechanism of corrosion is that the least noble microstructural phase, $MgZn_2$ is anodically dissolved, this then exposes the steel substrate which acts as a cathode, promoting rapid corrosion of the remaining coating. The time taken to expose the iron substrate can be measured during immersion experiments. A link between the time to iron exposure and the susceptibility of the coating to filiform corrosion has been confirmed, in that the shorter the time to iron exposure, the more susceptible the coating is to filiform corrosion. Thicker coating weights have a longer time to iron exposure, and therefore are less susceptible to filiform corrosion. Increasing aluminium additions to the hot dip coating also increases the time to iron exposure and the resistance to filiform corrosion.

Filiform corrosion can also be inhibited by adding active pigments to the organic coating. Phenylphosphonic acid reduced filiform corrosion levels by up to 80% after 5 weeks by reacting with the surface of the Zn-Al-Mg hot dip coating and forming a layer of insoluble $Zn^{2+}PP^{2-}$ salt. This acts as a barrier for electron transfer to the cathodic site reducing the overall rate of corrosion. Hydrotalcite is also added to the PVB organic coating. HT is an anion exchange clay, which will convert acetate in to carbonate. HT also reduced filiform corrosion by up to 70%.

**Future work**

The work in this thesis was completed to the highest possible standard with the equipment and time available. With more time it would be possible to gain a further understanding of phenomena discussed in this thesis. In chapter 4 it is stated that higher levels of aluminium in the hot dip coating alloy leads to an increase in filiform corrosion resistance due to the formation of a passive aluminium oxide layer. Given more time this oxide layer could be characterized using a technique such as XPS. Furthermore the oxide on other samples could also be characterized and this could be used to predict the filiform corrosion resistance of novel alloys. A similar characterization could be used to understand the salt layer which is deposited when PPA is added to the organic coating. Hydrotalcite described in chapter 6 has a finite capacity for anion exchange reactions. When the HT has been exhausted no more anion exchange reactions can take place, and the coating will effectively be uninhibited. Further work which could be carried out is to understand the lifetime of HT coatings, and understand there usable life span.

A more fundamental understanding of how Zn-Al-Mg coating corrode could be obtained using x ray diffraction studies. This would give a greater understanding to the corrosion mechanism, and also a highly visual output for explaining the corrosion mechanism.

Finally some initial studies were carried out on hot dip zinc coatings where a thin layer of magnesium has been deposited by PVD. These coatings are also susceptible to filiform corrosion. Potentially layers of magnesium and aluminium could be deposited, to create a more controlled coating, with various surface properties. Diffusion times could also be altered to that the magnesium is diffused in to just the surface, or down to the steel substrate.

# References


1. Association, World steel. *World Crude steel Production.* 2012 (annual report)

2. *Handbook of Environmental Degradation of Materials.* Norwich : M.Kutz. Willaim Andrew Publishing, 2005. ISBN = 8155 1500 6 (0-8155).

3. *Ecconomic effects of metalic corrosion in the United States,* L.H Bennet, J.Kruger . National Burear of standards special publication, 1978. ISBN = N/A

4. *Corrosion Costs and preventative stratagies in the United States.* G.H.Koch, M.P.H Brongers. 2002, NACE internalional annual report

5. *Introduction to Corrosion Science.* New York : E.McCafferty. Springer, 2009. ISBN 978-1-4419-0454-6.

6. *Corrosion Prevention and Protection, practical solutions.* V.S.Sastri, E.Ghali, M.Elboujdaini. Chichester : cs-books, 2007 ISBN = 978-0-470-02402-7

7. *Chemistry (9th Edition).* E Davis, M Peck, G Stanley. Belmont : Mary Finch, 2010 ISBN = 978-1133610663

8. *Corrosion Tests and Standards: Application and Interpretation.* R.Baboian. MD : Baltimore, 2005. ISBN = 0-8031-2098-2

9. *Introduction to Corrosion Science.* E.McCafferty. London : Springer, 2010. ISBN = 978-1-4419-0454-6

10. *Anode activation polarization on Pt(h k l) electrodes in dilute sulphuric acid electrolyte.* R.F.Mann, J.C.Amphkett, B.A.Peppley, C.P.Thurgood. 2, s.l. : Journal of Power Sciences, 2007, Vol. 163. 679-687.

11. *Axial mass transport in liquid–liquid Taylor–Couette–Poiseuille flow.* X.Zhu, R.J.Campero, R.D.Vigll. 21, s.l. : Chemical engineering science, 2000, Vol. 55. 5079-5087.

12. *Area effects in aluminum electrodes.* W.M.Macnevin, R.M.Wilson. s.l. : Analytica Chemica Acta, 1960, Vol. 23. 390-395.

13. *The corrosion product morphology found on sacrificial zinc anodes.* J.Perkins, R.A.Bornhold. 5, s.l. : Corrosion Science, 1977, Vol. 17. 377-384.

14. *Cathodic Protection.* J.H.Morgan. NACE 1987. ISBN = 0915567288

15. *Cathodic disbondment of epoxy coating with zinc aluminum polyphosphate as a modified zinc phosphate anticorrosion pigment.* R.Naderi, M.Attar. 4, s.l. : Progress in Organic Coatings, 2010, Vol. 69. 392-395.

16. *Cathodic disbonding of a thick polyurethane coating from steel in sodium chloride solution.* J.L.Luo, C.J.Lin, Q.Jang, S.W.Guan. 4, s.l. : Progress in Organic Coatings, 1997, Vol. 31. 289-295.

17. *Cathodic disbonding of an unpigmented epoxy coating on mild steel.* H Bi, J Sykes. s.l. : Corrosion Science, 2011, Vol. 53. 3416-3425.

18. *Using ceramic membranes to recycle two nonionic alkaline metal-cleaning solutions.* A-Chen, N.Stencel, D.Ferguson. 1-2, s.l. : Journal of Membrane Science, 1999, Vol. 162. 219-234.

19. *An investigation of the influence of physical vapour deposited aluminium layers on the kinetics of organic coating disbondment on iron.* G.J.Reynolds, Z.S.Barrett, N.H.McMurray, G.Willaims. s.l. : Corrosion Science, 2013, Vol. 70. 82-92.

20. *Filiform underfilm corrosion of lacquered steel surfaces.* C.F.Sharman. 1944, Nature, p. 621.

21. *Filiform corrosion in polymer coated metals.* A.Bautista. 1996, Progress in Organic Coatings, pp. 49-58.

22. *Machanism of Filiform Corrosion.* W.H.Slabaugh, M.Grotheer. 1954, Industrial and Engineering Chemistry, pp. 1014-1016.

23. *Effect of climatic parameters on filiform corrosion of coated aluminium alloys.* N.LeBozec, D.Persson, D.Thierry. 2004, Nace international annual conference.

24. *Chloride-induced filiform corrosion of organic-coated magnesium.* G.Williams, R.Grace. 2010, electrochemica Acta, pp. 1894-1903.

25. *Blistering of Paint Films and Filiform corrosion.* Funke, W. 1981, Progress in organic coatings, pp. 29-46.

26. *Filiform corrosion of bianry aluminum model alloys.* A.Afseth, J.Nordlien, G.Scamans, K.Nisancioglu. 2002, Corrosion Science, pp. 2529-2542.

27. *effect of thermo-mechanical processing on filiform corrosion of aluminum alloy AA3005.* A.Afseth, J.Nordlien, G.Scamans, K.Nisancioglu. 2002, corrosion science, pp. 2491-2506.

28. *The breakdown in the barrier properties of organic coatings due to filiform corrosion.* A.T.A.Jenkins, R.D.Armstrong. 7, s.l. : Corrosion Science, 1996, Vol. 38. 1147-1157.

29. *Scanning kelvinprobe investigations of filiform corrosion on aluminum alloy 2024-t3.* W.Schmidt, M.Stratmann. 8, s.l. : Corrosion Science, 1998, Vol. 40. 1441-1443.

30. I*nhibition of filiform corrosion on organic-coated AA2024-T3 by smart-release cation and anion-exchange pigments.* G.Williams, H.N.McMurray. 2012, electrochemica Acta, pp. 287-294.

31. *Filiform corrosion: interactions between electrochemistry and mechanical properties of the paints.* J.Delplancke, S.Berger, X.Lefebvre, D.Maetens, A.Pourbaix, N.Heymans. 2001, Progress in Organic Coatings, pp. 64-74.

32. *Investigations of filiform corrosion of varnighed steel plates.* Kaesche, H. 1959, werkstoffe Korros, p. 668.

33. *The influence of contaminants on the failure of protective organic coatings on steel.* E.Koehler. 1977, Corrosion, pp. 209-217.

34. *A review of filiform corrosion.* Hoch, G. 1974, NACE, p. 134.

35. *Pourbaix diagrams for the iron–water system extended to high-subcritical and low-supercritical conditions.* s.l. : Corrosion Science, 2012, Vol. 55. 326-331.

36.. *The science of construction materials.* Berlin : H Freiesleben. Springer Heidelberg, 2009.

37. *The morphology of coating/substrate interface in hot-dip-aluminized steels.* G.Awan, F.Hasan. 1-2, s.l. : Materials Science and Engineering, 2008, Vol. 472. 157-165.

38. *Microstructure and high temperature oxidation behavior of hot-dip aluminized coating on high silicon ductile iron.* M.Lin, C.Wang. 5, s.l. : Surface and Coatings technology, 2010, Vol. 205. 1220-1224.

39. *Chemistry, energy and the environment.* César A. C. Sequeira, John B. Moffat. ISBN 0-85404-703-4. Estoril : Bookcraft, 1997.

40. *The metallurgy of zinc coated steel.* A.R.Marder. Nethlehem : Progress in Materials Science, 2000, Vol. 45. 191-271.

41. *Hot dip galvanizing: A guide to process selection and galvanixing practice.* Hornsby, M.J. s.l. : ITDG publishing, 1995. 13:9781853391903.

42. *Comparison between the Cook-Nortenman and Sedzimir processes.* Bablik, H. London : Fifth international conference on hot dip galvanizing, 1958. 115-161.

43. *Handbook of hot dip galvanization.* Peter Maaß, Peter Peißker. Weinheim : Wiley-VCH, 1993 ISBN = 978-3-527-32324-1.

44. *Effects of zinc bath temperature on the coatings of hot dip galvanizing.* B Peng, J Wang, X.Su, Z.Li, F.Yin. 9, Xiangtan University : Surface and Coatings technology, 2008, Vol. 202. 1785-1988.

45. *Formation of intermetallic phases on 55wt% Al-Zn-Si hot dip strip.* D. Phelan, B Jiang Zu, R Dippenaar. 1-2, Wollongong : Materials Science and Engineering, 2006, Vol. 420. 144-149.

46. *The effect of magnesium additions on the microstructure and cut edge corrosion resistance of zinc aluminium galvanised steel.* J.Elvins, J. Spittle, J.Sullivan, D. Worsley. 6, Seansea : Corrosion Science, 2008, Vol. 50. 1650-1658.

47. *Morphology and properties of hot dip Zn+Mg and Zn+Mgh+Al alooy coatings on sheet steel.* M.Dutta, A.K.Halder, S.B.Singth. 2010, Surface coatings and technology, pp. 2578-2584.

48. *Corrosion behaviour of Zn+Al+Mg coated steel in sodium chloride conating environment.* S.Schuerz, M.Fleishanderi. 2009, Corrosion Science, pp. 2355-2363.

49. *The peformance of Zn+Al+Mg+Si hot dip galvanized sheet steel.* S.Tanaka, K.Honda, A.Takahashi, Y.Morimoto, M.Kurosaki, H.Shindo, K.Nishimura, M.Sugiyama. Brussels : s.n., 2001. Galvatrech. pp. 153-160.

50. *Corrosion peformance of Zn+Al+Mg coatings in open and confined zones in conditions simulating automotive applications.* T.Prosek, N.Larche, M.Volt, F.Goodwin, D.Thierry. 2010, Materials and Corrosion, p. 412.420.

51. *Solidification Structure of the Coating Layer on Hot-Dip Zn-11%Al-3%Mg-0.2%Si-Coated Steel Sheet.* H.shindo, K.Nishumura, K.Saito. Tokyo : s.n., 1988. Galvatec. pp. 1395-1400.

52. *Corrosion Resistance of pre-painted Zn-6%Al-hot dip coated steel.* S.Yamamoto, A.Komatsu, A.Andog. Osaka : s.n., 2007. Galvatec. pp. 659-664.

53. *Case study of the role of Mg alloying in Zn+Mg on sheet steel.* C.Schwerdt, M.Riemer, S.Kohler, B.Schumacher, M.Steinhorst, A.Zwick. Chicago : s.n., 2004. Galvatec. p. 783.

54. M.Dutta, A.Kumar Halder, S.Brat Singh. *Morphology and Properties of hot dip Zn-Mg and Zn-Mg-Al alloy coatings on steel sheet.* Jamshedpur : R&D Tata Steel, Jamshedpur, India, 2010.

55. *Corrosion mechanism of model zinc-magnesium alloys in atmospheric conditions.* T.Prosek, A.Nazarov. 2008, Corrosion Science, pp. 2216-2231.

56. *Structure and corrosion-resistance of zinc alloy coated steel sheets obtained by continuous vapor-deposition apparatus.* J.Kawafuka, J. Katoh, M.Toyama, H.Nisimoto, K.Ikeda, H.Satoh. 1991, TETSU TO HAGANE-JOURNAL OF THE IRON AND STEEL INSTITUTE OF JAPAN, pp. 995-1002.

57. *Self healing ability of zinc plated steel coated with magnesium electrodeposited from a molten salt.* M.Morishita, K.Koyama, Y.Mori. 1997, Materials Transactions, pp. 719-723.

58. *Magizinc, a new generation of hot dip galvanised products.* M.Vlot, R.Bleeker, T Maalman, E Van Perlstein. Dusseldorf : s.n., 2006. Galvatec.

59. *Properties and potential application of novel Zn-Mg alloy coatings on steel sheet by PVD.* T.Koll, K.Ullrich. 2004, Revue de Métallurgie, pp. 543-550.

60. *Inovative steel strip coatings by means of PVD in a continuous pilot line* : Process technology and coating development. B.Schuhmacher, C Scherdt, U Seyfert, O.Zimmer. 2003, Surface and coatings technology, pp. 703-709.

61. *Corrosion of zinc-magnesium coatings : Mechanism of paint delamination.* R.Hausbrand, M.Stratmann, M.Rohwerder. 2009, Corrosion science, pp. 2107-2114.

62. *Influence of Mgcontent in coating layer and coating structure on corrosion resistance of hot-dip Zn–Al–Mg–Si alloy coated steel sheet,.* . Tsujimura, A. Komatsu, A. Andoh. Brussels : s.n., 2001. Galvatic. pp. 145–152.

63. *Corrosion Behavior of Zn-Al-Mg Coated Steel in Different Environments.* S.Shuerz, G.Mori, G.Luckeneder, M.Fleischanderl, K.Heinz-Stellnberger. Houston : Nace international, 2011. NACE corrosion conference and expo 2011. pp. 1-16.

64. Kuznetsov, Y.I. *Organic Inhibitors of corrosion of metals ISBN 0-306-45169-7.* New York : Plenum, 1996.

65. *Anion-Exchange Propoerties of Hydrotalcite like compounds.* S.Miyata. 1983, Clays and Clay Materials , pp. 305-311.

66. *Smart release corrosion inhibitor pigments based on organic ion exchange resins.* G.Williams, S.Geary, N.H.McMurray. 2012, Corrosion Science, pp. 139-147.

67. *Anion-Exchange Inhibition of Filiform corrosion on Organic Coates AA2024-T3 Aluminium Alloy by hydrotalcite-Like pigments.* G.Williams, H.N.McMurray. 2003, Electrochemical and Solid State letters, pp. B9-B11.

68. *Clays and catalysis: a promising future.* A.Vaccari. 1999, Applied Clay Science, pp. 161-198.

69. *V.A.Drits, T.N.Sokolova, G.V.Sokolova, V.I.Cherkashin.* Group, New Members of the Hydrotalcite-Manasseite. 1987, Clays and Clay materials, pp. 401-417.

70. *Effective ionic radii in oxides of flourides.* R.D.Shannon, C.T.Prewitt. 1969, Chrystallographic Acta, pp. 925-946.

71. *Corrosion mechanism and inhibition on organic coated packaging steel.* T.Watson. 2007, EngD thesis, p. 45.

72. V.Rives. *Layered double Hydroxides: Pase Present and Future.* s.l. : Nova, 2001.

73. *Absorbtion Studies on Clay Minerals. A forumlation of the thermodynamics of Exchange Adsorption.* H.C.Thomas, G.L.Gaines. 1952, the jounral of chemical physics, pp. 714-719.

74. *Corrosion and the electrochemistry of zinc.* New York : Zhang, Xiaoge Gregory. Plenum, 1996. ISBN = 978-0306453342

75. *Chrome-Free Single-Step In-Situ Phosphazing Coatings on a Ti-6Al-4V Titanium Alloy.* H.Neuder, C.Tsu Lin. 2002, Journal of Coatings Technology, pp. 37-42.

76. *Effect of Zinc Phosphating on Corrosion Control for Carbon Steel Sheets.* M.Hafiz, J.Kashan, A.Kani. 2008, engineering and technology, pp. 501-511.

77. *Green chemistry in in situ phosphatizing coatings.* Lin, C.Tsu. 2001, Progress in organic coatings, pp. 226-235.

78. *Inhibition of Filiform Corrosion on AA6111-T$ Using In-Coating Phenlyphosphonic Acid.* A.J.Coleman, H.N.McMurray, G.Williams, A.Afseth, G.M.Scamans. 2007, Electrochemical and Solid State, pp. C35-C38.

79. *An In-Situ phosphating coating catalyzed by phenylphosphonic acid on AA6061.* Z.Ming. 2012, Metal Finishing.

80. *anion embedded sol-gel films on Al for corrosion protection.* M.Sheffer, A.Groysman, D.Starosvetsky, N.Savchenko, D.Mandler. 2004, Corrosion Science, pp. 2975-2985.

81. DC Bell, AJ Garratt-Reed. *Energy Dispersive X-Ray analysis in the electron microscope ISBN 0-203-48342.* Oxford : BIOS Scientific Publishers Ltd, 2005. ISBN 0-203-48342.

82. *SEM–EDX—a useful tool for forensic examinations.* G.Zadora, Z.Brozek-Mucha. 2-3, s.l. : Materials Chemistry and Physics, 2003, Vol. 81. 345-348.

83. Haugstad, Greg. *Atomic force microscopy.* New Jersey : John Wiley and Sons, 2012. ISBN 978-0-470-63882-8.

84. *A review of atomic force microscopy imaging systems: application to molecular metrology and biological sciences.* N.Jalili, K.Laxminarayana. 8, s.l. : Mechatronics, 2004, Vol. 14. 907-945.

85. *Atomic Force Microscopy, Scanning Kelvin Probe Force Microscopy and magnetic measurements on thermally oxidized AISI 304 and AISI 316 stainless steels.* B.Maachi, C.Pirri, A.Mehdaoui, N.E.Hakiki, J.L.Bubendorff. 3, s.l. : Corrosion Science, 2011, Vol. 53. 984-991.

86. *Microscopic aspects of electrochemical delamination: an SKPFM study.* M.Rohwerder, E.Hornung, M.Stratmann. s.l. : Electrochemica Acta, 2003, Vol. 48. 1235-1243.

87. P.Mass, P.Peissker. *Handbook of hot dip galvanizing.* Weinheim : Wiley-VHC, 1993. ISBN 978-3-527-32324-1.

88. *Aluminum Control on Stelco's Z-Line.* E.W.Fossen, P.J.Landriault, M.G.Lamb. s.l. : Galvatec, Iron and Steel society, 1995. 795-800.

89. *Numerical simulation of hot-dip metallic coating process.* H.Zhang. 2, s.l. : International Journal of heat and mass transfer, 1995, Vol. 38. 241-257.

90. M.Vlot. *Corriosion resistance of Zn-Al-Mg hot dip coated steels.* s.l. : Tata steel internal R&D report, 2006.

91. *Kinetics of atmospheric corrosion of mild steel, zinc, galvanized iron and aluminium at 10 exposure stations in India.* M.Natesan, G.Venkatachari, N.Palaniswamy. 11, s.l. : Corrosion Science, 2006, Vol. 48. 3584-3608.

92. *Chromate Inhibition of Corrosion-Driven Organic Coating Delamination Studied Using a Scanning Kelvin Probe Technique.* G.Williams, H.N.McMurray. 10, s.l. : Journal of the electrochemical society, 2001, Vol. 148. B377.

93. *Inhibition of NF-kappa B Binding to DNA by chromium, cadmium, mercury, zinc and arsenite in vitro: evidence of a thiol mechanism.* J.A Shumilla, K.E Wetterhahn. 2, s.l. : archives of biochemistry and biophysics, 1998, Vol. 349. 356-362.

94. *Comparative electrchemical studies of zinc chromate and zinc phosphate as corrosion inhibitors for zinc.* A.C Bastos, M.G.S Ferreira, A.M Simoes. 4, s.l. : progress in organic coatings, 2005, Vol. 52. 339-350.

95. *Study of the anticorrosive properties of zinc phasphate in vinyl paints.* B. Amo, R.Romagnoli, V.F Vetere, L.S Herna. 1, s.l. : Progress in organic coatings, 1998, Vol. 33. 28-35.

96. *Anticorrosive coatings containing modified phosphates.* V. Jaskova, A.Kalendova. 4, s.l. : Progress in organic coatings, Vol. 75. 328-334.

97. *Comparative electrochemical studies of zinc chromate and zinc phosphate as corrosion inhibitors for zinc.* A.C.Bastos, M.G.Ferreria, A.M.Simoes. 4, s.l. : Progress in organic coatings, 2005, Vol. 52. 339-350.

98. *Smart release corrosion inhibitor pigments based on organic ion-exchange resins.* G.Williams, S.Geary, H.N.McMurray. 1, s.l. : Corrosion Science, 2012, Vol. 57. 139-147.

99. *Active protection coatings with layered double hydroxide nanocontainers of corrosion inhibitor.* M.L.Zheludkevich, S.K.Poznyak, L.M.Rodrigues, D.Raps, T.Hack, L.F Dick, T.Nunes, M.G.S Ferreira. 2, s.l. : Corrosion Science, 2010, Vol. 52. 602-611.

100. *The effect of surface / primer treatments on the peformance of alkyd coated steel.* J.Marsh, J.Dlebury, S.B.LyonScan. 5, s.l. : Corrosion Science, 2001, Vol. 43. 829-852.

101. *Inhibition of filiform corosion on AA611-T4 Using In-Coating Phenylphosphonic Acid.* A.Coleman, N.H.McMurray, G.Williams, A.Afseth, G.M.Scamans. 5, s.l. : Electrochemical and Solid-State letters, 2007, Vol. 10. C35.

102. *Dopant effects in Polyaniline Inhibition of Corrosion-Driven Organic Coating Cathodic Delamination on Iron.* G.Williams, A.Gabriel, A.Cook, H.N.McMurray. 10, s.l. : Journal of the electrochemical society, 2006, Vol. 153. B425.

103. *Characterisation of barrier properties of organic paints: the zinc phosphate effectiveness.* M.Beiro, A.Collazo, M.Izquierdo, X.Novoa, C.Perez. 2, s.l. : Progress in organic coatings, 2003, Vol. 46. 97-106.

104. *Challenges of chromate inhibitor pigments replacement in organic coatings.* J.Sinko. 3-4, s.l. : Progress in organic coatings, 2001, Vol. 42. 267-282.

105. *Inhibition of corrosion-driven organic coating disbondment on galvanised steel by smart release group II and Zn(II)-exchanged bentonite pigments.* G.Williams, N.H.McMurray, M.Loveridge. 5, 2010 : Electrochemica Acta, Vol. 55. 1740-1748.

106. *Anion-Exchange Inhibition of Filiform Corrosion on Organic Coated AA2024-T3 Aluminum Alloy by Hydrotalcite-Like Pigments.* G.Williams, N.H.McMurray. 3, s.l. : Electrochemical and Solid state letters, 2003, Vol. 6. B9-B11.

107. Inhibition of Filiform Corrosion on Organic-Coated Aluminum Alloy by Hydrotalcite-Like Anion-Exchange Pigments. H. N. McMurray, G. Williams. 3, Swansea : Corrosion Science, 2004, Vol. 60. 219-228.

# Appendix

| week number | filament 1 | filament 2 | filament 3 | filament 4 | mean length mm | st dev | st dev of mean |
|---|---|---|---|---|---|---|---|
| | | | 0.5 mol/dm3 acetic acid | | | | |
| 0 | 0 | 0 | N/A | N/A | 0 | 0 | 0 |
| 1 | 1 | 1 | N/A | N/A | 0.25 | 0 | 0 |
| 2 | 2 | 1 | N/A | N/A | 0.375 | 0.707 | 0.5 |
| 3 | 7 | 5 | N/A | N/A | 1.5 | 1.414 | 1 |
| 4 | 10 | 8 | N/A | N/A | 2.25 | 1.414 | 1 |
| 5 | 14 | 11 | N/A | N/A | 3.125 | 2.121 | 1.5 |
| | | | 1 mol/dm3 acetic acid | | | | |
| 0 | 0 | 0 | 0 | 0 | 0 | 0 | 0 |
| 1 | 2 | 1 | 2 | 4 | 0.5625 | 1.258 | 0.629 |
| 2 | 5 | 4 | 4 | 8 | 1.3125 | 1.892 | 0.946 |
| 3 | 11 | 7 | 9 | 13 | 2.5 | 2.582 | 1.290 |
| 4 | 16 | 10 | 12 | 17 | 3.4375 | 3.304 | 1.652 |
| 5 | 21 | 13 | 16 | 25 | 4.6875 | 5.315 | 2.657 |
| | | | 1.5 mol/dm3 acetic acid | | | | |
| 0 | 0 | 0 | 0 | 0 | 0 | 0 | 0 |
| 1 | 3 | 4 | 4 | 4 | 0.9375 | 0.5 | 0.25 |
| 2 | 9 | 6 | 9 | 10 | 2.125 | 1.732 | 0.866 |
| 3 | 17 | 10 | 14 | 14 | 3.4375 | 2.872 | 1.436 |
| 4 | 25 | 13 | 17 | 20 | 4.6875 | 5.058 | 2.529 |
| 5 | 34 | 17 | 2 | 26 | 6.1875 | 7.182 | 3.591 |
| | | | 2 mol/dm3 acetic acid | | | | |
| 0 | 0 | 0 | 0 | 0 | 0 | 0 | 0 |
| 1 | 5 | 6 | 4 | 6 | 1.3125 | 0.957 | 0.479 |
| 2 | 10 | 12 | 7 | 12 | 2.5625 | 2.363 | 1.181 |
| 3 | 17 | 17 | 10 | 23 | 4.1875 | 5.315 | 2.658 |
| 4 | 22 | 21 | 13 | 28 | 5.25 | 6.164 | 3.082 |
| 5 | 28 | 31 | 16 | 36 | 69375 | 8.5 | 4.25 |

Figure 3-8 data set

Figure 3-6 data set

| week number | Defect 1 | Defect 2 | Defect 3 | Defect 4 | mean area cm2 | st dev | st dev of mean |
|---|---|---|---|---|---|---|---|
| | | | 0.5 mol/dm3 acetic acid | | | | |
| 0 | 0 | 0 | 0 | 0 | 0 | 0 | 0 |
| 1 | 0 | 0.00915 | 0.00468 | 0.10578 | 0.0299 | 0.051 | 0.025 |
| 2 | 0.02787 | 0.04271 | 0.02502 | 0.08096 | 0.0441 | 0.026 | 0.013 |
| 3 | 0.04759 | 0.17331 | 0.02461 | 0.1501 | 0.0989 | 0.074 | 0.037 |
| 4 | 0.10354 | 0.23657 | 0.18165 | 0.20911 | 0.1827 | 0.057 | 0.029 |
| 5 | 0.18633 | 0.30899 | 0.20240 | 0.20492 | 0.2506 | 0.065 | 0.033 |
| | | | 1 mol/dm3 acetic acid | | | | |
| 0 | 0 | 0 | 0 | 0 | 0 | 0 | 0 |
| 1 | 0.03906 | 0.16802 | 0.06631 | 0.05513 | 0.0821 | 0.058 | 0.029 |
| 2 | 0.04618 | 0.29841 | 0.20016 | 0.10069 | 0.1614 | 0.111 | 0.056 |
| 3 | 0.10942 | 0.24399 | 0.29068 | 0.20993 | 0.2625 | 2.139 | 0.070 |
| 4 | 0.15887 | 0.58767 | 0.45118 | 0.37185 | 0.3924 | 0.179 | 0.090 |
| 5 | 0.33015 | 0.90399 | 0.66334 | 0.45240 | 0.5875 | 0.252 | 0.126 |
| | | | 1.5 mol/dm3 acetic acid | | | | |
| 0 | 0 | 0 | 0 | 0 | 0 | 0 | 0 |
| 1 | 0.24247 | 0.02888 | 0.19039 | 0.28295 | 0.1861 | 0.111 | 0.056 |
| 2 | 0.55655 | 0.46644 | 0.22457 | 0.17758 | 0.3563 | 0.184 | 0.092 |
| 3 | 0.88202 | 0.69243 | 0.54048 | 0.43246 | 0.6368 | 0.195 | 0.098 |
| 4 | 1.26892 | 0.94182 | 1.07771 | 0.57750 | 0.9665 | 0.292 | 0.146 |
| 5 | 1.56062 | 1.07200 | 1.44039 | 0.75752 | 1.2076 | 0.365 | 0.182 |
| | | | 2 mol/dm3 acetic acid | | | | |
| 0 | 0 | 0 | 0 | 0 | 0 | 0 | 0 |
| 1 | 0.10679 | 0.30126 | 0.30459 | 0.15093 | 0.2158 | 0.102 | 0.051 |
| 2 | 0.46115 | 0.48962 | 0.68592 | 0.34540 | 0.4955 | 0.141 | 0.071 |
| 3 | 0.54658 | 0.72701 | 1.03641 | 0.47579 | 0.6964 | 0.250 | 0.125 |
| 4 | 0.97843 | 1.24389 | 1.25773 | 0.91930 | 1.0998 | 0.176 | 0.088 |
| 5 | 1.31855 | 1.60394 | 1.59052 | 1.03458 | 1.3868 | 0.269 | 0.134 |

Figure 3-6 data set

Figure 4-16 data set

| week number | Defect 1 | Defect 2 | Defect 3 | Defect 4 | area of corrosion | st dev | st dev of mean |
|---|---|---|---|---|---|---|---|
| | | | Zn-Al(1wt%)-Mg(1wt%) | | | | |
| 0 | 0 | 0 | 0 | 0 | 0 | 0 | 0 |
| 1 | 0.21 | 0.40 | 0.21 | 0.45 | 0.3175 | 0.125 | 0.063 |
| 2 | 0.36 | 0.62 | 0.35 | 0.72 | 0.5125 | 0.186 | 0.093 |
| 3 | 0.93 | 0.85 | 0.41 | 1.14 | 0.8325 | 0.307 | 0.154 |
| 4 | 1.35 | 1.29 | 0.46 | 1.43 | 1.1325 | 0.452 | 0.226 |
| 5 | 1.51 | 1.47 | 0.64 | 1.8 | 1.355 | 0.499 | 0.249 |
| | | | Zn-Al(1.5wt%)-Mg(1.5wt%) | | | | |
| 0 | 0 | 0 | 0 | 0 | 0 | 0 | 0 |
| 1 | 0.14 | 0.06 | 0.08 | 0.08 | 0.095 | 0.034 | 0.017 |
| 2 | 0.12 | 0.18 | 0.10 | 0.24 | 0.155 | 0.070 | 0.035 |
| 3 | 0.35 | 0.42 | 0.14 | 0.73 | 0.41 | 2.244 | 0.122 |
| 4 | 0.65 | 0.69 | 0.25 | 1.04 | 0.6575 | 0.323 | 0.161 |
| 5 | 1.10 | 0.98 | 0.36 | 1.41 | 0.9625 | 0.441 | 0.220 |
| | | | Zn-Al(3wt%)-Mg(3wt%) | | | | |
| 0 | 0 | 0 | 0 | 0 | 0 | 0 | 0 |
| 1 | 0.06 | 0.02 | 0.09 | 0.03 | 0.05 | 0.032 | 0.016 |
| 2 | 0.04 | 0.11 | 0.11 | 0.05 | 0.0775 | 0.037 | 0.019 |
| 3 | 0.05 | 0.14 | 0.11 | 0.05 | 0.0875 | 0.045 | 0.023 |
| 4 | 0.07 | 0.38 | 0.12 | 0.12 | 0.1725 | 0.140 | 0.070 |
| 5 | 0.06 | 0.71 | 0.13 | 0.20 | 1.275 | 0.295 | 0.148 |
| | | | Zn-Al(6wt%)-Mg(3wt%) | | | | |
| 0 | 0 | 0 | 0 | 0 | 0 | 0 | 0 |
| 1 | 0.01 | 0.02 | 0.01 | 0.0 | 0.01 | 0.008 | 0.004 |
| 2 | 0.02 | 0.03 | 0.00 | 0.02 | 0.0175 | 0.013 | 0.006 |
| 3 | 0.01 | 0.00 | 0.02 | 0.03 | 0.015 | 0.013 | 0.006 |
| 4 | 0.01 | 0.02 | 0.05 | 0.01 | 0.0225 | 0.019 | 0.001 |
| 5 | 0.02 | 0.02 | 0.03 | 0.04 | 0.0275 | 0.010 | 0.005 |

Figure 4-16 data set

Figure 4-26 data set

| week number | Defect 1 | Defect 2 | Defect 3 | Defect 4 | area of corrosion | st dev | st dev of mean |
|---|---|---|---|---|---|---|---|
| | | | 70g/m2 | | | | |
| 0 | 0 | 0 | 0 | 0 | 0 | 0 | 0 |
| 1 | 0.22 | 0.12 | 0.31 | 0.15 | 0.197 | 0.084 | 0.042 |
| 2 | 0.72 | 0.21 | 0.56 | 0.75 | 0.560 | 0.248 | 0.124 |
| 3 | 1.10 | 0.45 | 0.82 | 0.89 | 0.815 | 0.271 | 0.135 |
| 4 | 1.67 | 0.63 | 1.27 | 1.22 | 1.198 | 0.429 | 0.214 |
| 5 | 2.01 | 0.78 | 1.83 | 1.53 | 1.538 | 0.542 | 0.272 |
| | | | 100g/m2 | | | | |
| 0 | 0 | 0 | 0 | 0 | 0 | 0 | 0 |
| 1 | 0.08 | 0.12 | 0.14 | 0.26 | 0.077 | 0.077 | 0.039 |
| 2 | 0.38 | 0.46 | 0.26 | 0.42 | 0.086 | 0.086 | 0.043 |
| 3 | 0.48 | 0.78 | 0.52 | 0.71 | 0.145 | 0.145 | 0.072 |
| 4 | 0.71 | 1.15 | 0.74 | 1.10 | 0.232 | 0.232 | 0.116 |
| 5 | 0.84 | 1.53 | 0.97 | 1.42 | 0.336 | 0.336 | 0.168 |
| | | | 140g/m2 | | | | |
| 0 | 0 | 0 | 0 | 0 | 0 | 0 | 0 |
| 1 | 0.06 | 0.01 | 0.08 | 0.14 | 0.095 | 0.034 | 0.017 |
| 2 | 0.18 | 0.08 | 0.24 | 0.12 | 0.155 | 0.070 | 0.035 |
| 3 | 0.42 | 0.14 | 0.73 | 0.35 | 0.410 | 0.244 | 0.122 |
| 4 | 0.69 | 0.25 | 1.04 | 0.65 | 0.658 | 0.323 | 0.161 |
| 5 | 0.98 | 0.36 | 1.41 | 1.10 | 0.963 | 0.440 | 0.220 |
| | | | 200g/m2 | | | | |
| 0 | 0 | 0 | 0 | 0 | 0.000 | 0 | 0 |
| 1 | 0.01 | 0.05 | 0.02 | 0.03 | 0.028 | 0.010 | 0.005 |
| 2 | 0.04 | 0.04 | 0.14 | 0.04 | 0.065 | 0.034 | 0.017 |
| 3 | 0.14 | 0.08 | 0.47 | 0.14 | 0.208 | 0.085 | 0.043 |
| 4 | 0.46 | 1.11 | 0.83 | 0.32 | 0.430 | 0.138 | 0.069 |
| 5 | 0.89 | 0.27 | 1.35 | 0.53 | 0.760 | 0.235 | 0.117 |
| | | | 275g/m2 | | | | |
| 0 | 0 | 0 | 0 | 0 | 0 | 0 | 0 |
| 1 | 0.02 | 0.02 | 0.04 | 0.03 | 0.028 | 0.010 | 0.005 |
| 2 | 0.08 | 0.12 | 0.06 | 0.04 | 0.075 | 0.034 | 0.017 |
| 3 | 0.19 | 0.26 | 0.13 | 0.06 | 0.160 | 0.085 | 0.043 |
| 4 | 0.46 | 0.42 | 0.27 | 0.16 | 0.328 | 0.138 | 0.069 |
| 5 | 0.62 | 0.73 | 0.32 | 0.24 | 0.478 | 0.235 | 0.117 |
| | | | 350g/m2 | | | | |
| 0 | 0 | 0 | 0 | 0 | 0 | 0 | 0 |
| 1 | 0.01 | 0 | 0.03 | 0.02 | 0.015 | 0.013 | 0.006 |
| 2 | 0.01 | 0.05 | 0.02 | 0.02 | 0.025 | 0.017 | 0.009 |
| 3 | 0.04 | 0.01 | 0.05 | 0.04 | 0.035 | 0.017 | 0.009 |
| 4 | 0.06 | 0.26 | 0.12 | 0.22 | 0.115 | 0.104 | 0.052 |
| 5 | 0.11 | 0.32 | 0.18 | 0.38 | 0.248 | 0.124 | 0.062 |

**Figure 4-16 data set**

Figure 5-2 data set

Total area covered in corrosion product cm2

| week of mean | Defect 1 | Defect 2 | Defect 3 | Defect 4 | Average | st dev | st dev |
|---|---|---|---|---|---|---|---|
| | | | 0wt% PPA | | | | |
| 0 | 0 | 0 | 0 | 0 | 0 | 0 | 0 |
| 1 | 0.24 | 0.03 | 0.19 | 0.28 | 0.185 | 0.109 | 0.055 |
| 2 | 0.56 | 0.47 | 0.22 | 0.18 | 0.358 | 0.186 | 0.093 |
| 3 | 0.88 | 0.69 | 0.54 | 0.43 | 0.635 | 0.195 | 0.098 |
| 4 | 1.27 | 0.94 | 1.08 | 0.58 | 0.968 | 0.292 | 0.146 |
| 5 | 1.56 | 1.07 | 1.44 | 0.76 | 1.208 | 0.364 | 0.182 |
| | | | 2wt%PPA | | | | |
| 0 | 0 | 0 | 0 | 0 | 0 | 0 | 0 |
| 1 | 0.14 | 0.04 | 0.17 | 0.05 | 0.100 | 0.077 | 0.039 |
| 2 | 0.39 | 0.13 | 0.49 | 0.21 | 0.305 | 0.086 | 0.043 |
| 3 | 0.43 | 0.21 | 0.74 | 0.38 | 0.440 | 0.145 | 0.072 |
| 4 | 0.65 | 0.30 | 1.02 | 0.53 | 0.625 | 0.232 | 0.116 |
| 5 | 0.94 | 0.42 | 1.34 | 0.61 | 0.828 | 0.336 | 0.168 |
| | | | 4wt%PPA | | | | |
| 0 | 0 | 0 | 0 | 0 | 0 | 0 | 0 |
| 1 | 0.06 | 0.10 | 0.14 | 0.14 | 0.110 | 0.038 | 0.019 |
| 2 | 0.14 | 0.22 | 0.26 | 0.18 | 0.195 | 0.050 | 0.025 |
| 3 | 0.21 | 0.32 | 0.44 | 0.34 | 0.323 | 0.095 | 0.048 |
| 4 | 0.33 | 0.43 | 0.60 | 0.52 | 0.470 | 0.116 | 0.058 |
| 5 | 0.49 | 0.61 | 0.82 | 0.57 | 0.623 | 0.141 | 0.070 |
| | | | 6wt%PPA | | | | |
| 0 | 0 | 0 | 0 | 0 | 0.000 | 0 | 0 |
| 1 | 0.03 | 0.05 | 0.08 | 0.10 | 0.065 | 0.031 | 0.016 |
| 2 | 0.09 | 0.16 | 0.14 | 0.16 | 0.138 | 0.033 | 0.017 |
| 3 | 0.15 | 0.32 | 0.27 | 0.32 | 0.265 | 0.080 | 0.040 |
| 4 | 0.19 | 0.46 | 0.35 | 0.38 | 0.345 | 0.113 | 0.057 |
| 5 | 0.25 | 0.63 | 0.45 | 0.40 | 0.433 | 0.157 | 0.078 |
| | | | 8wt%PPA | | | | |
| 0 | 0 | 0 | 0 | 0 | 0 | 0 | 0 |
| 1 | 0.08 | 0.03 | 0.05 | 0.02 | 0.045 | 0.026 | 0.013 |
| 2 | 0.14 | 0.06 | 0.19 | 0.15 | 0.135 | 0.054 | 0.027 |
| 3 | 0.29 | 0.10 | 0.32 | 0.21 | 0.230 | 0.098 | 0.049 |
| 4 | 0.32 | 0.13 | 0.44 | 0.27 | 0.290 | 0.128 | 0.064 |
| 5 | 0.40 | 0.14 | 0.52 | 0.34 | 0.350 | 0.159 | 0.079 |
| | | | 10wt%PPA | | | | |
| 0 | 0 | 0 | 0 | 0 | 0 | 0 | 0 |
| 1 | 0.04 | 0.05 | 0.06 | 0.02 | 0.043 | 0.017 | 0.009 |
| 2 | 0.10 | 0.06 | 0.14 | 0.07 | 0.093 | 0.036 | 0.018 |
| 3 | 0.14 | 0.09 | 0.22 | 0.10 | 0.138 | 0.059 | 0.029 |
| 4 | 0.30 | 0.10 | 0.29 | 0.22 | 0.228 | 0.092 | 0.046 |
| 5 | 0.37 | 0.12 | 0.39 | 0.31 | 0.298 | 0.123 | 0.061 |

Figure 5-2 data set

Figure 5-8 data set

Number of filaments on cut edge per cm

| wt% PPA | Edge 1 | Edge 2 | Edge 3 | Edge 4 | Average | st dev | st dev of mean |
|---|---|---|---|---|---|---|---|
| 0 | 12 | 6 | 10 | 17 | 11.25 | 4.573 | 2.287 |
| 2 | 6 | 3 | 2 | 4 | 3.75 | 1.708 | 0.854 |
| 4 | 1 | 0 | 2 | 1 | 1 | 0.816 | 0.408 |
| 6 | 0 | 0 | 0 | 0 | 0 | 0 | 0 |
| 8 | 0 | 0 | 0 | 0 | 0 | 0 | 0 |
| 10 | 0 | 0 | 0 | 0 | 0 | 0 | 0 |

Figure 5-8 data set

Figure 6-5 data set

Total area covered in corrosion product cm2

| week | Defect 1 | Defect 2 | Defect 3 | Defect 4 | Average | st dev | st dev of mean |
|---|---|---|---|---|---|---|---|
| | | | 0.00VF HT | | | | |
| 0 | 0 | 0 | 0 | 0 | 0 | 0 | 0 |
| 1 | 0.24 | 0.03 | 0.19 | 0.28 | 0.185 | 0.109 | 0.055 |
| 2 | 0.56 | 0.47 | 0.22 | 0.18 | 0.358 | 0.186 | 0.093 |
| 3 | 0.88 | 0.69 | 0.54 | 0.43 | 0.635 | 0.195 | 0.098 |
| 4 | 1.27 | 0.94 | 1.08 | 0.58 | 0.968 | 0.292 | 0.146 |
| 5 | 1.56 | 1.07 | 1.44 | 0.76 | 1.208 | 0.364 | 0.182 |
| | | | 0.05VF HT | | | | |
| 0 | 0 | 0 | 0 | 0 | 0 | 0 | 0 |
| 1 | 0.10 | 0.16 | 0.03 | 0.08 | 0.093 | 0.054 | 0.027 |
| 2 | 0.19 | 0.26 | 0.09 | 0.18 | 0.180 | 0.069 | 0.034 |
| 3 | 0.29 | 0.46 | 0.20 | 0.22 | 0.293 | 0.118 | 0.059 |
| 4 | 0.37 | 0.62 | 0.34 | 0.36 | 0.423 | 0.132 | 0.066 |
| 5 | 0.61 | 0.85 | 0.40 | 0.55 | 0.603 | 0.187 | 0.093 |
| | | | 0.1VF HT | | | | |
| 0 | 0 | 0 | 0 | 0 | 0 | 0 | 0 |
| 1 | 0.05 | 0.10 | 0.08 | 0.14 | 0.093 | 0.038 | 0.019 |
| 2 | 0.10 | 0.15 | 0.12 | 0.30 | 0.168 | 0.091 | 0.045 |
| 3 | 0.19 | 0.19 | 0.24 | 0.39 | 0.253 | 0.095 | 0.048 |
| 4 | 0.30 | 0.20 | 0.38 | 0.47 | 0.338 | 0.115 | 0.058 |
| 5 | 0.37 | 0.22 | 0.48 | 0.54 | 0.403 | 0.141 | 0.070 |
| | | | 0.15VF HT | | | | |
| 0 | 0 | 0 | 0 | 0 | 0.000 | 0 | 0 |
| 1 | 0.01 | 0.05 | 0.07 | 0.08 | 0.075 | 0.021 | 0.010 |
| 2 | 0.13 | 0.07 | 0.09 | 0.11 | 0.100 | 0.026 | 0.013 |
| 3 | 0.29 | 0.10 | 0.14 | 0.15 | 0.170 | 0.083 | 0.041 |
| 4 | 0.35 | 0.11 | 0.22 | 0.17 | 0.213 | 0.102 | 0.051 |
| 5 | 0.45 | 0.14 | 0.28 | 0.24 | 0.246 | 0.179 | 0.090 |
| | | | 0.20VF HT | | | | |
| 0 | 0 | 0 | 0 | 0 | 0 | 0 | 0 |
| 1 | 0 | 0.02 | 0.04 | 0.05 | 0.028 | 0.022 | 0.011 |
| 2 | 0.10 | 0.06 | 0.07 | 0.05 | 0.070 | 0.021 | 0.011 |
| 3 | 0.12 | 0.08 | 0.10 | 0.06 | 0.090 | 0.026 | 0.013 |
| 4 | 0.17 | 0.10 | 0.13 | 0.11 | 0.128 | 0.031 | 0.015 |
| 5 | 0.20 | 0.11 | 0.14 | 0.13 | 0.145 | 0.039 | 0.019 |

## Figure 6-5 data set

Figure 6-5 data

Average length of filiform corrosion filaments. 1 Data point = 0.25mm

| week | Defect 1 | Defect 2 | Defect 3 | Defect 4 | Average filament length mm | st dev | st dev of mean |
|---|---|---|---|---|---|---|---|
| | | | 0.00VF HT | | | | |
| 0 | 0 | 0 | 0 | 0 | 0 | 0 | 0 |
| 1 | 3 | 4 | 4 | 4 | 0.94 | 0.500 | 0.250 |
| 2 | 9 | 6 | 9 | 10 | 2.13 | 1.732 | 0.866 |
| 3 | 17 | 10 | 14 | 14 | 3.44 | 2.872 | 1.436 |
| 4 | 25 | 13 | 17 | 20 | 4.69 | 5.058 | 2.529 |
| 5 | 34 | 17 | 22 | 26 | 6.19 | 7.182 | 3.591 |
| | | | 0.05VF HT | | | | |
| 0 | 0 | 0 | 0 | 0 | 0 | 0 | 0 |
| 1 | 4 | 2 | 2 | 2 | 0.63 | 1.633 | 0.816 |
| 2 | 8 | 5 | 7 | 4 | 1.50 | 2.872 | 1.436 |
| 3 | 11 | 8 | 11 | 7 | 2.31 | 3.266 | 1.633 |
| 4 | 16 | 11 | 15 | 10 | 3.25 | 3.415 | 1.708 |
| 5 | 19 | 12 | 17 | 12 | 3.75 | 4.249 | 2.175 |
| | | | 0.1VF HT | | | | |
| 0 | 0 | 0 | 0 | 0 | 0 | 0 | 0 |
| 1 | 2 | 2 | 3 | 2 | 0.56 | 1.258 | 0.629 |
| 2 | 5 | 3 | 6 | 6 | 1.25 | 1.500 | 0.750 |
| 3 | 8 | 5 | 10 | 10 | 2.06 | 1.500 | 0.750 |
| 4 | 12 | 7 | 12 | 14 | 2.81 | 1.732 | 0.866 |
| 5 | 15 | 8 | 13 | 16 | 3.25 | 2.754 | 1.377 |
| | | | 0.15VF HT | | | | |
| 0 | 0 | 0 | 0 | 0 | 0.00 | 0 | 0 |
| 1 | 2 | 3 | 2 | 2 | 0.56 | 0.010 | 0.005 |
| 2 | 4 | 3 | 2 | 3 | 0.75 | 1.000 | 0.500 |
| 3 | 7 | 6 | 4 | 3 | 1.25 | 1.291 | 0.645 |
| 4 | 10 | 8 | 5 | 4 | 1.69 | 1.708 | 0.854 |
| 5 | 12 | 10 | 6 | 6 | 2.13 | 2.217 | 1.108 |
| | | | 0.20VF HT | | | | |
| 0 | 0 | 0 | 0 | 0 | 0 | 0 | 0 |
| 1 | 2 | 2 | 2 | 0 | 0.380 | 1.000 | 0.500 |
| 2 | 6 | 2 | 5 | 1 | 0.880 | 2.380 | 1.190 |
| 3 | 8 | 2 | 6 | 3 | 0.190 | 2.754 | 1.377 |
| 4 | 9 | 2 | 8 | 5 | 0.150 | 3.162 | 1.581 |
| 5 | 9 | 3 | 9 | 6 | 0.690 | 2.872 | 1.436 |

## Figure 6-6 data set